

**Heterogeneous Polycomb Silencing of Incoming Herpes Simplex
Virus Genomes During Productive Infection**

Alison Katharine Francois
Vienna, Austria

MBiochemistry (1st class), University of St Andrews
St Andrews, Scotland, 2017

A Dissertation Presented to the Graduate Faculty of the
University of Virginia in Candidacy for the
Degree of Doctor of Philosophy

Department of Microbiology, Immunology, and Cancer Biology
University of Virginia
April 2024

Table of Contents

Abstract	vii
Acknowledgements	ix
Figures and Tables	xiii
Abbreviations	xvii
Chapter 1: An Introduction to Herpes Simplex Virus 1 Lytic Infection and Viral Chromatin	1
1.1. The Importance of Herpesvirus Research	3
1.1.1. Lytic and Latent Herpesvirus Infection	3
1.1.2. Clinical Impacts of Herpesviruses	4
1.1.3. Treating Lytic and Latent Infection	10
1.2. HSV-1 Replication and Chromatinization	12
1.2.1. The HSV-1 Lytic Replication Cycle	12
1.2.2. Modifying the Host Cell	15
1.2.3. Lytic HSV-1 Chromatin	16
1.2.4. Repressive Histone Modifications on HSV-1 Chromatin	19
1.2.5. Heterogeneous Lytic Infection	21
1.2. Mammalian Polycomb Silencing	24
1.3.1. Two Branches of Gene Silencing	24
1.3.2. H3K27 Methylation by PRC2	25
1.3.3. H2AK119 Ubiquitination by PRC1	30
1.4. Investigating Polycomb Silencing in HSV-1 Infection	37
1.4.1. Starting Questions	37
1.4.2. Technical Goals	39
1.4.3. Statement of Purpose	42

Chapter 2: PRC2-mediated Regulation of Lytic Infection Through Repressive H3K27 Dimethylation	43
2.1. Abstract	45
2.2. Importance	46
2.3. Introduction	47
2.4. Results	52
2.4.1. H3K27me3 Does Not Associate with the HSV-1 Genome Following Infection of Human Fibroblasts.	52
2.4.2. Analysis of Individual HSV-1 Genome Foci for Co-localization with H3K27me3 Using NucSpotA.	55
2.4.3. Inhibition of H3K27me3 Deposition or Removal Does Not Alter its Co-localization with HSV-1 Genomes in Fibroblasts.	60
2.4.4. H3K27 Demethylase Inhibition Restricts Lytic Gene Expression.	62
2.4.5. A Subpopulation of Genomes Co-Localizes With H3K27me2 When H3K27 Demethylation Is Inhibited.	64
2.4.6. CUT&RUN Reveals a Low Association of Lytic Gene Promoters With H3K27me2 That Increases With K27 HDM Inhibition.	68
2.4.7. Transcriptionally Repressed Genomes Are Enriched for H3K27me2 In The Absence Of PML-NBs.	70
2.4.8. Association of the H3K27me2 reader protein PHF20L1 with a subpopulation of HSV-1 genomes.	73
2.5. Discussion	77
2.5.1. Updating the Model for H3K27 Methylation on Lytic Genomes	77
2.5.2. Experimental Limitations and Considerations	78
2.5.3. Implications and Future Directions	79
Chapter 3: PRC1-mediated Regulation of Lytic HSV-1 Gene Expression	83
3.1 Abstract	85
3.2. Introduction	87

	v
3.3. Results	93
3.3.1. H2AK119ub Is Enriched on The Latent HSV-1 Genome <i>In Vivo</i> .	93
3.3.2. H2AK119ub is Not Detected on Lytic HSV-1 Chromatin.	94
3.3.3. PRC1 Inhibition Restricts Lytic Gene Transcription.	97
3.3.4. RING1A/B Co-localize with a Subset of Lytic HSV-1 Genomes.	99
3.3.5. PRC1 Inhibition Reveals RING1A at Input Genomes in Transcriptionally Active Infected Cells.	104
3.3.6. Pro-Transcriptional H2AK119ub Reader ZRF1 Co-Localizes with Lytic HSV-1 Genomes and Replication Compartments.	107
3.3.7. ZRF1 is Expressed in Neurons and Re-Localizes to Replication Compartments During Neuronal Lytic Infection.	110
3.3.8. Total ZRF1 Expression and S47 Phosphorylation Change as a Consequence of Lytic Infection In Fibroblasts.	113
3.4. Discussion	115
3.4.1. A Pro-Transcriptional Role for PRC1 in HSV-1 Lytic Infection	115
3.4.2. Inability to Detect H2AK119ub on Lytic Chromatin	117
3.4.3. Non-specific ZRF1 Antibody Binding	120
3.4.4. Future Directions	120
Chapter 4: Implications and Future Directions	123
4.1 Future Directions	125
4.1.1. Potential Mechanisms for Repression by PHF20L1 in HSV-1 Infection	125
4.1.2. An Integrated Model for Polycomb Regulation of HSV-1 Chromatin	129
4.1.3. HSV-1 as a Tool to Study Host Epigenetics	132
4.2. Technical Lessons and Advances	133
4.2.1. Capturing Heterogeneity During Lytic Infection	133
4.2.2. Antibody Specificity is Key	134
4.2.3. Next Gen Sequencing Approaches to Viral Chromatin	135

4.3 Conclusions	139
Chapter 5: Materials and Methods	141
5.1. Reagents	143
5.1.1. Non-Neuronal Cells	143
5.1.2. Primary Neuronal Cells	143
5.1.3. Viruses	144
5.1.4. Inhibitors	145
5.1.5. PML Nanoblade and Knock-Out Cell Production	145
5.1.6. Production of EdC-labeled Virus Stocks	146
5.2. Infections	151
5.2.1. Lytic Infections	151
5.2.2. Establishment of Latent HSV-1 Infection in Primary Neurons	151
5.2.3. <i>In Vivo</i> Latent Infection	151
5.3. Immunofluorescence	152
5.3.1. Click Chemistry and Immunofluorescence	152
5.3.2. Image Analysis	152
5.3.3. Expressing FLAG-tagged ZRF1	153
5.4. Other Quantitative Methods	155
5.4.1. Quantification of Viral Gene Expression	155
5.4.2. Western Blotting	155
5.4.3. Histone Peptide Array	156
5.5. Epigenetic Assays	158
5.5.1. ChIP-qPCR	158
5.5.2. CUT&RUN	158
Appendix: Supplementary Data	161
References	173

Abstract

Herpes simplex virus 1 (HSV-1) establishes life-long infection with distinct lytic and latent phases in the epithelial mucosa and peripheral nervous system respectively.

Reactivation is triggered by factors including stress, fever, sun exposure and hormonal changes, leading to renewed lytic replication. How lytic and latent infection are shaped in these distinct contexts is unclear, but must be understood to inform the goal of preventing reactivation.

During latency, viral DNA exists in the nucleus as repressive heterochromatin. Latent HSV-1 chromatin features the histone post-translational modification H3K27me₃, laid by Polycomb repressor complex 2 (PRC2). In non-neuronal cells, viral chromatin is instead permissive to lytic gene expression. We tested the assumption in the field that H3K27me₃ is rapidly deposited and removed from the viral genome in fibroblasts, and determined that H3K27me₃ does not associate with lytic HSV-1 genomes. Using a novel assay imaging individual viral genomes, we found that H3K27me₂ forms on a subset of genomes and represses lytic gene expression. We determined that H3K27me₂ reader PHF20L1 co-localizes with incoming viral DNA, indicating that transcriptional repression by H3K27me₂ could be mediated via PHF20L1 activity.

We then explored whether the other branch of Polycomb silencing, Polycomb repressor complex 1 (PRC1)-mediated H2AK119ub, regulates HSV-1 gene expression. H2AK119ub was detected on viral chromatin from latency established *in vivo*, providing an updated picture of latent chromatin that features both Polycomb-associated modifications. We did not detect H2AK119ub on lytic chromatin, but found that PRC1 activity is pro-transcriptional to lytic gene expression. PRC1 subunits RING1A/B both co-

localized with lytic viral genomes, and pro-transcriptional H2AK119ub reader Zuotin-related factor 1 (ZRF1) co-localized with incoming genomes and replication compartments. These findings point to PRC1 promoting lytic gene expression through reader protein ZRF1.

We conclude that both branches of Polycomb silencing contribute to the transcriptional regulation of HSV-1 infection. PRC2 activity represses lytic gene expression, whereas PRC1 activity is pro-transcriptional in lytic infection of fibroblasts. We also identify reader proteins PHF20L1 and ZRF1 that may mediate the transcriptional regulation by PRC2 and PRC1 activity respectively. We propose these two axes of transcriptional regulation by Polycomb complexes, aspects of which may differ between non-neuronal and neuronal infection and shape the cell type-specific outcomes. We also illustrate the value of capturing heterogeneity between viral genomes, an approach that revealed previously unobserved roles for Polycomb regulation of HSV-1 infection.

Acknowledgements

I have been incredibly supported in my life thus far and have many to thank. I received an excellent education in international schools in the Netherlands and Austria. My teachers believed in my intelligence, and at the same time fostered my creativity. My parents trusted me to learn at my own pace and ask for help when needed, and my dad Joe spent many evenings helping me tackle math homework through my frustration and tears. My mom Mary-Lynne has always been there for me, and never doubted my ability to achieve my academic goals. My older siblings Brendan and Chloe believed in me while being appropriately annoyed by their little sister, eventually accepting that I did actually know more than them about something. I had the privilege of growing up in a household that values reading and education, and following our interests.

I am thankful for the International Baccalaureate program's emphasis on interdisciplinary learning and critical thinking, and the teachers who taught me those subjects at Vienna International School. I have fond memories of my IB higher level biology class, taught by David Ford. Mr. Ford saw and matched my curiosity for biology, challenged my thinking and never doubted my goals, and his support is a large factor in my choice to pursue science.

I attended the University of St Andrews for my degree in biochemistry where I was taught by world-class researchers passionate about their subjects, many of whom informed my interests today. Dr David Jackson was my mentor during my fourth year and for my masters research the following year, and he was patient and understanding when a series of events in both our lives made completing my research seem

impossible. Dr Gerald Prescott stands out in my memory as an incredibly effective educator, and I am particularly thankful for Dr Prescott's support at the end of my degree.

When I came to UVA, I felt welcomed by the BIMS program and the MIC Department. Amy Anderson (administrator at the time) made our lives infinitely easier as we adjusted to graduate school. I am thankful for Amy, as well as our current administrator Jennifer Hamlin. I was thrilled to join Dr Anna Cliffe's lab at the end of my rotations, and was struck by Anna's creativity, passion and ambition in research. I was 24 when I joined, and I've been able to grow up with the lab in my time here. I have had the privilege of seeing the lab grow, and see Anna grow as a mentor. I appreciate her scientific guidance, as well as her understanding when health or other life factors had to take priority. Anna also let me go down rabbit holes teaching myself new computational skill sets, and I am thankful for that space and the skills I've been able to develop. I am certainly a better scientist because of Anna's guidance, and I look forward to seeing the work the lab produces in the coming years. I am also grateful for my thesis committee members Dr Dan Engel, Dr Lucy Pemberton, Dr Mitch Smith and Dr Patrick Grant, and their guidance during the winding journey of my research (particularly those who physically left UVA and still attended meetings over zoom).

Lastly, I met some very important people while living in Charlottesville. My cohort member Dr Liz Gonye has been a loyal and kind friend since 2017, and I can't wait to see whatever she does next. My fellow lab members have created a welcoming and supportive environment, and I am particularly thankful to Dr Sara Dochnal for her encouragement, Dr Sean Cuddy for his distinct laugh barreling down the hallways, and (eventual Dr) Abby Whitford for her white board artwork. I met my partner Tim a month before my qualifying exam, and I got through grad school with his support and

unwavering belief in my capabilities. Our three dogs Penny, Zoe and Luna have also been crucial for my survival, and coming home to you and three overjoyed dogs every day is my favorite thing.

Figures and Tables

Table 1. Composition and abbreviations used for Polycomb-associated proteins.	xvii
Table 2: Non-Polycomb complex abbreviations and acronyms.	xix
Figure 1.1: The eight human herpesviruses and the specialized cell types known to undergo lytic replication and latent infection.	4
Figure 1.2: The three clinical stages of prototypical HSV-1 infection.	6
Figure 1.3: Diseases caused by herpes simplex viruses 1 and 2.	8
Figure 1.4 An overview of the lytic replication cycle of Herpes simplex virus (HSV-1).	14
Figure 1.5: An overview of the events during Polycomb-mediated facultative heterochromatin formation in pluripotent cells.	25
Figure 1.6: The composition of PRC2.1 and PRC2.2 complexes.	27
Figure 1.7: The components of canonical and variant PRC1 complexes and interacting transcription factors.	31
Figure 1.8: Conflicting mechanisms of transcriptional regulation by H2AK119ub on mammalian chromatin.	36
Figure 2.1: CUT&RUN during early infection shows little H3K27me3 enrichment on lytic HSV-1 chromatin.	54
Figure 2.2: Image analysis using NucSpotA to quantify the enrichment of nuclear protein(s) at viral genomes.	58
Figure 2.3: Incoming HSV-1 genomes do not co-localize with H3K27me3 during early lytic infection.	60
Figure 2.4: Inhibition of H3K27me3 dynamics does not impact H3K27me3 co-localization with lytic genomes.	62
Figure 2.5: Inhibition of H3K27 demethylase activity restricts lytic gene expression, but inhibition of H3K27 methylation does not impact lytic gene transcription.	64
Figure 2.6: A subpopulation of viral genomes co-localizes with H3K27me2 when H3K27 demethylation is inhibited.	66

Figure 2.7: Bulk-level analysis of viral chromatin by CUT&RUN shows modest H3K27me2 enrichment at viral promoters, and less across gene bodies, during lytic infection.	70
Figure 2.8: Transcriptionally repressed viral genome association with H3K27me2 is favored in the absence of PML expression.	73
Figure 2.9: H3K27me2 reader PHF20L1 co-localizes with a subpopulation of lytic genomes, including transcriptionally repressed genomes in the absence of PML expression.	75
Figure 3.1: HSV-1 genomes from latently infected ganglia show enrichment for H2AK119ub at the lytic ICP27 and ICP8 promoters.	93
Figure 3.2: H2AK119ub is not seen at individual HSV-1 genomes or bulk chromatin by ChIP-qPCR.	96
Figure 3.3: Lytic gene expression is restricted by PRC1 inhibition in both fibroblasts (HFFs) and epithelial cells (ARPE-19s).	99
Figure 3.4: RING1B co-localizes with a subset of lytic genomes.	102
Figure 3.5: RING1A also co-localizes with a subset of lytic HSV-1 genomes 4 HPI.	103
Figure 3.6: PRC1 inhibitor RB-3 causes loss of RING1A at input genomes in cells expressing ICP4.	107
Figure 3.7: H2AK119ub reader ZRF1 co-localizes with lytic genomes and is recruited to replication compartments in fibroblasts.	110
Figure 3.8: ZRF1 is expressed in neuronal cells and recruited to replication compartments during lytic neuronal infection.	112
Figure 3.9: ZR1, pZRF1 and ID1 protein levels shift over 6 hours of lytic infection.	114
Figure 4.1: The repressive PHF20L1-NuRD-PRC2 mechanism that could be occurring on viral chromatin	129
Figure 4.2: An integrated model for PRC1 and PRC2 activity regulating HSV-1 transcription.	131
Figure 4.3: An overview of the CUT&RUN data analysis pipeline established for HSV-1 infected cells	138

Table 5.1: Antibodies used and their applications	147
Table 5.2: Oligonucleotide primer sequences used for qPCR	149
Table 5.3: Promoter locations on reference genome used for CUT&RUN data analysis	150
Figure 6.1: Histone peptide binding arrays for H3K27me3 and H3K27me2 antibodies show variable target specificity and non-specific binding affinities.	163
Figure 6.2: Validation of inhibitor activity and lack of interferon-stimulated gene induction.	164
Figure 6.3: Certain H3K27me2 antibodies show evidence of non-specific binding to the viral genome.	165
Figure 6.4: H2AK119ub antibody binding specificity assessed by western blot.	166
Figure 6.5: ZRF1 staining with a mouse antibody shows concentration at replication compartments.	167
Figure 6.6: Western blots of ZRF1 showed non-specific protein bands.	168
Figure 6.7: Optimizing CUT&RUN for H2AK119ub in HFF cells.	169
Figure 6.8: Integrative Genome Viewer coverage plots for CUT&RUN samples.	170
Figure 6.9: Assessing PHF20L1 protein levels by western blot is made complicated by bands of unexpected sizes.	171

Abbreviations

Table 1. Composition and abbreviations used for Polycomb-associated proteins.

This is a direct adaptation from Dochnal, Francois and Cliffe et al., 2021 (1) and originally compiled by Sara Dochnal.

Complex	Full-Length Name	Abbreviation
Polycomb repressive complex 1		PRC1
	Ring Finger Protein 1A, B	RING1A, B
	Polycomb group RING finger protein	PCGF
Canonical PRC1		cPRC1
	Polycomb group RING finger protein 2, melanoma nuclear protein 18	PCGF2/ME L18
	Polycomb group RING finger protein 4	PCGF4/BMI 1
	Chromobox 2, 4, 6, 7, 8	CBX2, 4, 6, 7, 8
	* Runt-related transcription factor 1	RUNX1
	* RE1-silencing transcription factor/ neuron-restrictive silencing factor	REST/NRS F
Non-canonical/variant PRC1		vPRC1
	RING1 and YY1-binding protein	RYBP
	YY1-associated factor 2	YAF2
	Lysine (K)-specific demethylase 2B	KDM2B
	Polycomb group RING finger protein 1–6	PCGF 1–6
	* E2F transcription factor 6	E2F6
	* MAX gene-associated protein	MGA
	* Heterogeneous nuclear ribonucleoprotein K	hnRNPK
Polycomb Repressive complex 2		PRC2
	Enhancer of Zeste 1, 2	EZH1, 2
	Suppressor of Zeste 12	SUZ12
	Embryonic ectoderm development	EED
	Retinoblastoma-associated proteins 46	RbAp46/RB BP4
	Retinoblastoma-associated proteins 48	RbAp48/RB BP7
PRC2.1		
	Elongin BC	No abbreviation

	Elongin BC- and PRC2-associated Protein	EPOP
	PRC2-associated LCOR isoform1, 2 C-terminal binding protein	PAL1, 2 CTBP
	Polycomb-like protein 1/PHD finger protein 1	PCL1/PHF1
	Polycomb-like protein 2/metal response element binding transcription factor 2	PCL2/MTF2
	Polycomb-like protein 3/PHD finger protein 19	PCL3/PHF1 9
PRC2.2		
	Jumonji and AT-rich interaction domain 2	JARID2
	Adipocyte enhancer-binding protein 2	AEBP2

* Accessory proteins linked with complex recruitment.

Table 2: Non-Polycomb complex abbreviations and acronyms.

Acronym	Full-Length Name
ACV	Acyclovir
AD	Activation domain
AML	Acute myeloid leukemia
ATRX	Alpha Thalassemia/Mental Retardation Syndrome X-Linked protein
CNS	Central nervous system
CSK	Cytoskeletal buffer
ChIP	Chromatin immunoprecipitation
CUT&RUN	Cleavage under targets and release using nuclease
DAXX	Death domain-associated protein
DMSO	Dimethyl sulfoxide
DSBs	Double-stranded breaks
EBV	Epstein-Barr virus
FBS	Fetal bovine serum
FISH	Fluorescence in situ hybridization
HCMV	Human cytomegalovirus
HFFs	Human foreskin fibroblasts
HHV	Human herpesvirus
HIV	Human immunodeficiency virus
HMBA	Hexamethylene bis-acetamide
HPI	Hours post-infection
HSVEdC	EdC-labeled HSV-1
IE	Immediate early
LAT	Latency-associated transcript
MNase	Micrococcal nuclease
MOI	Multiplicity of infection
MSL	Male-specific lethal
NBs	Nuclear bodies
NER	Nucleotide excision repair
NGS	Next gen sequencing
NPCs	Neural progenitor cells

NSL	Non-specific lethal
NuRD	Nucleosome remodeling and deacetylase
PBS	Phosphate-buffered saline
PFU	Plaque-forming units
PHD	Plant homeodomain
PML	Promyelocytic leukemia protein
PTMs	Post-translational modifications
PcG	Polycomb group protein
RCs	Replication compartments
RPEs	Pigmented retinal epithelial cells
SCG	Superior cervical ganglia
TG	Trigeminal ganglia
VHS	Virus host shutoff
VZV	Varicella-zoster virus
fHC	Facultative heterochromatin
iPSCs	Induced pluripotent stem cells
lncRNA	Long non-coding RNA
mESCs	Mouse embryonic stem cells
qPCR	Quantitative polymerase chain reaction
scRNAseq	single cell RNA sequencing

Chapter 1: An Introduction to Herpes Simplex Virus 1 Lytic Infection and Viral Chromatin

Some sections of this chapter have been adapted from the following publication:

Dochnal SA*, Francois AK*, Cliffe AR. 2021. De Novo Polycomb Recruitment:
Lessons from Latent Herpesviruses. *Viruses* 13:1470.

*Co-first authors

Blank page

1.1. The Importance of Herpesvirus Research

1.1.1. Lytic and Latent Herpesvirus Infection

All herpesviruses (*Herpesvirales Orthoherpesviridae*) are capable of both productive (lytic) and quiescent (latent) infection in specific cell types. Latent herpesvirus infection is life-long with continued potential for reactivation. Reactivation from latency causes renewed lytic replication and viral shedding, facilitating transmission to new hosts. Within the order and family *Herpesvirales Orthoherpesviridae*, the herpesviruses are categorized as alpha, beta and gamma. Each human herpesvirus (HHV) uniquely interacts with the host, but some shared features exist within each subfamily. The human alphaherpesviruses establish latency in peripheral neurons, which are notably non-dividing cells. Betaherpesviruses establish latency in hematopoietic progenitor and myeloid cells, while gammaherpesviruses persist in lymphoid cell populations, both dividing cell populations. The specialized cell types for latent and lytic infection by the nine HHV are represented in Figure 1.1.

The factors shaping lytic replication, latent infection and reactivation from latency are a focus of herpesvirus research, as they represent potential treatment targets. Although this dissertation focuses on alphaherpesvirus herpes simplex virus 1 (HSV-1), all subfamilies of HHV are associated with global health burdens. The human herpesviruses are widely prevalent, and threaten reactivation for the rest of the host's life. Some of the acute and long-term impacts of HHV infection are summarized in the following section.

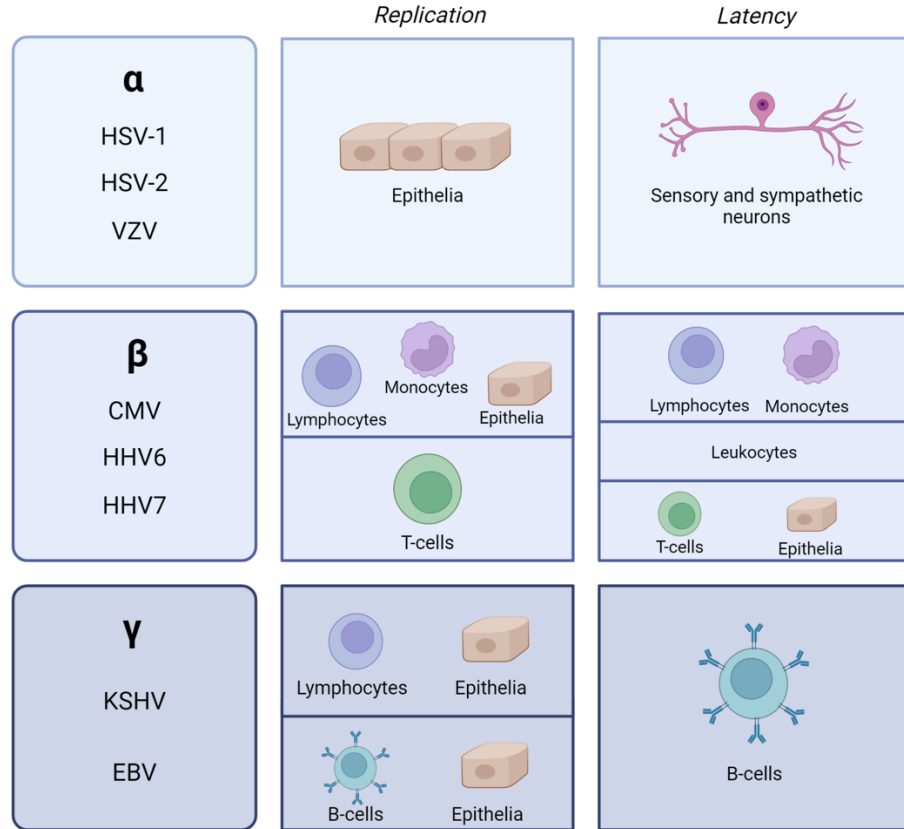


Figure 1.1: The eight human herpesviruses and the specialized cell types known to undergo lytic replication and latent infection.

Table created using information adapted from Cohen et al. (2), created with Biorender.

1.1.2 Clinical Impacts of Herpesviruses

The Human Alphaherpesviruses

Detection of latent herpesviruses *in vivo* is difficult, due to a lack of viral gene expression during this stage. Serum antibodies generated during prior lytic infection are used to estimate prevalence. The World Health Organization estimates that 67% of the world's population is latently infected with HSV-1, and 13% with HSV-2. HSV-1 and HSV-2 are

distinct species, but share approximately 70% nucleotide sequence and a similar genomic structure (3).

A common site of initial lytic HSV-1 infection is the oral mucosa, from which nearby sensory or autonomic neurons are infected and latency established in the neuronal nucleus (Figure 1.2). Like all herpesviruses, infection with HSV-1 is life-long and asymptomatic in the latent phase, with symptomatic reactivation events triggered by a variety of stressors at an unpredictable frequency. Most commonly known as the cause of oral cold-sores, primary HSV-1 infection or reactivation can cause life-threatening neonatal herpes (4, 5) or encephalitis (the latter particularly in individuals with specific interferon signaling gene mutations (6). HSV-2 can also cause encephalitis and meningitis (7). Primary or reactivated infection of the eye causes herpes keratitis, and possible blindness if untreated (8).

HSV-1 is also capable of primary infection at the genital mucosa, and latency establishment in neurons of the dorsal root ganglia. Conversely, HSV-2 is typically considered the cause of genital herpes (9), but is capable of infecting the oral mucosa. However, the number of new genital infections caused by HSV-1 is increasing, shifting this paradigm (10). HSV-1 reactivates less frequently in the dorsal root ganglia (25% of patients) than HSV-2 (60-90% of patients) (11–13). Taking this crossover into account, a 2020 study estimated a prevalence of half a billion genital infections with HSV-1 or HSV-2, and several billion orally infected with HSV-1 (14).

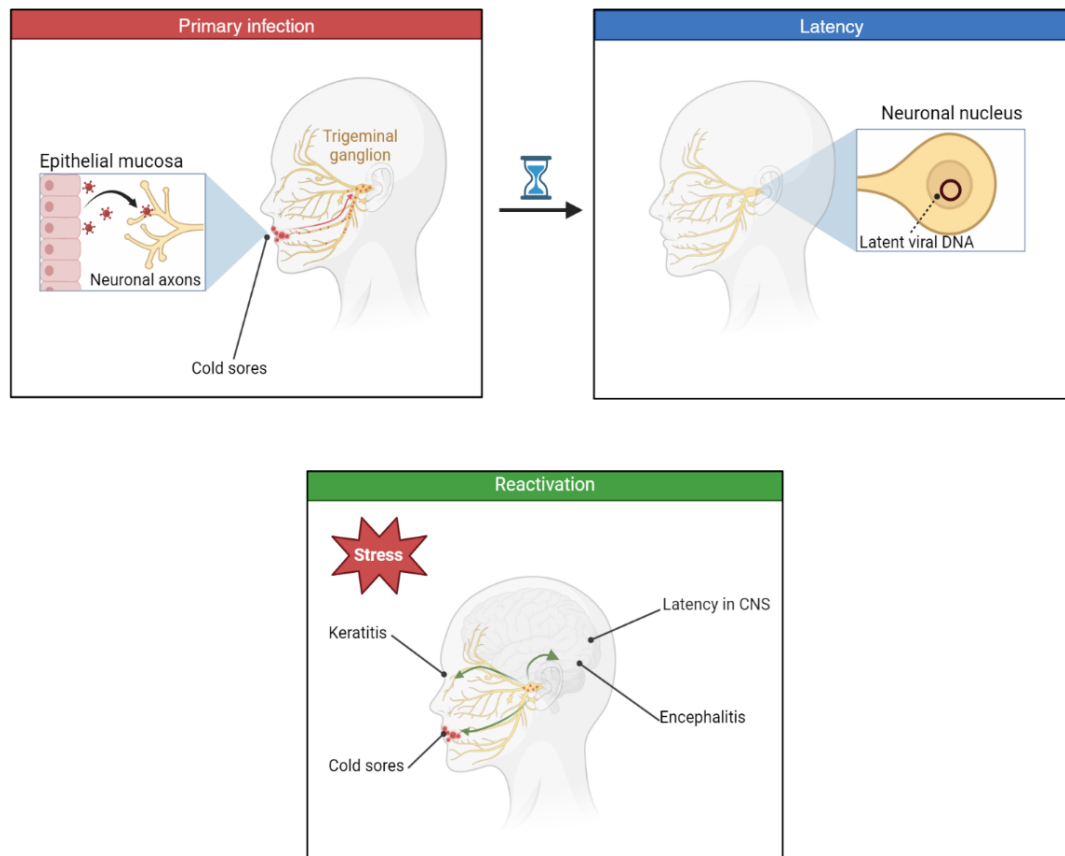


Figure 1.2: The three clinical stages of prototypical HSV-1 infection.

A. At primary infection of the epithelial mucosa, lytic replication results in production of new virions. Virions then infect the distal axons of nearby peripheral neurons. The face's sensory neurons' cell bodies (somata) are clustered together into a ganglion, the trigeminal ganglion. **B.** Within the infected neuron's nucleus, the viral genome establishes latency, persisting for the lifetime of the host. **C.** Following a stressor such as UV exposure, fever or psychological stress, the latent genome can reactivate. Transcription of lytic genes resumes, and newly assembled virus particles can travel back down the axon and re-infect the original site of primary infection. This results in a cold sore. In some cases, neighboring sensory neurons are infected. *De novo* infection of these neurons then causes lytic infection of that neuron's innervated site. In the case of the neurons innervating the eye, herpes keratitis occurs. In rare cases, usually in immunocompromised individuals or neonates, reactivated virus can infect the central nervous system, with serious implications including encephalitis. (15) Created with Biorender.

Beyond the acute risks of lytic virus replication, there are potentially long-term impacts of life-long infection with HSV-1. Growing evidence links HSV-1 latency in the brain and neurodegenerative disease, an association hypothesized to result from repeated reactivation events and subsequent immune responses (15–20). Genital infection with HSV-2 is also associated with increased risk for human immunodeficiency virus (HIV) infection, contributing to the global HIV crisis. This link underlines the necessity of understanding the impacts of life-long infection, in addition to the acute complications of lytic replication. The aforementioned HSV-related conditions are shown with their location on an adult body in Figure 1.3.

Varicella-zoster virus (VZV) is the third human alphaherpesvirus, but the only one we currently vaccinate against. Known as the cause of chickenpox, a VZV vaccine became available in 1995 and changed public perception of childhood infection from inevitable to preventable (21, 22). VZV infection can be severe, causing complications including encephalitis, but usually resolves with latent infection of the sensory ganglia (23). Reactivation (typically in later adulthood) causes herpes zoster (shingles), in which virus is transported back down the axon to the skin and causes significant pain from neuronal damage. This feature is shared with HSV-1 and HSV-2, although VZV infects a broader range of peripheral ganglia throughout the body (23–25). This pain, termed post-herpetic neuralgia, can be long-lasting and debilitating (26).

For all three human alphaherpesviruses, reactivation causes potentially permanent damage to neurons, which is especially impactful for these non-dividing cells that must persist for the life of the host. Antivirals are a treatment option for actively lytic infection, inhibiting viral DNA replication effectively, but it is difficult to catch reactivation early enough to administer the medication before any neuronal damage (24).

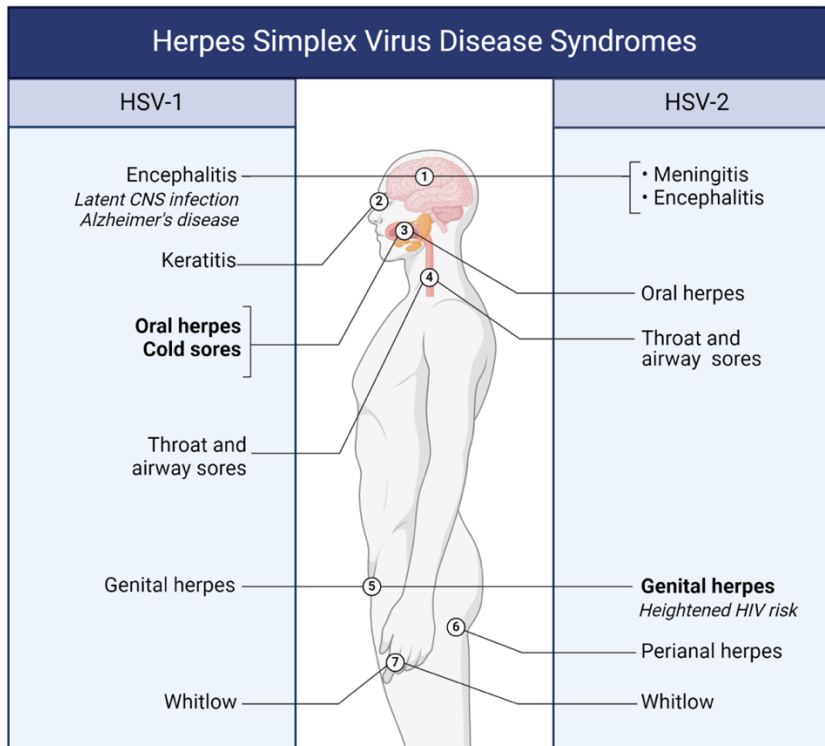


Figure 1.3: Diseases caused by herpes simplex viruses 1 and 2.

Figure adapted from a Biorender pre-existing template, with information added from (7, 11, 12, 14). Conditions in bold are classically considered characteristic of each virus at its main infection route. Conditions in italics are long-term risks of latent infection. Created with Biorender.

Beta and Gammaherpesviruses of Importance

Beta and gammaherpesviruses are of comparable clinical importance, and either shared or distinct findings around lytic infection and latency can broadly inform herpesvirus research. Like the alphaherpesviruses, long-term health impacts from latent infection are still being identified.

Human cytomegalovirus (HCMV) is a betaherpesvirus that asymptotically infects 40-99% of the world's population (27–29). HCMV is the leading infectious cause

of birth defects in the United States, posing the greatest risk to immunocompromised individuals, including organ transplant recipients (29, 30). Hematopoietic and myeloid cells are the latent reservoir, and reactivation can be triggered by the cells' differentiation (31). In addition to latency and lytic infection, a chronic "smoldering" phenotype with low level lytic replication and viral shedding can occur, specifically in endothelial or epithelial cells (27, 31, 32). The complex interactions with the host and the importance of differentiation state in regulating HCMV latency and reactivation have made its study (both *in vivo* and *in vitro*) difficult (30, 33).

Gammaherpesviruses Epstein-Barr virus (EBV) and Kaposi's sarcoma-associated herpesvirus (KSHV) are the only HHVs known to cause malignancy in humans, sometimes decades after primary infection and latency establishment. EBV contributes to cancers including lymphoma, while KSHV is named for the visible Kaposi's sarcoma lesions associated with HIV/AIDS patients (34, 35). An estimated 90% of the population are infected with EBV, primary infection typically occurring in childhood (36). Primary EBV infection during adolescence, however, is linked with infectious mononucleosis, a prolonged viral syndrome. Epidemiological evidence has mounted for latent EBV infection preceding multiple sclerosis, as well as proposed links between EBV and other autoimmune diseases (37, 38). The global impacts of these human herpesviruses further demonstrate the need to understand lytic and latent infection, working towards the goal of reducing health impacts by preventing or interrupting reactivation.

1.1.3. Treating Lytic and Latent Infection

Antiviral Treatments

In cases where HHV lytic replication is not adequately controlled by the host's immune system, nucleoside analog drugs are often used (24, 39, 40). Acyclovir is a nucleoside analog that must be phosphorylated by a viral protein (thymidine kinase) to become its active form, making it highly specific to virally-infected cells. Other drugs in the same class have the same mechanism of action, such as valacyclovir. This target specificity helps limit side effects experienced by the patient, but there are rare cases of neurotoxicity (41).

Phosphorylated acyclovir inhibits viral DNA replication by causing chain termination, limiting further viral replication. However, HSV-1 strains resistant to acyclovir activity occur, more so in immunocompromised patients with chronic lytic replication (42–47). Acyclovir resistance is also more frequent in immune-privileged tissues like the eye, and frequent reactivation and use of the antiviral increases the risk of resistance (46). Acyclovir resistance is achieved through mutation of the viral thymidine kinase (43, 46). The other main antivirals against herpesviruses are helicase-primase inhibitors, which also restrict viral DNA synthesis. Other processes can be targeted, such as cell attachment, cell entry, RNA translation and viral assembly, and novel approaches are required to bypass drug resistance and side-effects experienced by some patients (47, 48).

Preventing Reactivation

It is certainly beneficial to interrupt lytic replication as soon as possible, but particularly in the case of alphaherpesvirus neuronal infection, in which damage can be done before administration of antivirals. Unfortunately, targeting lytic replication does not resolve the underlying latent infection. The “shock and kill” approach is often brought up in discussions of eliminating latent viral reservoirs, particularly for human immunodeficiency virus (HIV) patients (49–51). Shock and kill consists of inducing reactivation of the latent reservoir, allowing the immune system to detect reactivating virus and attack those cells. The aim is to eliminate the latent reservoir altogether, avoiding future reactivation events. However, reactivating a latent virus and wiping out its reservoir is not appropriate for alphaherpesviruses, as the infected neurons need to be preserved to retain their function. A possible approach for alphaherpesviruses is “block and lock”, targeting epigenetic regulation of the viral genome to force maintenance of latency (50–52). During reactivation events, newly produced virus can infect nearby neurons and establish new reservoirs of latency, including in the central nervous system (CNS) (15, 53, 54). A treatment preventing future reactivation and administered during lytic infection, would be a valuable preventative tool. Drug resistance and the risks of repeated reactivation motivate the aim to understand regulation of lytic and latent infection.

1.2. HSV-1 Replication and Chromatinization

1.2.1 The HSV-1 Lytic Replication Cycle

HSV-1 is an enveloped DNA virus with a complex 152 kbp genome encoding 80 proteins. The HSV-1 genome also encodes regulatory microRNAs (miRNAs) and a long non-coding RNA (lncRNA) under the control of a neuron-specific promoter, the latency-associated transcript (LAT). During lytic infection of epithelial cells at the oral mucosa, lytic replication (mediated by both viral and host machinery) produces progeny virus. The order of events during lytic infection is represented in Figure 1.4, and each step in the figure is referred to by its label number (#).

Cell entry results in the viral capsid entering the cytoplasm and transportation to the cell nucleus by cellular microtubule machinery (#1) (55). When new virions are being assembled, viral DNA is packaged inside the capsid under high pressure driven by an ATP-dependent portal motor, and stored as repulsive energy between the negatively charged DNA residues (56–59). Once the capsid has bound the nuclear pore complex, DNA release through the capsid's portal vertex is propelled by this stored pressure, and host RNA polymerase helps pull the rest of the DNA fully into the nucleus (#2a) (59–61). Viral DNA extruded into the nucleus is then thought to circularize (#3) (55, 62, 63). This process occurs in both neuronal and non-neuronal cells, with viral DNA existing as an episome in the cell nucleus, amongst the cellular chromatin.

At the same time as viral capsid release, tegument proteins are released into the cytoplasm (#1). A matrix of tegument proteins surrounds the capsid, all of which is contained by the envelope. Tegument proteins have a variety of functions shaping the optimal cell environment for lytic gene transcription. One essential tegument protein is

the transcriptional activator VP16, which translocates to the nucleus, binds the viral genome (#2b and #3) and cooperates with cellular transcription factors (HCF and Oct-1) and RNA polymerase II to activate transcription of the immediate early (IE or α) genes (#4) (64–66). This is the start of an ordered cascade of gene expression: IE proteins promote transcription of early (β) genes (#5); early proteins carry out viral DNA replication (#6); late (γ) genes are transcribed following DNA replication (#7); late proteins are assembled with newly replicated viral DNA (#8) and this capsid undergoes egress out of the nucleus (#9). During egress, the tegument matures and the capsid is enveloped by either a trans-Golgi network-derived or plasma membrane-derived vesicle (#10) (67). This membrane that later fuses with the cell membrane to release the mature progeny virus (#11).

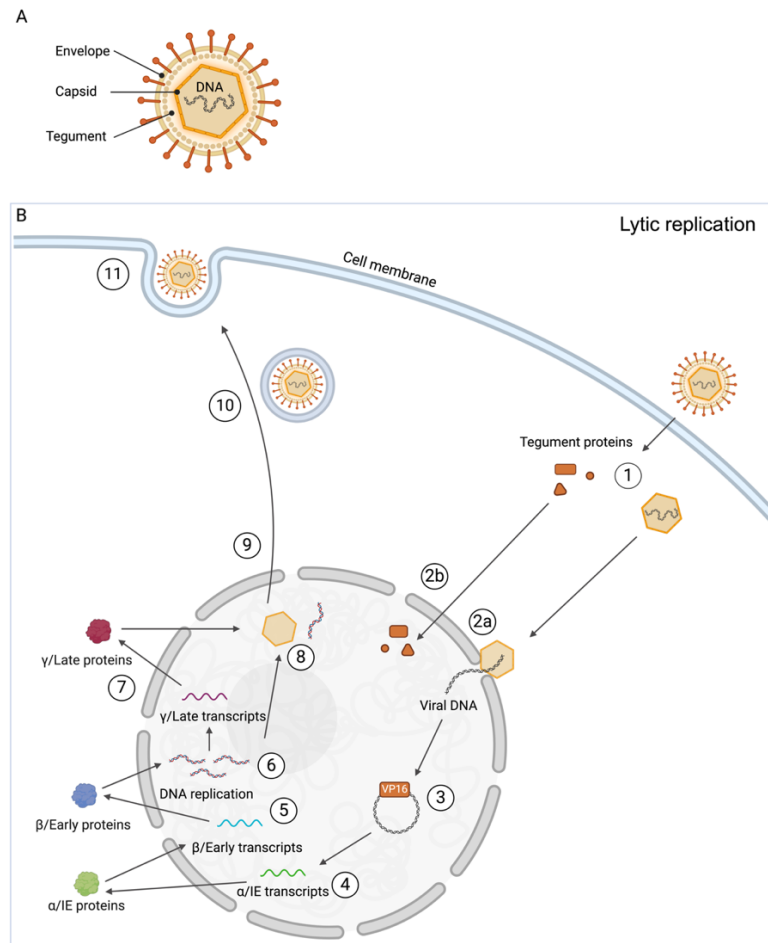


Figure 1.4 An overview of the lytic replication cycle of Herpes simplex virus (HSV-1).

Labels numbers on the image are referred to with #. **A.** The virion is composed of a viral capsid containing the DNA genome, surrounded by the tegument (a proteinaceous matrix), then the viral envelope derived from cell membranes. **B.** Following cell entry, the viral capsid and tegument proteins are each released into the cytoplasm (#1). The capsid, containing the naked DNA genome, is transported to the nucleus and docks at a nuclear pore (#2a). The viral genome is extruded into the nucleus, where it forms a circular episome. Tegument protein VP16 also translocates to the nucleus (#2b) and transactivates immediate early (IE) lytic gene transcription (#3). The sequential cascade of IE genes (#4), early genes (#5), DNA replication (#6) and then late genes occurs (#7), with newly assembled virions (#8) exiting the nucleus (#9) to continue egress (#10) from the cell and maturation. (63) Created with Biorender.

1.2.2. Modifying the Host Cell

Upon cell entry, viral proteins begin regulating the host cell environment in support of virus replication. This section describes the events in a non-neuronal cell, with the caveat that neuronal morphology leads to some differences. One such difference is the slower transport of VP16 along the axon relative to the viral capsid (68, 69). Arriving with the potent transcriptional activator VP16, tegument protein virus host shutoff (VHS) shuts down host cell protein synthesis with endoribonuclease digestion of host mRNA.

Once present in the nucleus, naked HSV-1 DNA rapidly associates with cell histone proteins and assembles into nucleosomes (61, 63, 70–72). The viral genome begins forming a replication compartment within the nucleus, reorganizing the cell's nuclear architecture (71–74). In a lytically infected, permissive cell, the majority of immediate early (IE) gene expression occurs 2-4 hours and early gene expression 6-12 hours post-infection. DNA synthesis occurs in a broad window from 3-12 hours post-infection, and mature progeny virus accumulates from 6 to 18 hours post-infection (HPI) (63, 75, 76).

Within the nucleus, immediate early gene product ICP0 (a viral E3 ubiquitin ligase) targets intrinsic defenses for degradation, impairing the cell's first line of defense. These ICP0 targets include promyelocytic leukaemia protein (PML) of PML nuclear bodies (PML-NBs), also referred to as nuclear domain 10 (ND10)-NBs, which are subnuclear hubs for many proteins and shown to physically entrap incoming HSV-1 genomes in the absence of ICP0 (77–81). Some PML-associated proteins are known to restrict lytic infection including speckled protein 100 (Sp100), death domain-associated protein (DAXX) and Alpha Thalassemia/Mental Retardation Syndrome X-Linked protein (ATRX) (82–89). All proviral functions for ICP0 targets have not been described, but its effect on the host proteome is robust (81).

As the viral gene cascade begins, host proteins are recruited to facilitate lytic gene expression. Notably, many ICP0 targets are histone chaperones or histone modifiers. Proteomics approaches also show that in the first hours of infection, many interacting proteins carry out chromatin formation and remodeling (90, 91). Chromatin structure confers transcriptional regulation, a valuable resource to both the cell and the virus.

1.2.3. Lytic HSV-1 Chromatin

Establishing the Existence Of Lytic HSV-1 Chromatin

Lytic HSV-1 chromatin was initially studied using micrococcal nuclease (MNase) digestion to determine DNA fragment size. DNA associated with histones is protected from digestion at the site of occupancy, resulting in DNA fragments from protected DNA, and digestion of non-nucleosomal DNA. In 1980, Leinbach and Summers used this approach to determine that very little parental (input) viral DNA from Vero cells was nucleosomal (92). In 1990, Lentine and Bachenheimer published findings in agreement with the non-nucleosomal structure (93).

However, subsequent studies using partial or serial MNase digestion argued for some nucleosome occupancy. Kent et al. concluded that nucleosomes are present and carry histone post-translational modifications (PTMs) associated with active gene transcription (94). It is worth noting, however, that this study used a neuroblastoma cell line that isn't particularly relevant to *in vivo* lytic infection. Chromatin immunoprecipitation (ChIP) and quantitative PCR (qPCR) was later used to demonstrate association with histone proteins, supporting the notion of viral chromatin formation (94, 95). Cliffe et al. found H3

levels on HSV-1 chromatin comparable to host chromatin in HeLa cells (96), conflicting with experiments suggesting low nucleosome occupancy. HeLa cells are not an ideal model cell for HSV-1 infection, but are of epithelial origin and are thus somewhat relevant to the cell types infected with HSV-1 *in vivo* (96).

The addition of CHIP-qPCR also allowed identification of specific histone PTMs at lytic promoters, including acetylation at histone H3 lysine 9 (H3K9) and histone H3 lysine 14 (H3K14) (94) and histone H3 lysine 4 (H3K4) tri-methylation (in HeLa cells) (97). Additional studies identified the chromatin-modifying host proteins regulating lytic gene expression, such as H3K4 methyltransferase Set1 (97–99). For some host factors, knock-downs showed minimal or redundant contributions to transcriptional activation (100). For others, individual knockdown has revealed roles in epigenetic modulation of the viral genome, such as the pro-viral activity of H3K9 demethylase LSD1 towards lytic gene transcription (52, 101–103). The relative importance of these factors can also vary by cell line (104, 105).

Using fractionation in combination with serial MNase digestion and short-read deep sequencing, infected Vero cell DNA was characterized by Hu et al. (106). Insolubility corresponds to less accessible chromatin, and solubility to accessibility. HSV-1 DNA in both populations showed a broadly accessible chromatin structure, regardless of gene class, indicating that lytic HSV-1 DNA is not modulated at the individual gene level (106). Another 2019 study using a next gen sequencing (NGS) approach, chromatin immunoprecipitation-sequencing (ChIP-seq) revealed immediate early protein ICP4 binding to accessible regions of the viral genome (107), further supporting the role of broad chromatin accessibility in regulating viral gene expression.

Human foreskin fibroblasts (HFFs), a primary cell type, are now frequently used to study lytic HSV-1 infection. The field currently accepts the existence of lytic HSV-1

chromatin (although lower nucleosome occupancy than host chromatin), and roles for histone tail PTMs in regulating lytic gene expression (99, 108).

Histone Chaperones and Variants

Histone variants on host chromatin, which carry out distinct functions, are exchanged into the nucleosome by histone chaperone proteins (109–113). Histone variants are also observed on viral chromatin and contribute to the methods of transcriptional regulation. PML-NBs act as a scaffold for various histone chaperones and are targeted by ICP0 for degradation as discussed earlier. PML-NBs promote H3.3 loading (via chaperone HIRA), as well as deposition of repressive post translational modifications (PTMs) di- and trimethyl H3.3K9 onto the viral genome via chaperones ATRX and DAXX (77, 79, 80, 85, 114). The result of PML-NB association is a transcriptionally repressed viral genome (115). H3.3 and H3.1 are differentially mobilized in the nucleus during lytic infection, H3.3 is first mobilized away from host chromatin and loaded onto incoming viral genomes (116). H3.1 is mobilized somewhat later and incorporated into newly synthesized viral genomes. This behavior mirrors cellular chromatin, where H3.1 loading is primarily coupled with DNA replication (116, 117).

It is also worth noting that histone variants have functions in cell DNA damage response and DNA repair processes, such as γ H2AX marking double-stranded breaks (DSBs) for repair (118). Proteomic studies have shown associations of viral DNA with DNA damage-related complexes, both pro- and anti-viral roles identified for some DNA repair factors (74, 91, 119–121).

1.2.4 Repressive Histone Modifications on HSV-1 Chromatin

Latent HSV-1 Chromatin

In contrast to lytic infection of fibroblasts, latent infection of neurons requires transcriptional silencing of lytic genes. A long-non-coding RNA (lncRNA) transcript, the latency-associated transcript (LAT), is instead expressed under a neuron-specific promoter *in vivo* and *in vitro* (122–124). The LAT is not required for latent infection, but its promoter features pro-transcriptional histone PTMs that contrast with the repressive modifications on lytic promoters (124–129). The LAT promotes the formation of the repressive histone PTMs H3K9me_{2/3} and H3K27me₃ during neuronal infection (124, 126, 128, 130–132). Viral chromatin from latently-infected mouse brainstems is relatively resistant to micrococcal nuclease digestion, indicating a compact latent chromatin structure (133). Following *in vivo* murine infection, latently infected trigeminal ganglia (TG) can be harvested and processed to analyze latent viral chromatin. Chromatin immunoprecipitation (ChIP) performed on *in vivo* latently infected mouse ganglia indicated that the repressive histone modifications H3K9me_{2/3} and H3K27me₃ were enriched on latent HSV-1 chromatin (129, 133). However, H3K27me₃ is not detectable on the viral genome until latency (10-14 days post-infection) *in vivo* and the chromatin structure leading up to this point (during latency establishment) has not been described (129).

On the host genome, H3K27me₃ is characteristic of facultative heterochromatin (fHC) and mediated by Polycomb repressive complex 2 (PRC2) (134). H3K9me₂ and H3K9me₃ are also found on heterochromatin, in a pattern mutually exclusive with H3K27me₃ occupancy. The balance of H3K27me₃ to H3K9me₃ is regulated by PML-NB-associated H3.3 chaperones ATRX/DAXX and HIRA (135). Knowledge of host

PRC2 activity can inform hypotheses around *de novo* H3K27me3 formation on the HSV-1 genome, keeping in mind that the process is not necessarily the same as for host chromatin.

Facultative heterochromatin has the capacity to be remodeled and transcriptional repression lifted, unlike the more permanently silenced constitutive heterochromatin (136). Functionally, this type of heterochromatin permits quiescence while retaining the capacity to resume lytic gene expression. Additionally, the histone remodelers that regulate reactivation from latency corroborate this reversible silencing; H3K9 and H3K27 demethylase activity (LSD1, JMJD2, and JMJD3, UTX respectively) is required for reactivation from latency (52, 101, 137, 138). Both H3K9 and H3K27 histone methylations being linked to latent HSV-1 chromatin point to heterogeneity in the repressive chromatin structures formed (132).

Proposed Lytic Heterochromatin Formation

ChIP-based studies of lytic HSV-1 chromatin in fibroblasts have informed a model in which lytic HSV-1 DNA is rapidly subjected to H3K9me_{2/3} and H3K27me₃ formation, which is then removed to allow lytic gene expression (99, 139). On host chromatin, H3K27 methylation is sequential, the end point being H3K27me₃, and each of these states is carried out by the PRC2 complex. Based on knowledge of host chromatin, H3K27me₃ dynamics are slow compared to lytic infection (140). The rationale behind challenging this model is discussed further in chapter 2, but we set out to test this hypothesis given the inconsistency with host H3K27 methylation dynamics. This was also informed by the knowledge that H3K27me₃ is not detectable until latency establishment *in vivo* (129), suggesting that there is another mechanism carrying out silencing prior to this modification's deposition. Whether or not H3K27me₃ formation

occurs on lytic HSV-1 chromatin is important to conclusively determine. If H3K27me3 is rapidly formed on lytic genomes in non-neuronal cells, cell type-specific factors can be identified by comparing the mechanism with our knowledge of latent chromatin.

1.2.5. Heterogeneous Lytic Infection

Cell to Cell Heterogeneity

Heterogeneity is a fundamental aspect of HSV-1 infection. This is reflected in the range of reactivation frequencies experienced by HSV-1 infected patients, as well as experimental findings of *in vivo* and *in vitro* latency (88, 131, 141, 142). Heterogeneity during lytic infection has been elucidated in the last few years with recent technical advances. One side of this heterogeneity is at the cell level.

Viruses with fluorescent reporters for lytic gene transcripts have constituted one approach to lytic heterogeneity, used to identify variables such as the number of viral genomes replicating in a nucleus correlating to lytic gene expression (143). Drayman et al. used single cell RNA sequencing (scRNAseq) and time-lapse microscopy to show high variability in lytic gene transcription within a population of infected fibroblasts (144). A fluorescent reporter virus for ICP4 expression allowed the categorization of cells by successful or unsuccessful (abortive) infections and found only 55% of cells expressing ICP4 (within which ICP4 expression levels varied). Lytic transcription was also impacted by cell cycle stage, among other variables (144).

Antiviral gene expression programs have also been defined in sub-populations of cells by scRNA-seq, allowing the identification of restrictive factor NRF2 (145). Cohen et al. cultured non-neuronal cells that survived lytic HSV-1 infection and found they held the viral genomes in a quiescent or abortive state with the potential to reactivate lytic gene

expression (146). This study determined that abortive infection is common during non-neuronal infection, and notable variability by cell line in the proportion of cells abortively infected (146). These analyses underlined the extent of cell-to-cell variability during lytic infection that bulk methods could obscure.

Individual Genome Heterogeneity

Another aspect of lytic HSV-1 heterogeneity is variation between individual viral genomes, even within a single nucleus. Fluorescent reporters for lytic gene expression have also proven useful for observing replication compartment (RC) dynamics. RCs are essentially factories set up by a viral genome, which begin with lytic gene transcription and expand as gene expression progresses and DNA replication takes place (147). RCs are not encased by a membrane, forming within the nuclear environment. After arriving in the nucleus, the HSV-1 genome decompacts and the RC grows in size within the nucleus. One RC descends from one genome, first visualized using pseudorabiesvirus (PRV), a herpesvirus livestock pathogen (71). RCs have been shown to coalesce as infection progresses, shown to facilitate homologous recombination between viral genomes by DNA fluorescence in situ hybridization (FISH) (148). IE gene product ICP4 is proposed to mediate phase separation of the compartment (149).

Bioorthogonally-labeled HSV-1 DNA, a product of propagating virus in the presence of a nucleoside analog (EdC, EdA or EdU), has allowed observation of the RCs forming from input genomes and characterization of the spatial and temporal dynamics at individual genomes (72). The molecule's incorporation allows covalent attachment of molecules to the DNA by click chemistry. This has proven useful for DNA pulldown and bulk proteomics experiments, identifying host factors interacting with viral RCs (91, 150, 151). The method also allows individual genome imaging by attachment

of a fluorophore to the DNA, an alternative to DNA FISH with the additional benefit of specifically identifying input genomes (and not newly replicated genomes) (72).

Replicating HSV-1 genomes in pigmented retinal epithelial cells (RPEs) are heterogeneous, with RCs of varying sizes and diffusing fluorophore signal as the compartment grows (72). Our collaborator Dr Chris Boutell has used bioorthogonal labeling to characterize input genome association with PML-nuclear bodies, detectable within 30 minutes of infection in fibroblasts (79). Interestingly, a low multiplicity of infection (MOI) with an ICP0 mutant virus (avoiding PML-NB degradation) results in entrapment of the HSV-1 genomes by PML-NBs, but higher MOI infection in which the PML-NBs are saturated allows free HSV-1 genomes to be unimpaired by the PML-NBs repressive functions (79). The amount of infectious virus should thus be considered when studying viral heterogeneity and interaction with intrinsic immune mechanisms in the nucleus.

These studies emphasize that within a nucleus, one HSV-1 genome may successfully initiate gene transcription and decompact, while another might fail to initiate robust gene expression and remain compacted. The valuable insights from these techniques to visualizing viral DNA underline the continued need for single-genome resolution methods that capture heterogeneity during HSV-1 infection.

1.2. Mammalian Polycomb Silencing

1.3.1. Two Branches of Gene Silencing

Polycomb group protein (PcG)-mediated heterochromatin is laid down and maintained by the activities of two major protein-complexes: the Polycomb repressive complex 1 (PRC1) and Polycomb repressive complex 2 (PRC2). The activity of these complexes will be referred to as “Polycomb silencing”. PRC2 was long considered the initial depositor of fHC, as it contains H3K27me ‘writer’ activity, carrying out mono-, di- or trimethylation (H3K27me1, H3K27me2, or H3K27me3) (152–154). Because H3K27me3 can then be recognized by the PRC1 complex, the formation of PcG-mediated silencing was thought to occur hierarchically with PRC2-mediated H3K27me3 followed by the recruitment of PRC1 to result in H2A lysine 119 mono-ubiquitination (H2AK119ub1) and/or chromatin compaction (155).

Our understanding of mammalian polycomb repression has since evolved beyond this model and the order of events in polycomb silencing seems far from straightforward (156), as represented in Figure 1.5. The current paradigm involves variant PRC1 (vPRC1) carrying out the majority H2AK119 ubiquitination, with which PRC2 can then be recruited and perform H3K27 methylation. This is reversed from the order previously described, and also reflects the different roles for distinct sub-complexes of both PRC1 and PRC2. Mammalian polycomb silencing likely occurs through a variety of mechanisms specific to cellular context and results in potentially divergent association with protein complexes and mechanisms to restrict gene expression. It is likely that herpesviruses have evolved to take advantage of host processes of heterochromatin formation.

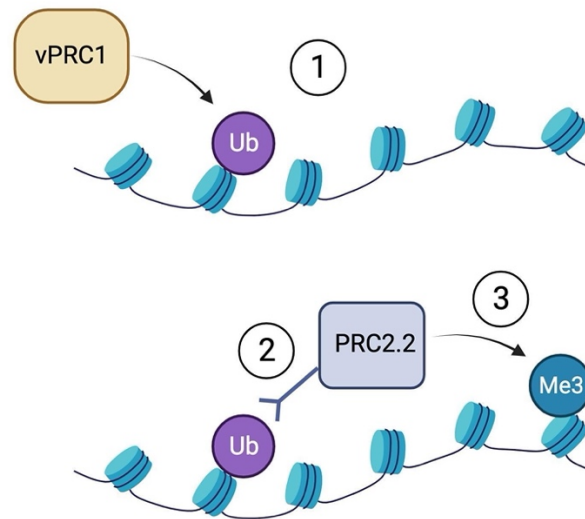


Figure 1.5: An overview of the events during Polycomb-mediated facultative heterochromatin formation in pluripotent cells.

H2AK119 mono-ubiquitination by variant PRC1 (vPRC1) occurs first. PRC2.2 can recognize the Ub modification via associated accessory proteins, allowing the H3K27 methylation to H3K27me3. Created with Biorender.

1.3.2. H3K27 Methylation by PRC2

PRC2 Recruitment for De novo Heterochromatin Formation

PRC2 contains a core of three components: EZH1/2, SUZ12 and EED (see Figure 1.6). EZH1/2 is catalytically active, but the full trimeric core is required for *in vitro* H3K27 methylation activity (136, 152, 157). All three methylation states of H3K27 (mono, di and tri-methylation) are carried out by PRC2. The formation and function of K27 methylation has been most extensively studied in mouse embryonic stem cells (mESCs) and human-induced pluripotent stem cells (iPSCs), where H3K27me2 is most abundant of the three, existing across 50–70% of total histone H3, predominantly at intergenic regions (140).

Despite being the most predominant form of H3K27 methylation and a substrate for PRC2, PRC2 levels are undetectable at regions of H3K27me2 (140). H3K27me1 and H3K27me3 are each found on approximately 10–15% of total H3 in mESCs (158, 159).

H3K27me3 is found centered around CpG islands of transcriptionally silent genes, and is the only methylation state to which PRC2 stably binds (140). Hence, these CpG islands can act as nucleation sites for facultative heterochromatin formation and propagation (140).

As summarized in Figure 1.6, the PRC2 core is built upon with accessory proteins, defining two distinct PRC2 variants with mutually exclusive binding patterns: PRC2.1 and PRC2.2 (160). These accessory proteins interact with the main complex, mediating recruitment of the complex to different genomic features. There are also redundant or compensatory mechanisms observed for PRC2.1 and PRC2.2 and inhibition of both complexes is required for the full inhibition of PRC2 activity in pluripotent cells (161). The possible combinations of accessory proteins for a single PRC2 variant reflect the built-in complexity in regulating PRC2 activity.

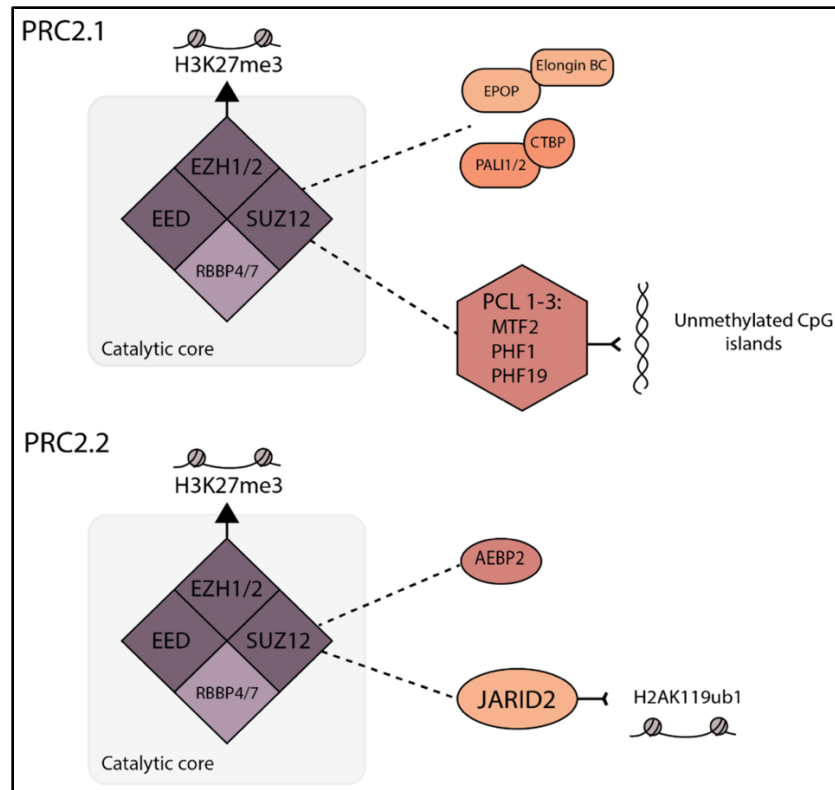


Figure 1.6: The composition of PRC2.1 and PRC2.2 complexes.

Polycomb repressive complex 2 (PRC2) has a catalytic core of EED, EZH1/2 and SUZ12 along with RBBP4/7. PRC2 carries out all three methylation states of H3K27, but H3K27me3 is the only one stably bound by the complex. To form the **PRC2.1** complex, the core can interact with either PALI1/2 and CTBP or EPOP and Elongin BC. One pair excludes the other from joining the complex. SUZ12 in PRC2.1 also interacts with one of three PCL proteins, but this interaction does not compete for the aforementioned interacting pairs. PCL proteins enable binding to unmethylated CpG islands. **PRC2.2** forms by SUZ12 in the same catalytic core interacting with JARID2 and AEBP2. Unlike PRC2.1, JARID2 enables PRC2.2 recruitment to sites of H2AK119ub1. *Figure and text adapted from Dochnal, Francois and Cliffe, 2021 (1).*

Transcriptional Regulation by Accessory Proteins

PRC2.2 (see Figure 1.6) accessory protein JARID2 interacts with SUZ12 with the help of AEBP2, recognizing the other Polycomb-mediated modification H2AK119ub. This interaction allows for cross-talk between the PRC1 and PRC2.2 pathways. Different accessory proteins may also be present in distinct cell types. For example, full length JARID2 is down-regulated with differentiation, although a cleaved protein lacking the PRC2-interacting domain (DeIN- JARID2) is present, at least in differentiated keratinocytes. The shorter form of JARID2 negatively regulates PRC2 function and is proposed to release PRC2-mediated repression of differentiation genes (162). This serves as an example of the function of a Polycomb protein changing in the context of differentiation, one facet of the complexities of Polycomb repression that must be considered in heterochromatin formation.

The PRC2.1 complex (see Figure 1.6) includes one of three PCL proteins (PCL1/2/3), also known as PHF1, MTF2 and PHF19, respectively, which enable PRC2.1 binding to unmethylated CpG islands (160). SUZ12 also interacts with either PALI1/2 and CTBP, or EPOP and Elongin BC, and these pairs exclude the other from binding. PALI1/2 promote methyltransferase activity alongside transcriptional repressor CTBP (163), while EPOP and Elongin has been shown to allow low-level expression of PRC2-repressed genes (134, 164, 165).

Consequences of Distinct PRC2 Complexes

It should also be noted that studies of PRC2.1/2.2 function on cellular chromatin have been carried out with some residual epigenetic template. In addition, it is likely that there are differences in the resulting epigenetic structures when fHC is laid down by PRC2.1

versus PRC2.2 that could result in different mechanisms for the re-expression of genes. This is supported by a recent study that has uncovered subtle differences in PRC2.1 versus PRC2.2 by inducing mutations in SUZ12 to shift preference towards forming one complex over the other. This revealed that PRC2 occupancy was significantly higher for PRC2.1 target regions than PRC2.2 bound regions, suggesting that differential accessory proteins bound to either PRC2.1 or 2.2 can result in differing PRC2 occupancy levels, at least in human iPSCs (166). Whether this has long-term implications for gene expression and chromatin compaction is not known.

As gene expression patterns change during differentiation, there is evidence that PRC2.2 is important for *de novo* silencing during this transitional process, whereas MTF2-containing PRC2.1 was required to maintain high amounts of H3K27me3 at already repressed CpG dense promoters (167). These results do not conflict with findings of redundancy between PRC2.1 and PRC2.2 in mESCs (134, 168), instead suggesting that, during differentiation, their roles shift.

Hence, when considering the mechanisms of PRC2 recruitment and function, it is important to consider changes in Polycomb group expression and activity upon differentiation and in distinct cell types, which is reflected in the differential composition of PRC2 in different cell types. One aspect that varies between pluripotent and differentiated cells is the presence of EZH1 versus EZH2. EZH2 is highly expressed in dividing cells and minimally in differentiated cells (169, 170). EZH1 is widely expressed and believed to be predominant in terminally differentiated cells, specifically in the maintenance of H3K27me3 (171). Studies in mESCs indicate that EZH1/2 use different mechanisms to repress chromatin, with EZH2 largely catalyzing H3K27me2/3 and EZH1 contributing to chromatin compaction (169).

Models of herpesviruses latency and reactivation serve as excellent systems to investigate *de novo* fHC formation in differentiated cells, and also track the potential differential regulation of gene expression from regions of fHC within distinct epigenetic structures.

1.3.3. H2AK119 Ubiquitination by PRC1

PRC1 Recruitment for De Novo Heterochromatin Formation

The composition of PRC1 complexes (see Figure 1.7) appears to be even more diverse than PRC2, falling into two broad categories: canonical (cPRC1) and non-canonical/variant (vPRC1) (172, 173). All PRC1 complexes contain dimerized RING1A or B, which interact with one of six possible PCGF proteins (PCGF1-6). The variability in composition of PRC1 complexes is reflective of their differential effects on chromatin and mechanism to impact gene expression.

cPRC1 complexes contain either PCGF2 (also called MEL18) or PCGF4 (also called BMI1) together with one of five chromobox (CBX2, 4, 6, 7 and 8) proteins (174). The CBX subunit of cPRC1 directly binds H3K27me₃ for recruitment to chromatin; therefore, the activity of cPRC1 is dependent on PRC2 (175–177).

vPRC1 complexes can contain any of the six PCGF proteins but lack CBX proteins, instead containing either RYBP or YAF2 (156, 174, 178). Hence, vPRC1 complexes lack H3K27me₃ binding ability and are recruited to chromatin independently of PRC2 (156, 179). Recruitment of vPRC1 can occur through direct DNA binding activities; for example, KDM2B-containing vPRC1 directs the complex to non-methylated CpG islands (180). vPRC1 can interact with sequence-specific DNA binding proteins such as E2F6, REST and RUNX1 (181). vPRC1 can also be recruited by interaction with

RNA, as appears to be the case for vPRC1 recruitment to the presumptive inactive X-chromosome in mESCs by interaction of the non-coding RNA Xist via hnRNPK.

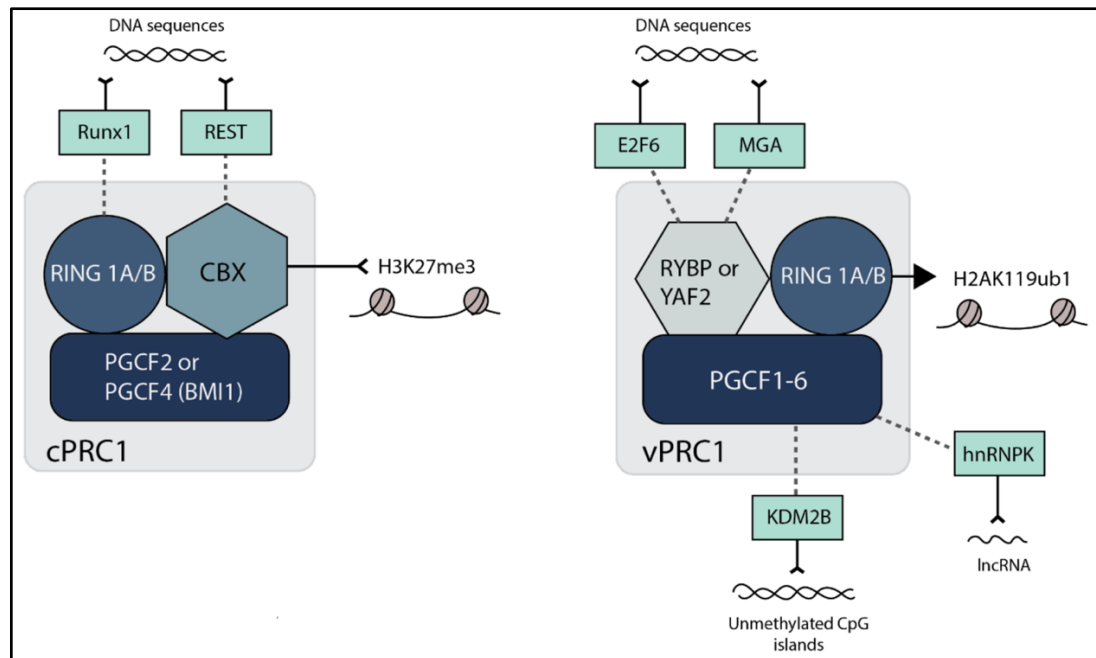


Figure 1.7: The components of canonical and variant PRC1 complexes and interacting transcription factors.

Canonical PRC1 (cPRC1) consists of one of two PGCF proteins (PGCF2 or PGCF4), along with RING1A/B and one of five chromobox (CBX) proteins. Although catalytically active, cPRC1 is thought not to contribute to the majority of H2AK119ub1. CBX proteins directly bind to H3K27me3, so cPRC1 recruitment to chromatin is dependent on PRC2 H3K27 methylation activity. **Variant PRC1 (vPRC1)** contains any of the six PGCF proteins, RING1A/B, and RYBP or YAF2. RYBP/YAF2 do not bind H3K27me3 and vPRC1 recruitment is thus independent of PRC2 activity. RYBP stimulates RING1A/B activity, and vPRC1 writes H2AK119ub1. Transcription factors RUNX1 and REST can interact with cPRC1 via RING1B and CBX7/8, respectively, recruiting the complex to specific target sequences of DNA. E2F6 and MGA can similarly recruit vPRC1 to specific DNA sequences by interaction with RYBP/YAF2, while hnRNPK can do so through interaction with PGCF3/5 and long-noncoding lncRNA. KDM2B can recruit vPRC1 to non-sequence specific, unmethylated CpG islands. *Figure and text adapted from Dochnal, Francois and Cliffe, 2021 (1).*

Implications of Distinct PRC1 Complexes

Although all complexes contain the RING1/2 catalytic subunit, vPRC1 is predominantly responsible for mediating H2AK119ub1, likely because RYBP stimulates PRC1 E3 ubiquitin ligase activity (156, 177, 179, 182). There is evidence, at least in embryonic stem cells, that H2AK119ub1 is required for PRC2 recruitment and the subsequent binding of both vPRC1 and cPRC1 (183, 184). These studies also revealed a direct role for H2AK119ub1 in repression of gene expression, and there is evidence for H2AK119ub1 inhibiting RNA polymerase elongation (185, 186), perhaps by preventing the eviction of H2A/H2B dimers (187).

Whilst vPRC1 is likely responsible for the majority of H2AK119ub1, cPRC1 appears to be responsible for repressing gene expression through chromatin compaction, in addition to mediating long-range chromosomal interactions (188). For regions of chromatin that are bound by either vPRC1 or cPRC1 in ES cells, those bound by cPRC1 exhibit increased transcriptional repression compared to those bound by vPRC1 (189). cPRC1 compaction is driven by the CBX proteins, in particular CBX2, 6 and 8, which contain a highly basic region that can drive chromatin compaction, at least *in vitro* (172). Thus, CBX2, 6 and 8-containing cPRC1 likely prevents gene expression by limiting access to transcriptional machinery. CBX7, which is the most abundant CBX in ES cells, lacks this basic domain and instead may function in transcriptional repression via mediating long-range chromosomal interactions (172, 189, 190). Other CBX proteins can also mediate long-range chromosomal interactions. Notably, CBX2 contains an intrinsically disordered region, which drives the formation of nuclear condensates known as Polycomb group bodies by phase separation (191). Therefore, differential expression of CBX paralogs in different cell types can lead to different

degrees of compaction, the significance of which in herpesvirus latency remains to be resolved.

In mESCs, enzymatic activity of RING1A/1B is required for H2AK119ub1 and the majority of H3K27me3, indicating that at least in stem cells vPRC1-mediated Polycomb repression is the predominant pathway (183, 184). Inhibition of this pathway also results in decreased association of cPRC1 at target genes usually bound by both vPRC1 and cPRC1 (183, 184). However, in these studies, small subsets of genes were found to be associated with H3K27me3 and cPRC1 via PRC2.1-mediated H3K27me3 deposition. There is evidence for a pathway of vPRC1-PRC2.2-mediated fHC formation during early development of neural progenitor cells (NPCs), where the RING1A/B E3 ligase activity was found to be essential for the repression of genes initially silenced during early neuronal development, but PRC1-mediated repression switched over to Ub-independence as stable silencing was maintained (192). This result highlights the importance of considering cell type and differentiation state when exploring mechanisms of Polycomb repression on herpesvirus genomes.

H2AK119ub-mediated Transcriptional Regulation

Beyond the variability in PRC1 complexes, H2AK119ub itself carries out transcriptional regulation. Traditionally considered a repressive histone PTM, recent studies have added interesting aspects to its repertoire. These are summarized in Figure 1.8.

There are a few H2AK119ub reader proteins thought to carry out transcriptional regulation (193). JARID2, an accessory protein to PRC2.2 discussed earlier, enables cross-talk between the two Polycomb silencing pathways (134, 161, 194, 195). It can recruit PRC2 to sites of H2AK119ub in pluripotent cells, facilitating the nucleation of

repressive domains (140, 154, 171, 194, 196). JARID2 has also been shown to interact with non-coding RNAs that are thought to help recruitment of PRC2 (197, 198). RYBP is a component of vPRC1, and promotes RING1B activity through binding H2AK119ub (199, 200).

H2AK119ub reader RSF1 is part of the non-Polycomb RSF complex, which controls nucleosome spacing and deposition (201, 202). The RSF complex is one of many ISWI family complexes, which carry out chromatin remodeling functions (203). RSF1 has been described as an H2AK119ub reader that stabilizes H2AK119ub nucleosome arrays and mediates transcriptional silencing in *Xenopus* embryogenesis (202). Like many chromatin-related proteins, RSF1 has been described in the pathogenesis of certain cancers, interacting with components of DNA repair, mitotic checkpoint, centromeric cohesion, chromosome segregation and arrangement and nucleosome compaction pathways (204).

Despite its reputation as a repressive histone modification, H2AK119ub has been shown to promote transcription through reader ZRF1 (also called DNAJC2). ZRF1 is involved in the response to UV-damage, its recruitment to damage-induced G quadruplex structures stabilizing the DNA (205). Additionally, nucleotide excision repair (NER) following UV damage can be mediated by H2AK119 ubiquitination by RING1B in the UV-RING1B complex (not in a Polycomb complex) (206). ZRF1 can also work with DICER to decondense chromatin at sites of H2AK119ub during global genome NER (GG-NER) (207, 208). In addition to these DNA damage roles, ZRF1 is involved in maintenance of neural progenitor cell identity (209). The protein ID1 blocks ZRF1 activity, but ID1 expression is lost during neuronal differentiation and ZRF1 takes over to activate the required Polycomb genes (209). ZRF1 helps maintain neuronal cell identity and can block PRC1 binding to chromatin (210). Additionally, ZRF1 activates genes

necessary for cardiomyocyte differentiation (211). ZRF1 is thought to act as a tumor suppressor, while contrarily contributing to acute myeloid leukemia (AML) pathogenesis (212, 213), illustrating how an epigenetic regulator can carry out seemingly contradictory roles depending on the cell context. These studies have been carried out by a small number of research groups, representing the understudied nature of ZRF1 as a transcriptional activator at sites of H2AK119 ubiquitination.

A 2024 study demonstrated both activating and repressive mechanisms mediated by H2AK119ub, one in which the modification recruits histone H1 and chromatin compaction (repressive) and one in which the modification inhibits cPRC1 activity and relieves repression (activating) (214). These are notably structural, as opposed to reader mediated, highlighting the importance of chromatin structure and compaction. The histone modification is implicated in some conflicting functions, and factors including differentiation state must be considered when characterizing functional outcomes of H2AK119 ubiquitination.

H2AK119ub-Mediated Transcriptional Regulation

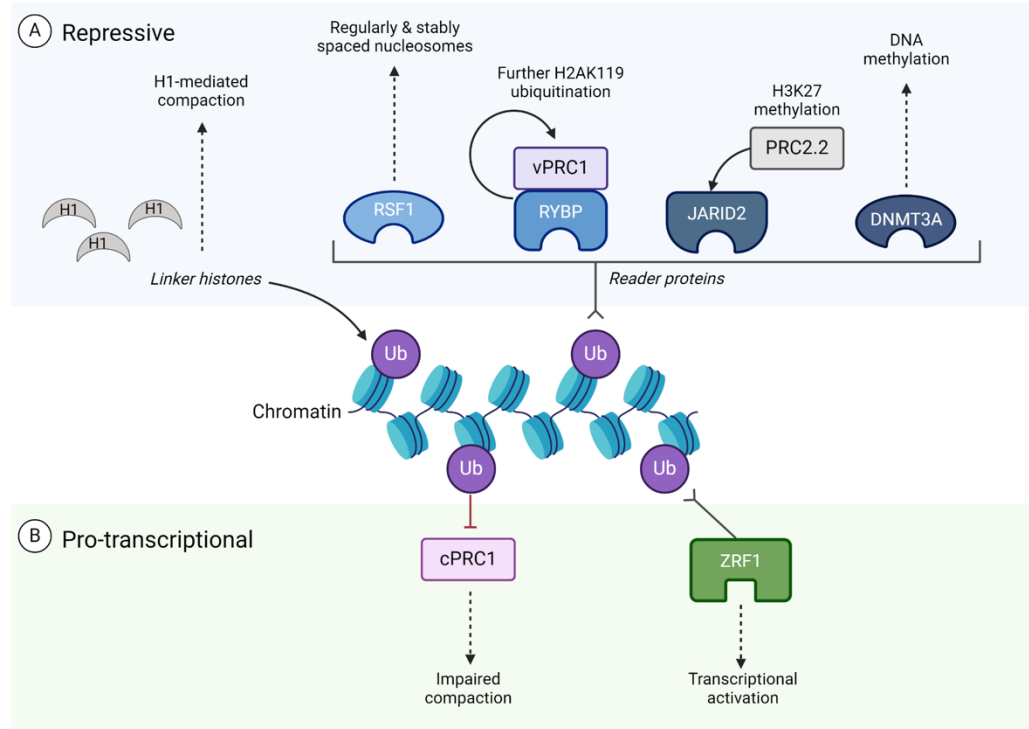


Figure 1.8: Conflicting mechanisms of transcriptional regulation by H2AK119ub on mammalian chromatin.

A. Repressive interacting partners. Linker H1 histones are recruited to H2AK119ub, and mediate compaction of the bound chromatin (214). Reader protein RSF1 (part of the RSF complex) is known to stabilize and ensure regular spacing of nucleosome arrays (202, 204). Variant PRC1 component RYBP can recognize H2AK119ub, promoting further vPRC1 activity on nearby chromatin (199, 200). JARID2, an accessory protein to PRC2.2, can bind H2AK119ub and recruit PRC2.2 to carry out H3K27 methylation (140, 171, 215). This acts as cross-talk between the PRC1 and PRC2 pathways. DNMT3A carries out methylation of the DNA itself, which is also repressive. **B.** H2AK119ub inhibits cPRC1-mediated chromatin compaction, preventing the structural form of transcriptional repression (214). ZRF1 is a reader protein that, in contrast to the above reader proteins, transcriptionally activates sites of H2AK119ub (216). Created with Biorender.

1.4. Investigating Polycomb Silencing in HSV-1 Infection

1.4.1. Starting Questions

In order to understand how HSV-1 achieves the distinct outcomes of lytic or latent infection, it is necessary to contrast the chromatin structures and processes directing this structure in both contexts.

Does PRC2-mediated H3K27 methylation regulate lytic infection of fibroblasts?

Latent HSV-1 chromatin features repressive H3K27me₃, but the contribution of PRC2-mediated H3K27 methylation in lytic infection is unclear. It is possible that H3K27me₃ formation occurs in a lytic context but is reversed to allow lytic gene expression, or that H3K27 methylation is skipped entirely in lytic infection and is exclusive to the establishment of latency in neuronal cells. In either case, clarifying whether this form of silencing occurs during lytic infection will inform our understanding of the cell type-specific contexts shaping viral chromatin.

Is PRC1-mediated H2AK119 ubiquitination present on the latent genome?

PRC1-mediated H2AK119 ubiquitination is thought to precede the majority of H3K27me₃ formation on mammalian chromatin (Figure 1.5). In *in vivo* latency models, H3K27me₃ has not been detected on the HSV-1 genome *in vivo* until 10-14 days post-infection (129). How lytic gene silencing is achieved prior to this point is unclear, and the other branch of Polycomb silencing (H2AK119ub) could initiate this silencing. We aim to

determine whether H2AK119ub is present on the latent genome *in vivo*, alongside H3K27me3 known to be present, thereby updating our understanding of latent HSV-1 chromatin.

Does PRC1-mediated H2AK119 ubiquitination regulate lytic infection?

Whether PRC1-mediated H2AK119ub is targeted to the incoming lytic genome as a mechanism of silencing is undetermined. In light of recent studies exploring the complexity and contrasting roles for PRC1 (214, 216–219), and the evidence for PRC1-mediated H2AK119ub formation on other herpesviruses (220–222), it is necessary to determine whether this histone modification is deposited on the lytic HSV-1 genome. Whether PRC1 regulation of HSV-1 occurs in lytic and/or latent contexts, and which host proteins mediate this modification, this branch of Polycomb silencing remains unexplored for HSV-1 lytic infection.

How does de novo heterochromatin formation occur in a differentiated cell?

Aside from the importance of understanding HSV-1 epigenetic regulation towards improving disease outcomes, these processes can offer insights into cell biology. HSV-1 infection provides a unique opportunity to deliver DNA absent of a pre-existing epigenetic template to the cell nucleus, allowing the observation of *de novo* heterochromatin formation in a terminally differentiated cell. As described above, Polycomb silencing has been studied extensively in the context of pluripotency and differentiation, given its importance in regulating developmental genes. The complexities being revealed in Polycomb-mediated heterochromatin formation, including how the

complexes' roles shift throughout differentiation, highlight the need to study the process in a differentiated cell. Any findings in this context could provide insights into an otherwise difficult to observe process.

1.4.2. Technical Goals

Alongside answering the academic questions outlined above, a major goal of this project is to tackle some of the technical limitations inherent to HSV-1 chromatin research.

Histone antibody specificity

The vast number of possible histone tail PTMs, and combinations thereof, highlights the potential for non-target binding by histone antibodies. Recent efforts to determine antibody specificity include peptide microarrays assessing an antibody's binding strength to a series of synthetically-produced histone peptides (223–225). Epigenetic assays often depend on use of an antibody that recognizes the histone or histone modification of interest, and this holds true for the characterization of HSV-1 chromatin.

We set out to use histone antibodies validated for their binding specificity in these studies and highlight the importance of considering antibody specificity in epigenetic assays. Our collaborators in the laboratory of Dr Scott Rothbart (Van Andel Institute) were willing to assess the binding specificity of our histone antibodies. Through this collaboration we were able to interpret the results of epigenetic assays with increased confidence.

Heterogeneity of HSV-1 infection

The use of nucleoside analogs to label HSV-1 DNA has already provided valuable insights into heterogeneous lytic infection, as described earlier. Our collaborator Dr Chris Boutell provided us with experimental details and labeled virus stock (79, 80), allowing us to optimize our own virus labeling and click chemistry protocols. This use of this technique in the context of neuronal infection was published by previous lab member Dr Jon Suzich (88).

A goal of this project was the establishment of an assay using EdC-labeled HSV-1, aiming to image individual lytic viral genomes and quantify co-localization with histone modifications of interest. This assay would be used to characterize the histone modifications associated with viral DNA at different times post-infection of fibroblasts. This assay and the quantitative methods we developed are introduced in Chapter 2.

Bulk chromatin assay resolution

Epigenetic assays using antibodies against histone modifications are a staple method for profiling HSV-1 chromatin. Chromatin immunoprecipitation (ChIP) with quantitative PCR (qPCR) is one such technique, and has been essential for many studies of HSV-1 and other herpesviruses' chromatin (65, 96, 129, 226). This approach inherently fails to capture heterogeneity amongst viral genomes, instead providing an average of a bulk population of viral genomes amongst a bulk population of infected cells. We were also aware that qPCR amplifies regions of the genome specified by the chosen oligonucleotide primers, and it is possible to unintentionally miss regions enriched for the histone modification of interest.

We chose to assess bulk chromatin in parallel with the aforementioned imaging assay, as it would provide a snapshot of the chromatin across the whole length of the viral genome. We also decided to perform bulk chromatin assays with histone antibodies validated for binding specificity, improving on one technical limitation of the assay. We set out to profile lytic HSV-1 chromatin using the more recently developed technique of CUT&RUN (Cleavage Under Target & Release Under Nuclease). CUT&RUN requires less input material than ChIP, and the antibody binding to chromatin occurs inside the native cell environment without fixation (227, 228). This would, in theory, yield data from a more native chromatin environment than a formaldehyde-fixed ChIP sample. Importantly, we needed data analysis capabilities for the sequencing data from CUT&RUN. We set out to acquire these computational skills and develop an analysis pipeline applicable to this and other CUT&RUN experiments.

1.4.3. Statement of Purpose

Primary Objectives

The purpose of this dissertation is to characterize and determine the functional role(s) of Polycomb-mediated silencing of viral chromatin on lytic gene transcription. This work follows the two branches of mammalian Polycomb silencing and is informed by the body of knowledge surrounding its roles regulating host chromatin and herpesvirus genomes.

The **hypotheses** we are testing are:

1. Polycomb silencing restricts HSV-1 gene expression through deposition of histone post-translational modifications during lytic infection of fibroblasts.
 - a. PRC2-mediated H3K27 methylation.
 - b. PRC1-mediated H2AK119ub ubiquitination.
2. PRC1-mediated H2AK119ub is present on the latent HSV-1 genome.

Technical Objectives

The secondary purpose of this research is to develop novel tools for improved resolution of HSV-1 chromatin. The technical goals of this are to:

1. Demonstrate the need for histone antibody binding specificity validation when profiling HSV-1 chromatin.
2. Observe heterogeneous viral chromatin structures amongst lytic HSV-1 genomes with a novel imaging assay.
3. Use CUT&RUN to profile heterochromatin-associated histone modifications across the length of the lytic HSV-1 genome.

Chapter 2: PRC2-mediated Regulation of Lytic Infection Through Repressive H3K27 Di-methylation

This chapter is a direct adaptation of the following publication:

Francois Alison K., Rohani Ali, Loftus Matt, Dochnal Sara, Hrit Joel, McFarlane Steven, Whitford Abigail, Lewis Anna, Krakowiak Patryk, Boutell Chris, Rothbart Scott B., Kashatus David, Cliffe Anna R. 2024. Single-genome analysis reveals a heterogeneous association of the herpes simplex virus genome with H3K27me2 and the reader PHF20L1 following infection of human fibroblasts.

MBio 0:e03278–23.

2.1. Abstract

The fate of herpesvirus genomes following entry into different cell types is thought to regulate the outcome of infection. For the Herpes simplex virus 1 (HSV-1), latent infection of neurons is characterized by association with repressive heterochromatin marked with Polycomb silencing-associated lysine 27 methylation on histone H3 (H3K27me). However, whether H3K27 methylation plays a role in repressing lytic gene expression in non-neuronal cells is unclear. To address this gap in knowledge, and with consideration that the fate of the viral genome and outcome of HSV-1 infection could be heterogeneous, we developed an assay to quantify the abundance of histone modifications within single viral genome foci of infected fibroblasts. Using this approach, combined with bulk epigenetic techniques, we were unable to detect any role for H3K27me3 during HSV-1 lytic infection of fibroblasts. By contrast, we could detect the lesser studied H3K27me2 on a subpopulation of viral genomes, which was consistent with a role for H3K27 demethylases in promoting lytic gene expression. In addition, viral genomes co-localized with the H3K27me2 reader protein PHF20L1, and this association was enhanced by inhibition of the H3K27 demethylases UTX and JMJD3. Notably, targeting of H3K27me2 to viral genomes was enhanced following infection with a transcriptionally defective virus in the absence of Promyelocytic leukemia nuclear bodies. Collectively, these studies implicate a role for H3K27me2 in fibroblast-associated HSV genome silencing in a manner dependent on genome sub-nuclear localization and transcriptional activity.

2.2. Importance

Investigating the potential mechanisms of gene silencing for DNA viruses in different cell types is important to understand the differential outcomes of infection, particularly for viruses like herpesviruses that can undergo distinct types of infection in different cell types. In addition, investigating chromatin association with viral genomes informs on the mechanisms of epigenetic regulation of DNA processes. However, there is a growing appreciation for heterogeneity in the outcome of infection at the single cell, and even single viral genome, level. Here we describe a novel assay for quantifying viral genome foci with chromatin proteins and show that a portion of genomes are targeted for silencing by H3K27me2 and associate with the reader protein PHF20L1. This study raises important questions regarding the mechanism of H3K27me2-specific targeting to viral genomes, the contribution of epigenetic heterogeneity to herpesvirus infection, and the role of PHF20L1 in regulating the outcome of DNA virus infection.

2.3. Introduction

The genomes of DNA viruses, especially those that replicate in the nucleus, have an intimate association with host chromatin. Herpesviruses are double-stranded DNA viruses that can undergo both lytic/productive replication and establish long-term latent infections. There is growing evidence that the regulation of herpesvirus latent versus lytic infection results from the deposition of cell type-specific types of chromatin, as active euchromatin is enriched during productive de novo infection and reactivation, whereas repressive heterochromatin is enriched on viral genome during latent infection (27, 106, 108, 117, 129, 220, 221, 226, 229–234). However, the mechanisms that regulate the deposition of heterochromatin, and functional outcomes in different cell types for many of the herpesviruses, remain unknown. The full meaning of abbreviated terms can be found in Table 1.

Polycomb-mediated silencing is a type of facultative heterochromatin, characterized in large part by the enrichment of lysine 27 tri-methylation on histone H3 (H3K27me3) and is associated with multiple latent herpesviruses (1, 128, 129, 132, 220, 221, 226, 230–232, 235–237). Facultative heterochromatin is more readily converted to transcriptionally active euchromatin than the more stable constitutive heterochromatin (238). Polycomb silencing is primarily established on the host genome during pluripotency and remodeled during cell specification. Hence, most data on Polycomb silencing come from studies investigating gene silencing in stem cells and during the early stages of development (1, 239). Many herpesviruses infect differentiated host cells and Polycomb silencing of latent herpesvirus genomes is believed to promote and/or maintain repression of the viral lytic phase genes during latent infection (1). The mechanisms of Polycomb silencing may differ between pluripotent and terminally

differentiated cells. Therefore, investigating the de novo deposition of chromatin onto incoming herpesvirus genomes has the potential to inform the mechanisms of heterochromatin formation in different cell types.

Herpes simplex virus type I (HSV-1) is the prototype alphaherpesvirus, and infection of neurons can result in a lifelong latent infection in which lytic genes are repressed. By contrast, infection of epithelial cells or fibroblasts results in productive (lytic) replication. The molecular mechanisms that regulate entry into lytic replication or silent latent infection are important to understand because HSV-1 (and the related HSV-2) latent infection causes significant morbidity and mortality. Periodically, the virus reactivates from latent infection to result in infectious virus production, which can lead to lesions at the body surface, keratitis, and encephalitis. In addition to these outcomes, HSV-1 infection has been linked to the progression of late-onset neurodegenerative disease (15, 16, 18, 20, 240).

When HSV-1 genomes initially enter the nucleus, they are devoid of chromatin. There is evidence for rapid association of histones with incoming genomes mediated by histone chaperone proteins (85, 94–96, 241). During a latent infection of neurons, HSV-1 lytic genes are associated with cellular histones carrying H3K27me3 as well as di- and tri-methylation of lysine 9 on histone H3 (H3K9me2/me3) (1, 124, 128–130, 242). One model for heterochromatin association with the HSV-1 genome involves immediate recognition of incoming viral DNA by the host cell, resulting in heterochromatin-mediated silencing, which the virus must overcome for lytic replication (52, 101, 108, 137, 139, 243). By contrast, the virus is thought to be unable to overcome gene silencing in neurons, and latency is established (108).

However, for Polycomb silencing, evidence supporting the initial deposition of H3K27me3 during lytic infection is limited. UTX (also known as Lysine-specific

Demethylase 6A; KDM6A) is one of two H3K27-specific demethylases, the second being Jumonji domain-containing protein-3 (JMJD3 or KDM6B). Previously, UTX was shown to contribute to HSV-1 gene expression in U2OS cells (104). A further study described the transient formation of H3K9me3 and H3K27me3 on a lytic promoter immediately upon infection, followed by distinct waves of removal (139). However, the absolute levels of H3K27me3 enrichment observed in this study were orders of magnitude lower than the enrichment on host chromatin. In addition, fully determining the presence of histone modifications can be problematic due to potential background enrichment in these assays, and interpretation is further complicated by appreciated issues with histone PTM antibody specificity (244). Another confounding factor is potential heterogeneity in the outcome of HSV infection, even in mitotic fibroblast cell lines (144–146, 148, 245, 246). These studies suggest that subpopulations of viral genomes may associate with certain types of heterochromatin, which would be difficult to detect in bulk assays like chromatin immunoprecipitation (ChIP). Assays that can measure the enrichment for certain types of chromatin at the single genome level would therefore be beneficial to take into account this potential heterogeneity.

Previous studies have identified the presence of the constitutive heterochromatin marks H3K9me2/me3 on the viral genome during lytic infection and defined their role in gene silencing (98, 101, 139, 247). Notably, H3K9me2/me3-marked histones associate with the histone chaperone protein DAXX prior to loading onto chromatin, facilitating rapid association of repressive PTMs with viral DNA (248). DAXX also associates with Promyelocytic leukemia (PML, also known as ND10) nuclear bodies (NBs), and previous literature supports a model in which PML-NBs are involved in constitutive heterochromatin formation (85, 109, 135, 249–252). Upon infection of non-neuronal cells, HSV-1 genomes rapidly associate with PML-NBs and there is evidence for

silencing through H3K9me₂/me₃ at these bodies (85, 146). Consistent with this observation, PML-NBs repress HSV-1 lytic replication, and the viral protein ICP0 degrades PML to overcome this repression (79, 80, 82, 253–256). However, histones pre-modified with methylated lysine H3K27 have not been previously detected (257). Given the association of viral genomes with PML-NBs and Daxx, and how the loss of PML shifts the balance of methylation from H3K9 to H3K27 (135), it is not clear whether incoming lytic genomes could be targeted for Polycomb silencing simultaneously with H3K9 methylation. Notably, we recently reported that primary neurons are devoid of PML-NBs (88), and hence if these bodies do protect against Polycomb silencing, viral genomes would still be targeted for H3K27me₃ deposition following neuronal infection. However, the presence of PML-NBs in non-neuronal cells could shift the balance of heterochromatin away from Polycomb silencing and toward initial H3K9me_{2/3} deposition.

The previously observed kinetics of H3K27me₃ formation (approximately 36 hours), at least in pluripotent cells, also do not support a role for this modification in restricting lytic HSV-1 infection (140, 153). However, it cannot be ruled out that there are different kinetics for de novo H3K27me₃ formation on incoming viral genomes in more differentiated cell types. Importantly, the deposition of H3K27me₂ is much more rapid (158). H3K27me₂ is also associated with gene silencing, and a recent study identified PHD Finger Protein 20-Like Protein 1 (PHF20L1) as a repressive reader protein of this PTM (258). H3K27me₂ is the most abundant H3K27 methylation state in embryonic stem cells (158) and yet the H3K27me₂ association with herpesvirus genomes, and any contribution to gene silencing, has not previously been reported.

Here, we set out to define the contribution of Polycomb silencing of HSV-1 genomes to lytic gene repression in non-neuronal cells. Using a combination of

epigenetic, imaging, and gene expression-based approaches, we determined that HSV-1 infection in primary human foreskin fibroblasts (HFFs) does not result in Polycomb-mediated H3K27me3 deposition or its subsequent removal. Importantly, we developed a novel assay quantifying co-localization between viral genome foci and histone PTMs in the nucleus, therefore accounting for heterogeneity between different genome epigenetic states. Combining this analysis with the inhibition of demethylases UTX and JMJD3, we found that a subpopulation of genomes was associated with H3K27me2 and PHF20L1. Furthermore, association with H3K27me2 increased on genomes of virus lacking the transactivating function of VP16 in the absence of PML-NBs, suggesting that association with PML-NBs limits H3K27me2 deposition on transcriptionally inactive genomes and instead promotes more constitutive heterochromatin formation.

2.4. Results

2.4.1. H3K27me3 Does Not Associate with the HSV-1 Genome

Following Infection of Human Fibroblasts.

To determine the potential contribution of H3K27 methylation mediated by Polycomb repressive complexes during HSV-1 lytic replication in non-neuronal cells, we set out to investigate the deposition of H3K27me3 on the viral genome following infection of human fibroblasts. In a previous study, data from ChIP followed by quantitative polymerase chain reaction (qPCR) suggested a low level of H3K27me3 was present at 1-2 hours post-infection (HPI) that was later reduced, co-incident with reduced total histone association and following ICP0 expression (139). However, without comparing H3K27me3 on the viral genome to regions of host chromatin that are enriched for this PTM, it cannot be concluded whether this modification is enriched on the viral genome. In addition, since this study was published, data have emerged that many antibodies against H3K27 methylation show non-specific binding to other histone PTMs (244), and it is therefore possible that antibody cross-reactivity with other PTMs complicated interpretation of these data.

To resolve these issues, we infected HFFs with HSV-1 strain 17 Syn+ at a multiplicity of infection (MOI) of 3 plaque-forming units (PFU) per cell and carried out CUT&RUN 2 and 4 HPI; time points chosen based on published observations that both H3K27me3 and total histone levels peak at these times and are removed by 4 HPI (96, 139). The H3K27me3 antibody used was chosen for its high target specificity, as determined by histone peptide array analysis (244) (Figure 6.1A). To quantify enrichment at specific promoter sequences, we analyzed the enrichment compared to

the non-specific IgG control aligning to the KOS reference strain (259). CUT&RUN data for both 2 and 4 HPI show very little enrichment for H3K27me3 on viral lytic promoters, shown as the geometric means of 2 replicates (linear enrichment over IgG) scaled to the host positive control (Myt1) promoter in Figure 6.1. All IE and early gene promoters are shown with a selection of late genes. In the presence of JMJD3 and UTX inhibition (GSK-J4), which would prevent H3K27 demethylation, the host genome showed higher enrichment for H3K27me3 at 4 HPI the Myt1 promoter, in addition to an increase compared to the 2 h time-point, which is consistent with previous reports (260). GSK-J4 activity was validated for uninfected HFF chromatin by western blot (Figure 6.2A), indicating that the lack of H3K27me3 accumulation on viral promoters is not due to a lack of inhibitor activity. In stark contrast to the host promoters, no viral lytic promoters showed notable enrichment for H3K27me3. Therefore, in bulk cultures, we were unable to detect positive enrichment for H3K27me3 in the regions of the viral genome examined.

H3K27me3 Enrichment at Human and Viral Promoters

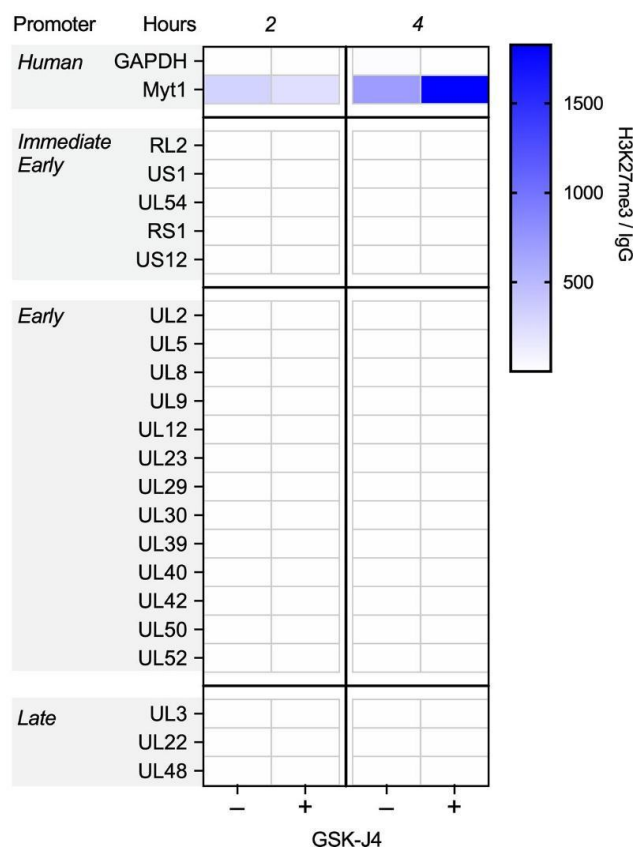


Figure 2.1: CUT&RUN during early infection shows little H3K27me3 enrichment on lytic HSV-1 chromatin.

HFFs were infected at an MOI of 3 PFU/cell untreated or treated with 10 μ M GSK-J4. Cells were processed for CUT&RUN, and fragments were sequenced and aligned to both human and viral genomes. The sum of coverage at defined promoter regions was used to calculate the fold enrichment of H3K27me3 over IgG. The geometric mean of the fold enrichment is plotted as a heat map scaled to the host gene Myt1 (N = 2). *Experiments and data analysis by Alison Francois. Sequencing provided by Novogene.*

2.4.2. Analysis of Individual HSV-1 Genome Foci for Co-localization with H3K27me3 Using NucSpotA.

Although the CUT&RUN data suggest that there was very little H3K27me3 enriched on the lytic HSV-1 genome following the infection of fibroblasts, we could not rule out the possibility that a subpopulation of viral genomes associates with H3K27me3 upon fibroblast infection, which may not be detected by these bulk population-level methods. Therefore, we developed an assay that would permit the quantification of histone modifications associated with HSV-1 DNA at an individual genome, or genome spot, resolution. Importantly, other studies have observed heterogeneity in the ability of cells to support lytic replication (144, 146). Therefore, heterochromatin may associate with a subpopulation of viral genomes following infection of fibroblasts.

We prepared viral stocks that contained EdC-labeled genomes as previously described (80). HFFs were infected with EdC-labeled HSV-1 (HSVEdC) and Click chemistry-based fluorescent staining (to visualize viral DNA) was carried out alongside immunostaining with the chosen histone antibody (79). To accurately quantify the enrichment of each histone PTM with the viral genome in an unbiased and high-throughput manner, we developed a custom program (NucSpotA) that measures the intensity of the signal at a viral genome compared to the intensity of positive signal throughout the nucleus (Figure 2.2). We first validated NucSpotA by quantifying the co-localization with proteins that have been found enriched at sites of viral genomes: RNA polymerase II (Figure 2.3A, top) and total histone H3 (Figure 2.3A, middle). H3 is known to be rapidly deposited on the lytic HSV-1 genome (65, 94, 108, 115, 261), while RNA polymerase II is essential for viral lytic gene expression (121) and has been shown

previously to co-localize with viral genomes (91). A higher intensity ratio represents a higher enrichment of a protein in viral genomes.

We then used NucSpotA to quantify the enrichment of individual viral genome foci with H3K27me3 (Figure 2.3A, bottom). We observed a reduced association of viral genomes with H3K27me3 compared to total H3 at 1 (HPI), which was statistically significant (Figure 2.3B). By contrast, RNA polymerase II intensity ratios were even higher than for H3, resulting in the strongest co-localization with viral genomes at each time post-infection. Therefore, H3 and RNA polymerase strongly co-localized with viral DNA as expected, but H3K27me3 appears not to co-localize with lytic genomes based on the results of the overall NucSpotA analysis.

The above data indicate that, overall, viral genomes show reduced association with the H3K27me3 compared to host chromatin, and reduced levels are also compared to total H3. However, this bulk NucSpotA analysis still did not take into account the possibility of a minority population of genomes that associate with H3K27me3. Therefore, we set a cutoff (intensity ratio 1.5) above which genomes look visually co-localized with H3K27me3 when assessed qualitatively. The percentages of genomes above this cutoff (labeled as a dotted line in Figure 2.3B through D and F) serve as an indicator of whether a subpopulation of genomes co-localizes with H3K27me3. Notably, this method can be used to assess the heterogeneous association of viral genomes with any nuclear protein of interest. Using this method, we observed that 11%, 9.8%, and 4.3% of viral genome foci had enrichment values for H3K27me3 above this threshold at 1-, 2- and 4 HPI, respectively (Figure 2.3B). As a positive control for H3K27me3 co-localization, we also performed Click chemistry and immunostaining for latent genomes in mouse SCG neurons (Figure 2.3E and F). In latently infected neurons, we observed enrichment of H3K27me3 on approximately 31% of latent HSV-1 genomes based on a

NucSpotA intensity ratio above 1.5. This is consistent with previous observations that H3K27me3 is enriched on the latent HSV genomes and its removal is important in reactivation (124, 128, 129, 138, 242, 262–264). These data also highlight the potential heterogeneity in the epigenetic nature of latent HSV genomes, which may relate to different levels of expression of the latency-associated transcript between individual neurons or differences in sub-nuclear genome localization (131, 265). Importantly, these data support our use of intensity ratios to quantify co-localization between HSV-1 genomes and H3K27me3.

It was not clear from this analysis whether positively co-localizing genomes represent a true association, or if they are more co-localized than we would expect by chance (random placement of a genome in the nucleus). We thus performed an additional analysis, using each image to generate its control by rotating the viral genome channel 90 degrees relative to nuclear and histone stain channels (Figure 2.2B). This allows paired analysis between an original genome's intensity ratio and that for its random placement within the same nucleus (266). Original image H3 co-localization was significantly greater than that for its random control image at each time point (Figure 2.3C), as is the co-localization of latent genomes with H3K27me3 (Figure 2.3F). However, co-localization with H3K27me3 in fibroblasts was similar to or below that expected by chance at all three time points post-infection (Figure 2.3D). In conclusion, assessing the co-localization of lytic viral genomes with histone modifications suggests that lytic genomes do not stably co-localize with H3K27me3, in contrast to co-localization with total histone H3.

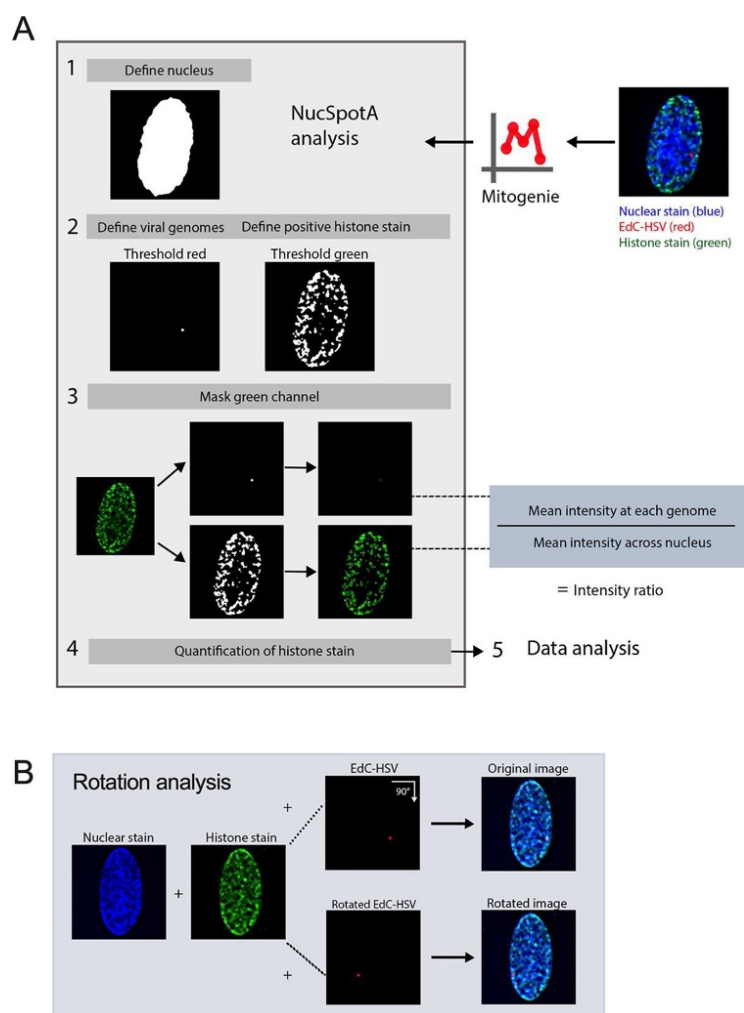


Figure 2.2: Image analysis using NucSpotA to quantify the enrichment of nuclear protein(s) at viral genomes.

A. The workflow was used for a batch of images of individual-infected nuclei using NucSpotA. An RGB image is thresholded to define the nucleus (blue channel), then viral genomes (red channel) and positive immunostain signal (green channel) within the nucleus. Representative images show a histone immunostain (H3K27me3). The mean intensity of the immunostain at each viral genome and across the nucleus is measured and used to calculate an intensity ratio. **B.** The rotation of the red channel relative to blue and green channels is used to generate pairs of original and rotated images. Rotation functions as random placement of viral genomes within the nucleus. Image pairs are processed in parallel. *Mitogenie* was developed in collaboration with Ali Rohani, formerly of the Kashatus lab with our feedback and test images. Figure generated by Alison Francois.

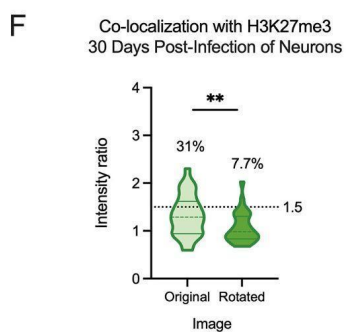
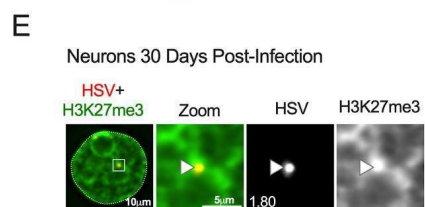
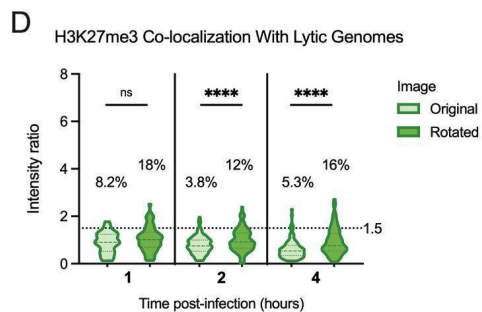
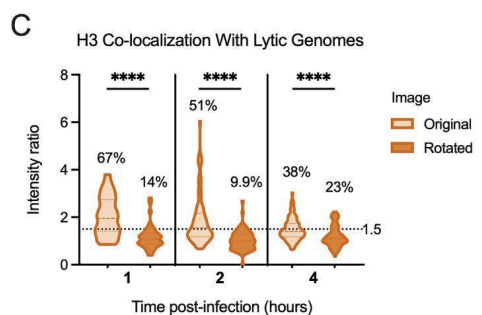
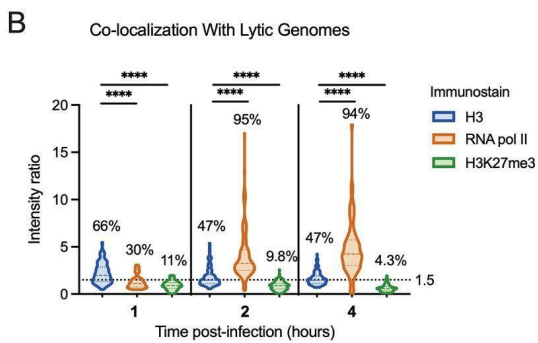
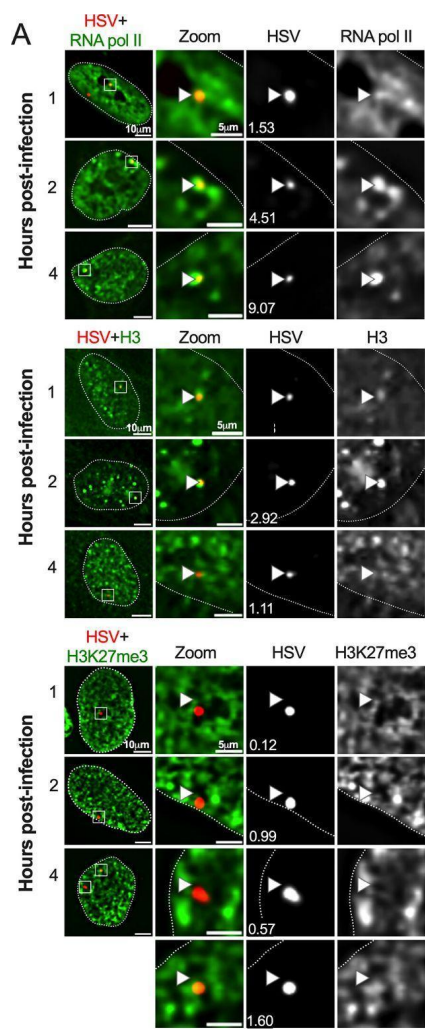


Figure 2.3: Incoming HSV-1 genomes do not co-localize with H3K27me3 during early lytic infection.

HFFs were infected at an MOI of 3 PFU/cell with HSVEdC, fixed at different times post-infection, and processed for click chemistry and immunostaining against H3K27me3. **A.** Representative images of HFF nuclei 1, 2, and 4 hours post-infection, and zoomed images of individual viral genomes. NucSpotA intensity ratios are superimposed on each viral genome's single-channel image, with arrows for reference in the same spot in each channel. **B.** NucSpotA quantification of image sets represented in A. The significance shown is based on the Kruskal-Wallis test. Each data point represents one viral genome. **C.** Rotation analysis of co-localization with H3 at each time point as outlined in Figure 2.2. Paired analysis was performed for each genome (Wilcoxon test). **D.** Rotation analysis for H3K27me3 intensity compared to those expected by chance (paired Wilcoxon test). Data shown in C and D were generated from the same original images quantified in B. **E.** A representative image shows the nucleus of a latently infected neuron, within which a viral genome is co-localized with H3K27me3. **F.** Rotation analysis of H3K27me3 co-localization with latent HSV genomes in neurons (paired Wilcoxon test). Percentages indicate the proportion of genomes with NucSpotA intensity ratios above the denoted co-localization threshold (dashed line). Adjusted P-values: **=<0.002, ****=<0.0001. $N \geq 3$. *Experiments and data analysis from panels A through D were performed by Alison Francois. Panels E and F were compiled using data provided by Sara Dochnal.*

2.4.3. Inhibition of H3K27me3 Deposition or Removal Does Not Alter its Co-localization with HSV-1 Genomes in Fibroblasts.

Although the rotation analysis suggested that a similar proportion of viral genomes could co-localize with H3K27me3 as those observed to co-localize by chance, it was still possible that a minority population is targeted for H3K27me3. Therefore, to thoroughly investigate whether this reflected deposition onto the viral genome, we pre-treated cells with UNC1999 (267), an inhibitor of the H3K27 methyltransferases EZH1 and EZH2 in the PRC2 complex, and quantified co-localization of viral genomes in the absence of H3K27 methyltransferase activity. Western blots of the total levels of H3K27me3 in fibroblasts demonstrated that 1.8 μM had the capability of reducing levels over time

(Figure 6.2B). Therefore, we pre-treated cells with 1.8 μ M UNC1999 followed by infection with HSV-1, maintaining drug treatment during and after infection. At 2 HPI, the co-localization of H3K27me3 at viral genomes was not significantly lower than for vehicle control (DMSO)-treated cells at the population level. The proportion of genomes above the intensity ratio threshold of 1.5 also did not decrease with PRC2 inhibition (Figure 2.4A). Therefore, we conclude that the small proportion of viral genomes with a threshold above 1.5 (5%) was not a result of active deposition of H3K27me3.

The final possibility was that H3K27me3 could be rapidly deposited and removed from viral genomes. Therefore, we added GSK-J4, an inhibitor of the H3K27me3 demethylases JMJD3 and UTX (268). Cells were again pre-treated with GSK-J4 (10 μ M), and the inhibitor was included during the infection. Inhibitor activity at this concentration was confirmed by assessing H3K27me3 retention on cellular chromatin by western blot (Figure 6.2A). At 4 HPI, we did not observe an increase in the proportion of viral genomes co-localizing with H3K27me3 in the presence of the inhibitor (Figure 2.4B), suggesting the mark was not added and then rapidly removed by the activity of these histone demethylases. Taken together, these data suggest that H3K27me3 is not deposited on lytic genomes in HFFs during the early stages of lytic infection of fibroblasts.

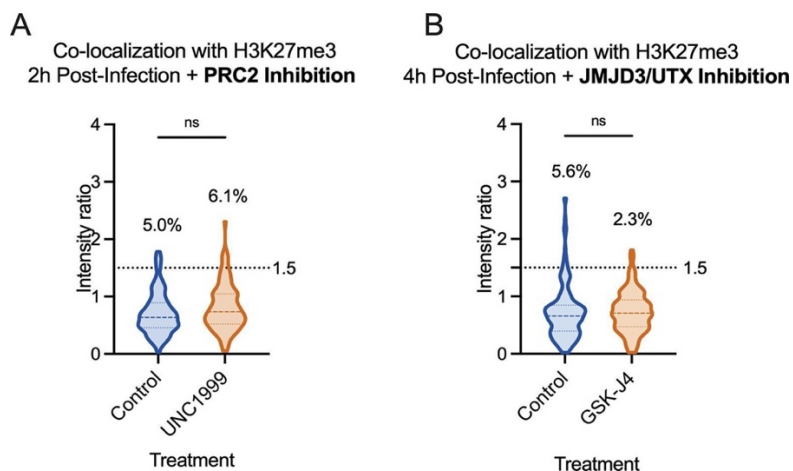


Figure 2.4: Inhibition of H3K27me3 dynamics does not impact H3K27me3 co-localization with lytic genomes.

HFFs were infected with HSV-EdC following pre-treatment with inhibitor or vehicle control, maintaining treatment throughout infection. **A.** Co-localization of viral genomes with H3K27me3 at 2 HPI, treated with vehicle control or UNC1999. **B.** Co-localization of viral genomes with H3K27me3 by 4 HPI, treated with vehicle control or GSK-J4 (10 μ M). Percentages represent genomes with co-localization above the threshold of 1.5. Kolmogorov-Smirnov tests, $N \geq 3$. *Experiments and data analysis by Alison Francois.*

2.4.4. H3K27 Demethylase Inhibition Restricts Lytic Gene

Expression.

To determine whether the presence of methylated H3K27 can impact HSV gene expression in fibroblasts, we carried out gene expression analysis on cells infected in the presence of UNC1999. HFFs were again pre-treated with UNC1999, and then infected with HSV-1, with the inhibitor treatment maintained throughout infection. We then performed reverse-transcription qPCR (RT-qPCR) to quantify lytic gene expression. We expected PRC2 inhibition with UNC1999 to enhance lytic gene expression if H3K27me3 were deposited on the viral genome. However, we did not observe any change in the

expression of the IE mRNA ICP27 and early mRNA ICP8 transcripts with UNC1999 treatment (Figure 2.5A and B). A previous study found that long-term treatment with a high dose of UNC1999 can result in the expression of anti-viral genes including, IL6, IFNA2, and IFNA1, and inhibition of viral gene expression (269). However, in our experiments using a lower dose of UNC1999 (3 μ M) and a shorter time frame of treatment, we did not observe changes in IL6 expression (Figure 6.2C), indicating the UNC1999 was not inducing an antiviral response in our cells that would otherwise impact the interpretation of these gene expression experiments. Therefore, these results indicate that the deposition of H3K27 methylation does not impact HSV-1 gene expression and supports our conclusion that H3K27me3 is not being deposited on the HSV-1 genome during lytic infection.

We also carried out the converse experiment and examined whether inhibition of the removal of H3K27 methylation impacted HSV-1 gene expression in fibroblasts using GSK-J4 (10 μ M). Unexpectedly, we observed a repressive effect with GSK-J4 treatment. Although data up to this point suggest that H3K27me3 is not forming on the lytic genome, preventing H3K27 demethylation led to repression of all the immediate early (IE), early and late transcripts checked at 2 HPI (approximately 3- to 5-fold, 50- to 80-fold, and 80-fold, respectively; Figure 2.5C). By 5 HPI, some effect was still seen for early genes (2- to 3.5-fold) and leaky late gene VP16 (5.4-fold), although less than that observed at 2 HPI, indicating the repression may be overcome later in infection (Figure 2.5D). Therefore, inhibition of JMJD3 and UTX activity limits, but does not fully prevent, HSV-1 lytic gene expression. This was surprising given our observation that inhibition of the H3K27 demethylases did not impact levels of H3K27me3 association. However, it was possible that inhibition of removal of other forms of H3K27 methylation would impact HSV-1 lytic gene expression.

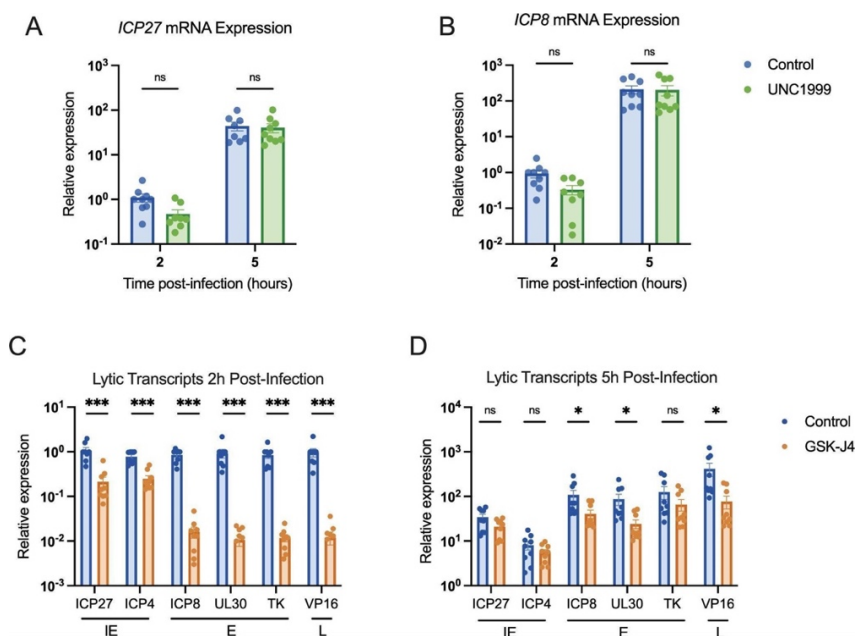


Figure 2.5: Inhibition of H3K27 demethylase activity restricts lytic gene expression, but inhibition of H3K27 methylation does not impact lytic gene transcription.

HFFs pre-treated with inhibitor or vehicle control were infected at an MOI of 3 PFU/cell, maintaining treatment throughout infection. RNA lysate was harvested, cDNA was synthesized, and transcript levels were determined by RT-qPCR. Fold expression change is relative to cellular g-actin transcript levels. **A.** Relative levels of IE transcript ICP27, **B.** and E transcript ICP8, in cells treated with vehicle control or UNC1999 (1.8 μ M). **C.** Transcription of all three lytic gene classes [immediate early (IE), early (E), and late (L), as indicated] 2 HPI, vehicle control-treated or treated with GSK-J4 (10 μ M). **D.** Transcription representative viral lytic genes 5 HPI. $N \geq 3$; biological repetitions shown. Mann-Whitney test, adjusted P-values: *= <0.05 , ***= <0.0005 . *Experiments and data analysis by Alison Francois.*

2.4.5. A Subpopulation of Genomes Co-Localizes With H3K27me2 When H3K27 Demethylation Is Inhibited.

Given that the PRC2 and JMJD3/UTX complexes are responsible for methylation dynamics between all three methylation states of H3K27, we considered that another methylation state other than H3K27me3 could be present and repressive to the lytic

genome. We focused on H3K27me₂, as this modification is also repressive to transcriptional activity (158, 258). In addition, we considered that previous studies investigating the mechanisms of de novo Polycomb silencing in murine embryonic stem cells (mESCs) have shown full tri-methylation of H3K27 to take approximately 36 hours, a time frame inconsistent with the rapid events unfolding during early HSV-1 infection (140, 159, 270). However, the same studies demonstrate that H3K27me₂ forms more rapidly. H3K27me₂ is relatively understudied but is also associated with gene silencing. It protects against the deposition of H3K27 acetylation (an activating modification), and the H3K27me₂ reader protein PHF20L1 has been shown to restrict transcription (158, 271). Notably, H3K27me₂ is also one of the most abundant histone PTMs on the host genome and is more prevalent than H3K27me₃ (158).

We therefore performed CUT&RUN and co-localization experiments, this time investigating the H3K27me₂ modification. We found it difficult to source an H3K27me₂ antibody with appropriate binding specificity and performed multiple experiments with one antibody (Diagenode C15410193) that turned out to have high binding affinity to unmodified histone H3 (Figure 6.1D). Histone peptide binding array analysis was conducted for four additional antibodies marketed to recognize H3K27me₂, but none were selective for this mark (Figure 6.1B through E). A comparison of co-localization and CUT&RUN viral genome coverage using Diagenode C15410193 is shown in Figure 6.3A and B. We note although we cannot fully rule out that the CUT&RUN signal is from H3K27me₂, the broad distribution across the genome pointed to non-specific binding. In addition, the co-localization of H3K27me₂ with the viral genome using Diagenode C15410193 is higher than other H3K27me₂ antibodies that were included in this study; therefore, we did not continue experiments using Diagenode C15410193. The explanation for the enhanced binding of this antibody to viral genomes is unclear but

may result from non-specific binding to unmodified histones. We include the data here as an example of the need to accurately validate the binding specificities of histone antibodies.

We analyzed H3K27me2 using a more specific antibody as determined by histone peptide arrays (Figure 6.1B; Active motif 39245). Figure 2.6A shows representative images of an infected nucleus at each time point post-infection. Without any inhibitor treatment, the co-localization of viral DNA with H3K27me2 was below that for total H3 (Figure 2.6B), and similar to or below that expected by chance from rotation control analysis (Figure 2.6C). Furthermore, PRC2 inhibition with UNC1999 (1.8 μ M) did not reduce the co-localization of viral DNA with H3K27me2, indicating that under these conditions we either could not detect active deposition of H3K27me2 onto viral genomes or that it was rapidly removed (Figure 2.6E). Inhibition of H3K27 demethylation using GSK-J4 (10 μ M) did cause a modest but significant increase in the fraction of viral genome foci that co-localize with H3K27me2, up to 15.5% of genomes (Figure 2.6F). Notably, the percentage increase in genomes co-localizing with H3K27me2 was reproducible between independent biological replicates, including biological repetitions with a separate H3K27me2 antibody (Active motif 61435; 5.1E; Figure 2.6G). Therefore, these viral genomes (representative images Fig. 6D) may represent a subpopulation of genomes that experience H3K27me2 deposition followed by removal by JMJD3 and/or UTX.

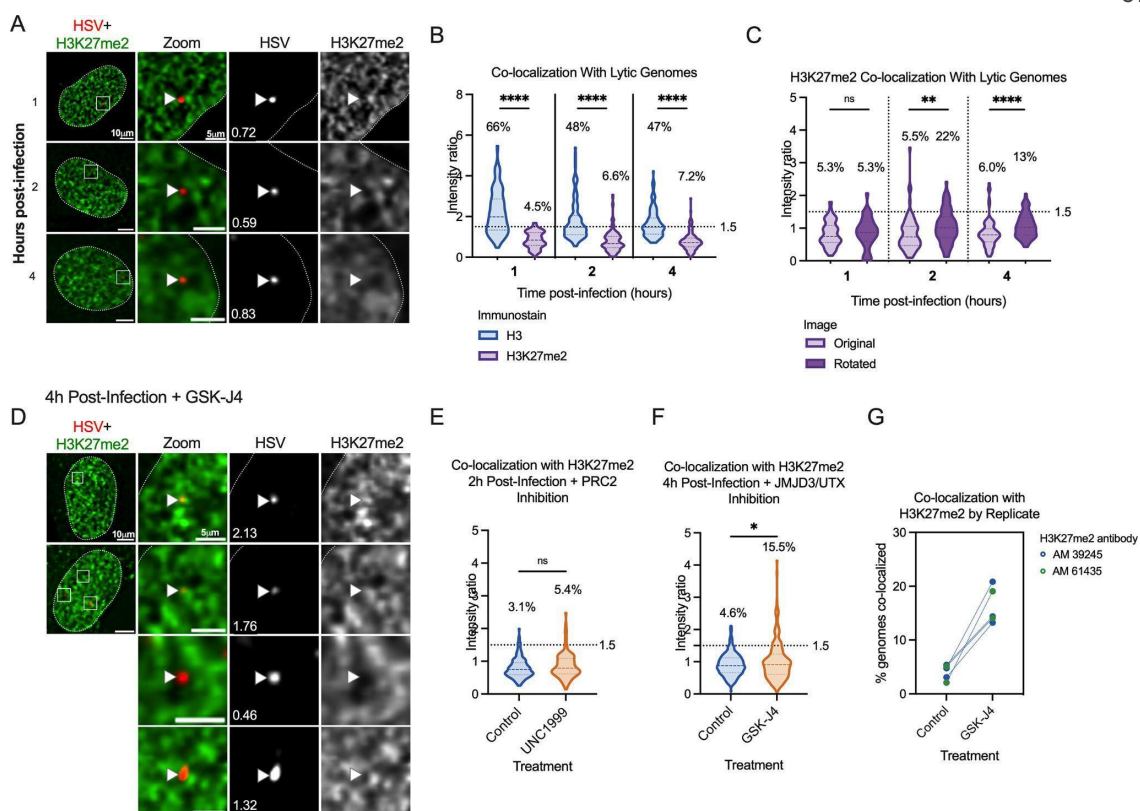


Figure 2.6: A subpopulation of viral genomes co-localizes with H3K27me2 when H3K27 demethylation is inhibited.

A. Representative images of HFF nuclei infected with HSVEdC at 1, 2, and 4 HPI (Active Motif 39245 antibody). Intensity ratios are superimposed on each viral genome's single-channel image.

B. H3K27me2 compared to H3 co-localization with lytic genomes. **C.** The rotation analysis for H3K27me2 images to compare actual co-localization to that expected by chance 1, 2, and 4 HPI.

D. Representative images of H3K27me2 co-localization with viral genomes in cells pre-treated and continuously treated with demethylase inhibitor GSK-J4 (10 µM). **E.** H3K27me2 co-localization with lytic genomes 2 HPI with vehicle control or UNC1999 treatment (1.8 µM). **F.** H3K27me2 co-localization with lytic genomes 4 HPI with vehicle control or GSK-J4 treatment (10 µM). **G.** Individual experimental replicates for GSK-J4-treated and vehicle control cells, including data included in F and two more data points with a different H3K27me2 antibody (Active motif 61435). *Experiments and data analysis by Alison Francois.*

2.4.6. CUT&RUN Reveals a Low Association of Lytic Gene

Promoters With H3K27me2 That Increases With K27 HDM Inhibition.

To investigate whether we could verify the association of H3K27me2 with the viral genome and any changes with GSK-J4 treatment, we performed CUT&RUN with paired-end sequencing, again using an antibody validated to bind H3K27me2 (CST D18C8 9728, Figure 6.1C). At 2 HPI, we were able to detect H3K27me2 on the viral genome that increased with GSK-J4 treatment. The H3K27me2 coverage on the viral genome 2 HPI is depicted as fold enrichment over IgG in Figure 2.7A and zoomed-in regions of representative viral promoters UL12 and UL54 are shown in Figure 2.7B. We were unable to find any previous studies investigating H3K27me2 association with the host genome in fibroblasts to compare the levels of H3K27me2 on the viral genome to those on known host-positive control regions. Therefore, we found regions with high and low associations in our data set for comparison with the HSV-1 genome. We chose the SERPINA1 promoter as a region of high enrichment and the GAPDH promoter as a region depleted for H3K27me2. In comparison to the SERPINA1 promoter, we observed modest enrichment on viral promoters at 2 HPI (Figure 2.7C). The enrichment of H3K27me2 was much lower at 4 HPI, likely because of ongoing viral DNA replication at this time point, active removal of the modification, or of histone H3 itself, which has previously been reported independently of viral DNA replication (96). Notably, we did observe an increase in H3K27me2 levels on the host genome between 2 and 4 hours post-infection. Although a comparatively low level of H3K27me2 was detected on viral genomes at 2 HPI, Figure 2.7D shows the same enrichment values plotted without scaling to the host-positive control. This representation shows an increase in H3K27me2 association in the presence of GSK-J4 at 2 HPI, indicating that a subpopulation of viral

genomes may retain H3K27me2 in the presence of H3K27 demethylase inhibition. There appeared to be no correlation with gene class for the IE and early genes, although UL54 (encoding ICP27) had the highest level of fold enrichment. Overall, the enrichment was higher in promoter regions compared to the gene bodies (Figure 2.7D). Taken together, these results indicate that H3K27me2 is deposited and removed on at least a subpopulation of viral genomes, and this removal enables more robust viral lytic gene expression at early times during infection.

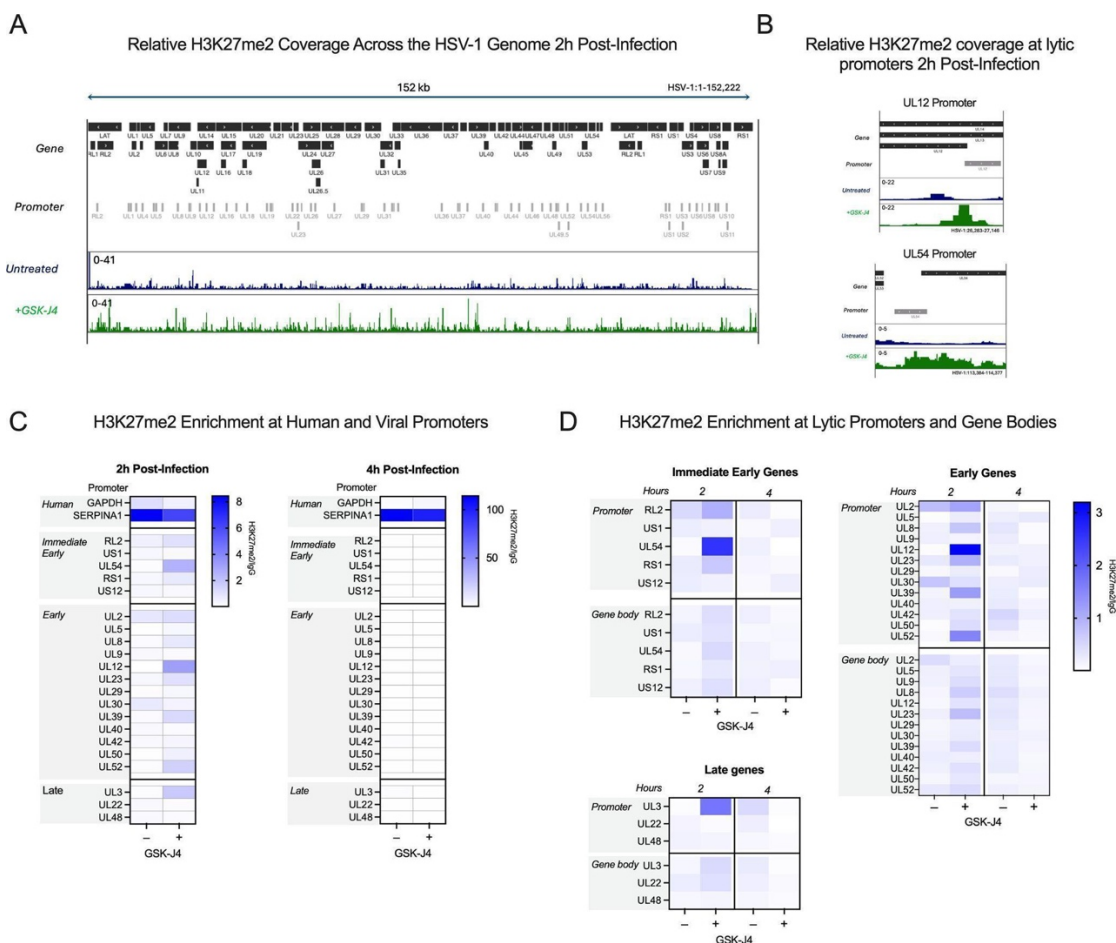


Figure 2.7: Bulk-level analysis of viral chromatin by CUT&RUN shows modest H3K27me2 enrichment at viral promoters, and less across gene bodies, during lytic infection.

HFFs infected at an MOI of 3 PFU/cell, untreated or treated with 10 μ M GSK-J4, 2 and 4 HPI. **A.** H3K27me2 coverage was normalized to IgG as linear fold enrichment, then used to generate relative coverage plots for the HSV-1 genome 2 HPI. Relative coverage (fold enrichment) files from two experimental replicates were combined to generate each plot. Promoter regions and gene bodies are included for reference. Both GSK-J4-treated and untreated cell data are shown using a scale of 0- to 41-fold coverage relative to IgG. Untreated (blue) and GSK-J4-treated (green). **B.** Zoomed-in views of the data in A, for lytic promoter regions (UL54 and UL12). **C.** The sum of coverage at defined promoter regions was used to calculate the fold enrichment of H3K27me2 over IgG. The geometric mean of two replicates' fold enrichment is plotted as a heat map scaled to host gene SERPINA1. **D.** The geometric mean of two replicates' fold enrichment at viral promoters and gene bodies, scaled to viral enrichment only. CUT&RUN and downstream processing were carried out in parallel for two independent infections (N = 2). *Experiments and data analysis by Alison Francois. Sequencing provided by Novogene.*

2.4.7. Transcriptionally Repressed Genomes Are Enriched for H3K27me2 In The Absence Of PML-NBs.

We next explored whether we could enrich viral genomes with the H3K27me2 modification, both to further validate that this modification is indeed targeted to viral genomes in fibroblasts and to determine under what conditions its deposition may occur. The methyltransferase activity of the PRC2 complex is known to be inhibited under conditions of active transcription (198, 272). Viral lytic gene expression is stimulated by the tegument protein, VP16, and the activation domain (AD) of VP16 recruits host proteins that promote transcription and limit total histone association (95). Therefore, taking into account this known function of the VP16AD, we investigated whether mutation of this domain resulted in increased H3K27me2 deposition.

We prepared EdC-labeled stocks of the previously described VP16AD mutant (RP5, KOS parent strain) (273). Initial parallel infections with RP5 compared to its rescued virus (RP5R) at an MOI of 3 PFU/cell showed a higher number of RP5 genomes reaching the nucleus than for RP5R, despite infection at the same PFU/cell; this is likely reflective of a reduced ability of RP5 to plaque on the U2OS cells used to grow and titer the viruses (data not shown). We thus adjusted the MOI of RP5 to achieve approximately 3 foci per nucleus when visualized with Click chemistry. The expected reduction in viral gene expression by RP5 compared to RP5R was confirmed by RT-qPCR from HFFs, although RP5 viral gene expression did still increase between 2 and 5 HPI albeit at a much-reduced level compared to the rescued virus (Figure 2.8A). We then analyzed the co-localization of RP5 genomes with H3K27me2 in HFF-telomerase immortalized cells (HFF-Ts) and observed approximately 24% that showed positive co-localization with H3K27me2. However, this was not significantly above the level for random placement determined using the rotated control images (Figure 2.8C).

However, it has previously been reported in several studies that transcriptionally inactive HSV genomes are associated with repressive PML-NBs in non-neuronal cells (88, 131, 253). PML-NBs can promote the deposition of H3K9me3 but are less linked to the deposition of H3K27me2/me3. Therefore, we asked whether the presence of PML-NBs was preventing association with H3K27me2 on these transcriptionally repressed genomes by promoting the more constitutive H3K9me3 association. We created PML knock-out HFF-Ts (Figure 2.8D), the infection of which resulted in a significant increase in H3K27me2 association with RP5 at 2 HPI over PML-expressing HFF-Ts (wild-type HFF-Ts). Therefore, these data indicate that H3K27me2 associates with the HSV-1 genome either as a consequence of transcription repression and/or lack of the VP16AD in the absence of PML-NBs. Finally, to determine whether PML-NBs increase the

association with constitutive heterochromatin, we also measured H3K9me3 co-localization with RP5 genomes. We found an increase in H3K9me3 association at 2 HPI in the wild-type HFF-Ts (Figure 2.8E), indicating that PML knock-out cells indeed favor H3K27me2 formation over H3K9me3 formation at transcriptionally inactive viral genomes.

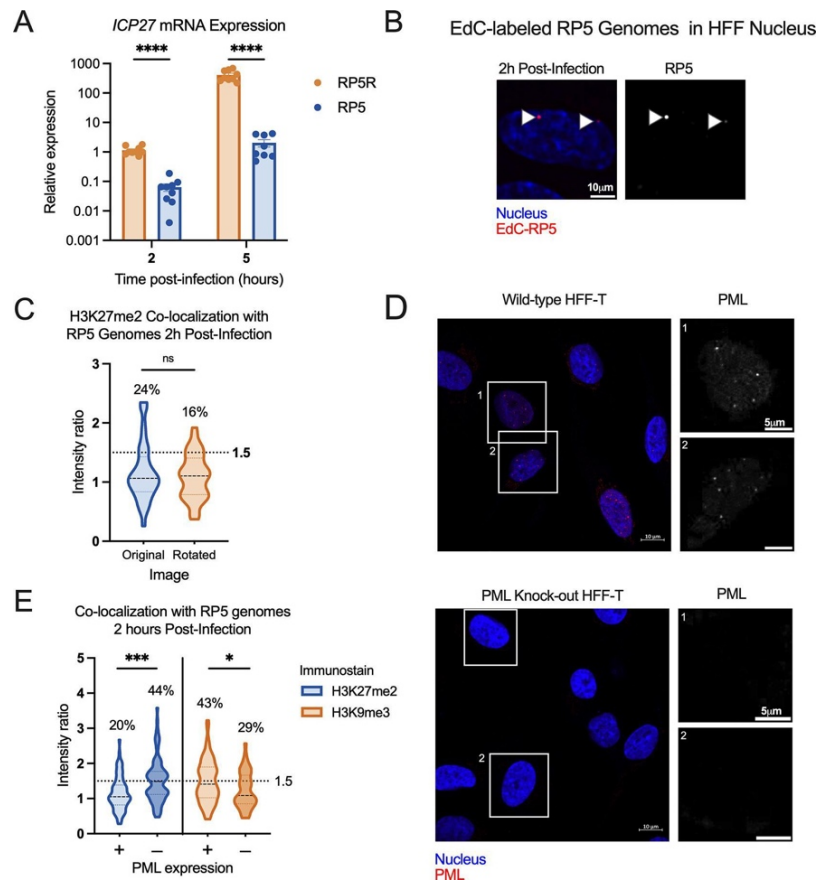


Figure 2.8: Transcriptionally repressed viral genome association with H3K27me2 is favored in the absence of PML expression.

A. HFFs were infected at an MOI of 3 PFU/cell with either VP16 activation domain mutant RP5 or its rescue RP5R. Relative ICP27 mRNA expression for RP5-infected cells, in comparison with RP5R-infected cells 2 and 5 HPI (multiple Mann-Whitney tests). Data are from three independent infections of 2–3 wells in parallel. **B.** A representative image showing EdC-labeled RP5 genomes in an HFF nucleus 2 HPI. **C.** H3K27me2 co-localization with RP5 genomes 2 HPI as determined using image rotation analysis (paired Wilcoxon test). **D.** Confirmation of nanoblade-mediated PML knock-out, comparing wild-type and knock-out HFF-Ts immunostained for PML. Cells were clonally selected following nanoblade treatment. Panels in grayscale are zoomed-in views of individual nuclei outlined in the left image. **E.** H3K9me3 and H3K27me2 co-localization with RP5 genomes 2 HPI in the absence of PML, co-localization in PML-expressing cells compared with PML knock-out cells (Kolmogorov-Smirnov tests). Percentages indicate the proportion of genomes with NucSpotA intensity ratios above the denoted co-localization threshold (dashed line) in C and E. Data are from 3 + independent infections. Active Motif 39245 antibody was used for H3K27me2 immunostaining. Adjusted P-values: *= <0.05 , ***= <0.0005 ., ****= <0.0001 . *Images in panel D acquired by Matt Loftus. PML nanoblades and cells in panels D and E generated by Matt Loftus. Experiments, data analysis from panels A-C and E by Alison Francois.*

2.4.8. Association of the H3K27me2 reader protein PHF20L1 with a subpopulation of HSV-1 genomes.

To explore the repressive functional outcome of H3K27me2 formation on lytic HSV-1 genomes, we investigated the co-localization of viral genomes with a reader of this histone PTM. PHD Finger Protein 20-Like Protein 1 (PHF20L1) was reported as an H3K27me2 reader in the context of breast tumor growth, working with PRC2 and nucleosome remodeling and deacetylase (NuRD) complexes to facilitate transcriptional repression (258). PHF20L1 co-localization was consistently found in approximately one-third of genomes at 4 HPI (34% of genomes), and an increase in co-localized genomes was observed with the GSK-J4 treatment. This increase is reflected in a 9% increase in

genomes above the co-localization cutoff, as well as a statistically significant difference between the two data sets (Figure 2.9B). Notably, the 9% increase in genomes co-localizing with PHF20L1 is similar to the 11% increase in co-localization with H3K27me2 (Figure 2.6F and G). Representative images in the presence and absence of GSK-J4 are shown, including one genome that is co-localized with PHF20L1 (intensity ratio 1.72) and one that is not (intensity ratio 0.69) within the same nucleus (Figure 2.9A).

Because we observed the highest levels of H3K27me2 association with RP5 genomes in PML knock-out cells, we also investigated the association of RP5 genomes with PHF20L1 in these same cells. Co-localization was indeed seen in a large proportion of RP5 genomes (46%) 4 HPI, as shown with representative images (Figure 2.9C and D). This further validates the potential for transcriptionally inactive genomes without PML-NBs to be targeted for H3K27me2 and read by PHF20L1.

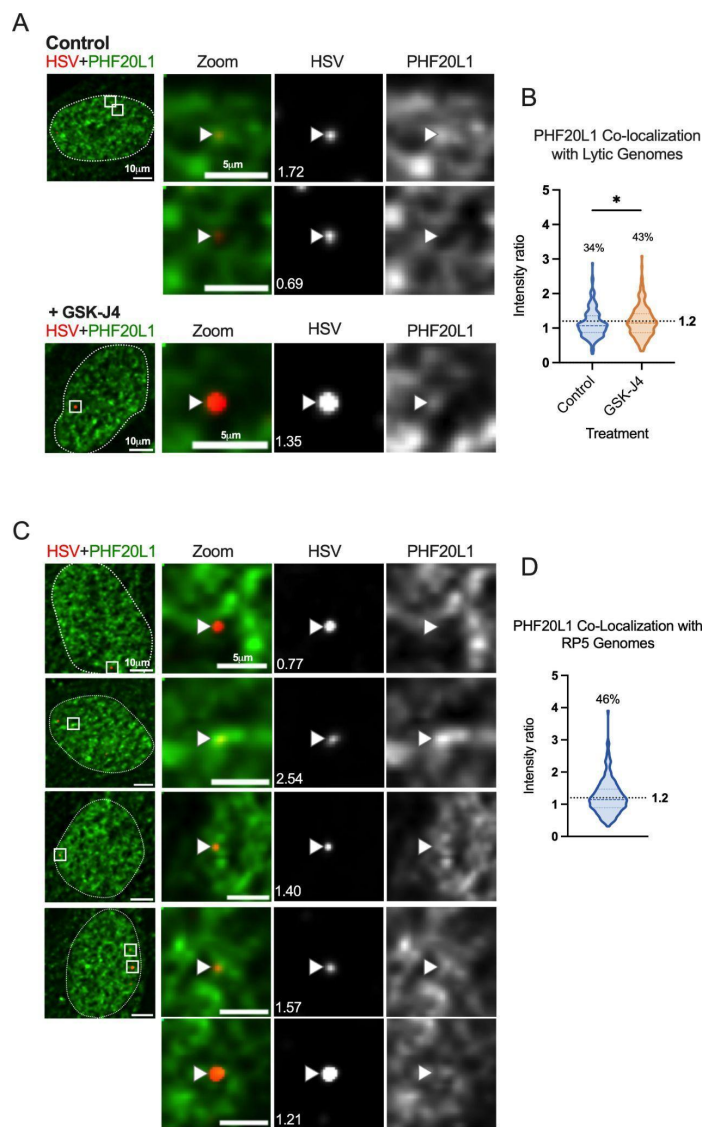


Figure 2.9: H3K27me2 reader PHF20L1 co-localizes with a subpopulation of lytic genomes, including transcriptionally repressed genomes in the absence of PML expression.

A. Representative images of HFFs infected with HSVEdC immunostained for PHF20L1 in both control and GSK-J4 (10 μ M) treated conditions 4 HPI. Cells were pre-treated for 2 hours before infection at an MOI of 3 PFU/cell, and treatment was maintained throughout infection. **B.** Quantification of images represented in A, showing NucSpotA intensity ratios for PHF20L1 co-localization (Kolmogorov-Smirnov test) in vehicle control or GSK-J4-treated (10 μ M) cells. **C.** Representative images showing PHF20L1 co-localization with transcriptionally inactive RP5 genomes in the absence of PML expression 4 HPI. PML knock-out HFF-Ts were infected with EdC-labeled RP5 to approximately 3 genomes per nucleus. **D.** Quantification of RP5 co-localization with PHF20L1 in PML knock-out HFF-Ts 4 HPI. Intensity ratios are superimposed on each viral genome's single channel image in A and C. Percentages indicate the proportion of genomes with NucSpotA intensity ratios above the denoted co-localization threshold (dashed line). *Experiments and data analysis by Alison Francois.*

2.5. Discussion

2.5.1. Updating the Model for H3K27 Methylation on Lytic Genomes

The process of lytic infection with HSV-1 is often described as a battle between the host cell and the infecting virus, with the host cell trying to silence gene expression by depositing repressive heterochromatin on the viral genome and the virus overcoming this silencing for gene expression to occur. However, for the Polycomb-associated modification, H3K27me3, there was little experimental evidence to support this model. Hence, using multiple techniques, we set out to determine whether any H3K27me3 could be detectably deposited on the incoming genome by the host, which the virus removes for lytic replication to take place. This was important to understand, first, to determine how the host cell attempts to silence incoming foreign HSV-1 DNA, and second, because this modification is ultimately enriched on the HSV-1 genome during latent infection of neurons (1, 124, 128, 129, 132, 242). Although we were unable to detect H3K27me3 enrichment on lytic genomes, our data suggest that a subpopulation of genomes is targeted for silencing by H3K27me2. This is intriguing because less is known about H3K27me2 versus the more commonly studied H3K27me3. The recent identification of a protein that specifically reads H3K27me2, PHF20L1, has illuminated the direct role of this modification in the recruitment of transcriptional repressors (258). In line with the role of H3K27me2 in lytic gene repression, we could also detect co-localization of viral genomes with PHF20L1 during lytic infection. Therefore, the deposition of H3K27me2 appears to play a more prominent role than H3K27me3 in repressing HSV-1 gene expression during lytic replication.

2.5.2. Experimental Limitations and Considerations

There are some caveats to our study. One is that we used small molecule inhibitors to this histone methyltransferases and histone demethylases and have not carried out knock-out or knock-down experiments. However, in attempting to do these experiments, we found that knock-down of the histone demethylases resulted in enhanced lytic gene expression, which is consistent with previous studies showing that a lack of these enzymes results in a reduction in anti-viral gene expression (268). Therefore, long-term loss of these enzymes in fibroblasts likely results in more indirect impacts on gene expression, making this approach a challenge. A further caveat is that antibody binding to histone PTMs can be influenced by neighboring PTMs. For example, binding to H3K27me2/me3 can be occluded by phosphorylation of H3S28. In preliminary studies using an H3K27me3/pS28 antibody, we were unable to detect co-localization with the viral genome. However, there are currently no antibodies that recognize the dual H3K27me2/pS28 modification state and therefore we cannot rule out the possibility that a subpopulation of viral genomes has these combined modifications.

Determining the presence or absence of a particular protein or histone PTM on viral genomes can be a challenge. Here, we decided to characterize the H3K27me2/me3 distribution across the early lytic HSV-1 genome by CUT&RUN using histone antibodies analyzed for their binding specificity (228). Using human genome loci to validate each antibody's DNA yield, we observed a relatively low level of H3K27me2/me3 across the viral genome. However, because of the known heterogeneity in the fate of HSV genomes following infection of fibroblasts (143–145, 245, 274–276) we developed a novel method for quantification of individual HSV genome foci with nuclear proteins. This is particularly important since comparison to host regions following CUT&RUN may obscure the enrichment at subpopulations of HSV genomes. NucSpotA analysis

accounts for variability among a set of images by thresholding the signal above a chosen percentage of its maximum intensity.

We visually determined an intensity ratio above which co-localization is occurring but found that it is important not to rely on the number's magnitude alone. Appropriate controls, such as a known positive control for co-localization or random placement in the nucleus through channel rotation, helped inform our interpretation of the data. In addition, statistical analysis of the data set applies to the whole population of genomes, but the shape of the violin plot (data point density) can be indicative of a subpopulation of genomes emerging. This assay was particularly informative in combination with other variables, such as inhibition of H3K27 methylation dynamics and the use of PML knock-out cells. In the future, we expect NucSpotA to be a useful tool for the field to analyze viral genome co-localization with nuclear proteins where heterogeneity in the fate of viral genomes can occur.

2.5.3. Implications and Future Directions

Our data suggest that H3K27me2 is deposited and removed from a subpopulation of lytic genomes. The combined data using H3K27 demethylase inhibitors and analyzing H3K27me2 genome co-localization and viral mRNA levels support a model by which H3K27me2 is repressive to lytic gene expression from a subset of viral genomes and is removed to permit more robust expression. The full spectrum of factors that regulate the deposition of H3K27me2 onto a subset of genomes is not clear. Our data point to differences in the subnuclear positioning of viral genomes and potentially viral transcriptional activity. Additional factors, which need not be mutually exclusive include the cell state, stage in mitosis, diversity in viral genome sequence, amount of infecting

virus, and responses from neighboring abortively or fully infected cells, which have all been linked to heterogeneous outcomes of HSV infection (143–145, 245, 274–276).

The H3K27me2 modification is understudied compared to H3K27me3 despite it being a predominant modification on the host genome and also being implicated in the repression of gene expression (1). There are several important implications of this observation. The first would be the mechanisms of targeting of H3K27me2 to the viral genome and investigating whether this is consistent between neurons and non-neuronal cells. The PRC2 complex can be targeted and activated to methylate H3K27 via different mechanisms (1). One model for H3K27me2/me3 involves general targeting to chromatin, potentially via RNA or binding to unmethylated CpG motifs, and inhibition by single-stranded RNA and activating histone PTMs (277–279). Our data showing increased deposition onto the VP16 mutant virus potentially supports these mechanisms; however, we cannot rule out other direct roles of VP16 in inhibiting PRC2 recruitment or inhibition. PRC2 can also be recruited following ubiquitination of lysine 119 on histone H2A (H2AK119ub) by PRC1 (156, 280). However, this pathway has only been described in pluripotent cells and the protein that links H2AK119ub to PRC2 recruitment may not even be present in more differentiated cells (162). Furthermore, it is unknown whether the HSV-1 genome is enriched in H2AK119ub in non-neuronal cells. However, as part of ongoing studies in our laboratory, we have found enrichment of H2AK119ub on latent viral genomes (see Chapter 3).

Previous studies have found that PML-NBs can promote H3K9me3 but not H3K27me3 (85). Therefore, our data showing that PML-NBs may also limit H3K27me2 are consistent with this model. Notably, we previously found that primary neurons are devoid of PML-NBs but can form with type I interferon treatment (88). In addition, targeting of viral genomes to PML-NBs only occurred with type I interferon exposure.

Therefore, by combining data from our previous study with our new data in fibroblasts, we can start to assemble a model by which the heterogeneity in the epigenetic structure of the latent genome arises. For those genomes that enter neurons exposed to type I interferon, and likely exposure specifically on the soma (88, 256, 281, 282), they would result in association with PML-NBs and H3K9me3 enrichment. For genomes that were not targeted to PML-NB, they would be more likely to become enriched for H3K27me2/me3. However, this model is based on extrapolating our findings here to neurons and therefore requires additional testing using relevant neuronal model systems.

Our findings that H3K27me2 can be deposited on incoming HSV-1 genomes but not H3K27me3 are consistent with our understanding of de novo H3K27me3 dynamics; reintroducing PRC2 activity leads to nucleation of H3K27me3 sites after 12 hours, and propagation across a region at 36 hours (140, 159, 270). However, these previous observations were made in undifferentiated, mouse embryonic cells, and we therefore had to consider that H3K27 methylation dynamics could be faster in the context of infecting a differentiated cell type. The factors that regulate the progression from H3K27me2 to H3K27me3 are not known. In the context of HSV latency establishment, this will be important to understand. A previous study showed that H3K27me3 did not form on latent genomes until 10–14 days post-infection of mice (129). Whether H3K27me2 forms prior to this and plays a role in lytic-gene repression during entry into latency is unknown.

Given the identified role for PHF20L1 as a repressive H3K27me2 reader, its co-localization with HSV-1 genomes strengthens the evidence for a mechanism by which H3K27me2 represses lytic genes soon after infection of a fibroblast. Hou et al. propose a model whereby PRC2 and NuRD complexes are recruited by PHF20L1 binding to

H3K27me₂, resulting in transcriptional repression in the context of breast tumorigenesis (258). This model may link H3K27me₂ on lytic HSV genomes with the transcriptional repression we observed with H3K27 demethylase inhibition. Interestingly, proteomic studies have shown NuRD complex components associated with both input and replicating HSV-1 genomes (90, 91). This axis would represent a previously undescribed defense mechanism against foreign DNA and a corresponding pro-viral role for H3K27 demethylation during lytic infection. Our data that PHF20L1 association increases following the inhibition of H3K27 demethylation support a role for PHF20L1 in reading H3K27me₂ on viral genomes. However, PHF20L1 can also read mono-methylated H3K4 and H4K20 (283), in addition to interacting with nonspecific lethal (NSL) complex (284, 285). The NSL complex is involved in the active transcription of housekeeping genes and promotes H4K16 acetylation (286). Therefore, it remains possible that PHF20L1 could play multiple roles in HSV-1 gene expression, and investigating these roles may shed some light on the differential functions of PHF20L1 in gene activation and repression. It also remains to be determined whether PHF20L1 plays a role during the establishment of latency in a neuron, where it could be an important component of the factors regulating cell type-specific transcriptional outcomes of HSV-1 infection.

Chapter 3: PRC1-mediated Regulation of Lytic HSV-1 Gene Expression

Some sections of this chapter have been adapted from the following publications in preparation:

Dochnal, SA, Francois, AK, & Cliffe, AR. Histone H2A ubiquitination mediates the establishment of reactivation-competent HSV-1 latent infection. In prep. (2024)

Francois, AK et al. Histone H2A ubiquitination promotes HSV-1 lytic gene expression through reader protein ZRF1. In prep. (2024 est.)

3.1 Abstract

Herpes simplex virus 1 (HSV-1) carries out distinct lytic and latent modes of infection in a host. Viral gene transcription is regulated differently in these contexts, and association with cell histones confers some epigenetic control over viral gene expression. Latent genomes form repressive heterochromatin marked by Polycomb-associated histone post-translational modification H3K27me3. Polycomb repressive complex 2 (PRC2) carries out H3K27 methylation on host chromatin, mediating one branch of Polycomb silencing.

Lytic HSV-1 chromatin is more dynamic, and we have previously shown that Polycomb-mediated H3K27me2 is deposited on a subset of lytic genomes in fibroblasts. We wished to determine whether the other branch of Polycomb silencing, Polycomb repressive complex 1 (PRC1)-mediated H2AK119 ubiquitination modifies HSV-1 chromatin. We first established through chromatin immunoprecipitation that H2AK119ub is present on the latent genome *in vivo*, indicating PRC1 activity contributes to the structure of latent chromatin. We then investigated whether PRC1 modifies lytic HSV-1 chromatin in fibroblasts, first through co-localization analysis with EdC-labeled viral genomes. Although we did not observe significant H2AK119ub co-localization with HSV-1 genomes, PRC1 inhibition with three different compounds restricted lytic gene expression in fibroblasts and epithelial cells. We found that PRC1 subunits RING1A and RING1B co-localize with a large proportion of lytic genomes, supporting the finding that PRC1 activity is pro-transcriptional for lytic HSV-1 genes. We then determined that pro-transcriptional H2AK119ub reader ZRF1/DNAJC2 co-localizes with lytic genomes and is recruited to replication compartments in both fibroblasts and lytic neuronal infection. We

propose a mechanism through which RING1A/B-mediated H2AK119ub promotes HSV-1 gene transcription via host factor ZRF1, a previously unidentified pro-viral host factor.

3.2. Introduction

Polycomb-mediated transcriptional silencing (Polycomb silencing) of mammalian chromatin has proven far from straightforward. Recent studies have revealed the variability in complex composition, accessory proteins, interplay between the two branches (PRC1 and PRC2), and their shifting functions during stages of differentiation (140, 219, 270, 287–289). Some of these findings are described in Chapter 1.

Additionally, cross-talk between the PRC1 and PRC2 pathways is an important feature of Polycomb silencing and *de novo* heterochromatin formation and maintenance (156, 161, 184, 194–196). When it comes to understanding Polycomb regulation of the HSV-1 genome, all these variables must also be considered.

Polycomb regulation is highly conserved, one study reporting that the core PRC1 and PRC2 complexes were present in the last eukaryotic common ancestor and gained complexity as species evolved (290). The more recent model for facultative heterochromatin formation during mouse embryonic development involves vPRC1-mediated H2AK119ub deposition, which then recruits PRC2 and facilitates H3K27 methylation (156, 280, 291–294). Multiple mechanisms of PRC1 recruitment have been observed (summarized in Chapter 1), including CpG island recognition, binding specific DNA sequences, and long non-coding RNA interaction (195, 270). In addition to the updated order of PRC1 activity relative to PRC2, more nuance exists in the existence of canonical (cPRC1) and variant (vPRC1, also referred to as non-canonical) complexes. Despite its name, vPRC1 appears to predominantly perform *de novo* H2AK119 ubiquitination, allowing heterochromatin to form independently from PRC2 activity (156, 270).

Although it does not seem to mediate much H2AK119 ubiquitination, cPRC1 can structurally compact chromatin (295–297). Polycomb domains span broad regions of chromatin and nucleosomes are physically compacted, physical restriction making the DNA inaccessible to transcriptional machinery (295). an important aspect of transcriptional repression. Chromobox (CBX) proteins are subunits of cPRC1 that can recognize H3K27me3, providing the opportunity for feedback in the PRC2 to PRC1 direction (174). Described by Yu et al. as reciprocal recruitment, the hypothetical series of events is as follows: vPRC1 ubiquitinates H2AK119ub, beginning *de novo* heterochromatin formation; PRC2.2 is recruited through accessory protein JARID2 binding the H2AK119ub; PRC2.2 carries out sequential H3K27 methylation, ultimately arriving at H3K27me3; PRC2.2 stably associates with H3K27me3; and cPRC1 is recruited to H3K27me3 via CBX protein binding, compacting the chromatin (140, 154). cPRC1 also contains the RING1A/B catalytic subunit and could thus continue the cycle by recruiting more PRC2. This feedback loop allows maintenance of repressive domains, a process distinct from initial *de novo* heterochromatin formation.

The PRC1-mediated branch of Polycomb silencing is now known to function in many processes, embryonic development and beyond, including: hematopoietic stem cell differentiation (190); X chromosome inactivation (298–300); neural progenitor cell maintenance (209, 210, 213); embryonic neurogenesis (192, 288, 301–303); marking damaged DNA for repair (304, 305); and UV damage-induced senescence (205, 306). Numerous cancers show perturbations in some aspect of PRC1-mediated gene regulation, demonstrating the continued importance of Polycomb regulation beyond embryogenesis (184, 188, 196, 204, 219, 288). PRC1 activity is no longer regarded as exclusively repressive, with transcriptional activation at sites of H2AK119ub through reader protein Zuo1in-Related Factor 1 (ZRF1) (207, 208, 216). This is an exciting and

relatively new aspect of PRC1 activity that is still being characterized in processes including neurodevelopment (209, 210, 213, 217).

In addition to the aforementioned roles, Polycomb silencing is involved in regulating herpesvirus gene expression. A herpesvirus genome enters the cell nucleus absent of nucleosomes, and thus absent of any pre-existing epigenetic template (234). Heterochromatin formed on the viral genome would be formed *de novo*, a process distinct from heterochromatin maintenance on mammalian chromatin. The terminally differentiated state of cells infected by HSV-1 *in vivo* is also distinct from the pluripotent context in which Polycomb silencing is frequently studied. In aiming to understand the roles of Polycomb silencing in HSV-1 infection, and particularly which complex variants may be responsible, these distinctions should be kept in mind.

Polycomb silencing through vPRC1 has been described on the latent KSHV genome, with accompanying H2AK119ub deposition (222, 230). In comparison with murine gammaherpesvirus MHV-68, the KSHV genome more efficiently and broadly recruits PRC1 (222). Gunther et al. conclude that genomic features (CpG islands) enriched on the KSHV genome promote this recruitment through KDM2B binding (180). This study specifically names vPRC1, which is consistent with the vPRC1-dominant mechanism of *de novo* Polycomb silencing on host chromatin (156, 184). The authors suggest these findings reflect herpesvirus adaptation of *cis*-acting genomic features to exploit host Polycomb silencing (222). Another study using siRNA-mediated knockdown screens identified KDM2B as restrictive to lytic KSHV replication, supporting the notion that this cell factor represses viral gene expression (307). Intriguingly, vPRC1 component RYBP has also been shown to repress KSHV lytic gene transcription outside of the PRC1 complex (308), demonstrating the potential for individual Polycomb subunits to functionally repress transcription by separate mechanisms. BMI1, a component of the

cPRC1 complex, is important for maintaining KSHV latent infection and BMI1 knockdown induces reactivation (309), a finding that aligns with heterochromatin maintenance mediated by cPRC1 (154). Epstein-Barr virus (EBV) similarly uses epigenetics to regulate latency and lytic gene expression, with the addition of repressive DNA methylation at CpG motifs (231, 233), while HSV-1 latent chromatin does not show evidence of DNA methylation (125). These studies highlight that individual herpesviruses can have unique means of exploiting host Polycomb silencing, likely selected for in their specific cell types for lytic and latent infection.

In the previous chapter, H3K27 di-methylation was shown to repress incoming HSV-1 genomes in fibroblasts. These findings contribute to our understanding of the relatively understudied role of PRC2 and the virus' exploitation of the H3K27 demethylases. Following latent infection *in vivo*, the detection of H3K27me3 on HSV-1 chromatin only after 10-14 days post-infection implies that other chromatin modifications could precede H3K27me3 (129, 132). PRC1 subunit BMI1 was first detected on latent HSV-1 chromatin (242), albeit at very low levels on the lytic promoters, and a further study confirmed this low level of recruitment (129). Regardless, BMI1 is only one of two PGCF proteins that form cPRC1 that form vPRC1, and its absence does not rule out PRC1 involvement.

H3K27me3 detected on latent HSV-1 chromatin likely represents the maintenance of Polycomb repression, but the onset of *de novo* heterochromatin formation has been difficult to observe. The same mechanism underlying H3K27me2 formation on lytic HSV-1 chromatin could occur during the establishment of latency, when *de novo* heterochromatin formation occurs, eventually fully methylated to the H3K27me3 state for the maintenance of latency. Given the evidence for vPRC1 activity preceding PRC2 recruitment during *de novo* heterochromatin formation on mammalian

chromatin, it is possible that vPRC1 activity precedes any PRC2 recruitment on HSV-1 genomes. This model would apply to the *de novo* heterochromatin formation stage during early *in vivo* infection with HSV-1. Given the cross-talk between the two branches of Polycomb silencing (194, 195, 280), and the evidence for PRC1 involvement in other latent herpesvirus' chromatin structures (129, 222, 242, 308), we must establish whether PRC1 informs HSV-1 chromatin structure. Any roles for the PRC1 complexes and H2AK119 ubiquitination in shaping *de novo* HSV-1 chromatin formation would be novel insights into both viral and cell Polycomb silencing.

We hypothesize that H2AK119ub is laid down first by PRC1 before PRC2 can carry out H3K27 methylation previously described. H2AK119ub kinetics on host chromatin are more rapid than those of full H3K27 trimethylation, which lends itself to this sequence of events (270). It is thus possible that HSV-1 transcriptional silencing during the establishment of latency is mediated by PRC1 activity, followed by later PRC2 activity. Whether or not PRC1 regulates lytic gene expression is also of interest for comparison with the events of non-neuronal, lytic infection.

We first set out to confirm whether H2AK119ub is present on the latent HSV-1 genome *in vivo* by ChIP-qPCR of trigeminal ganglia from latently infected mice. We find enrichment of H2AK119ub on lytic promoters, informing an updated model for latent HSV-1 chromatin featuring both H3K27me3 and H2AK119ub. To observe *de novo* heterochromatin dynamics, we then tested the hypothesis that H2AK119ub on the lytic genome represses lytic gene transcription in non-neuronal cells, first examining whether H2AK119ub co-localizes with individual viral genomes in the nucleus. Despite a lack of robust co-localization with H2AK119ub, inhibition of PRC1 activity caused a strong change in lytic gene expression in fibroblasts. In contrast to our hypothesis, PRC1 inhibition significantly impaired lytic gene transcription. We then determine that RING1A

and RING1B co-localize with viral DNA, as does the H2AK119ub reader protein ZRF1 (DNAJC2). We propose an axis through which H2AK119ub is deposited on the lytic genome by RING1A/B and lytic gene transcription activated by reader ZRF1, skirting Polycomb repression and exploiting the mechanism in non-neuronal cells.

3.3. Results

3.3.1. H2AK119ub Is Enriched on The Latent HSV-1 Genome *In Vivo*.

Ocular infection with HSV-1 allows the virus to establish latency *in vivo* in the trigeminal ganglia. Latently infected trigeminal ganglia have been used to characterize latent HSV-1 chromatin, and determine the presence of Polycomb-related proteins. (124, 129, 242). Trigeminal ganglia were harvested from latently infected mice 30 days post-ocular infection. ChIP was performed against an IgG negative control, total H2A and H2AK119ub. Quantification of enrichment over input material by qPCR showed both H2A and H2AK119ub were enriched at the ICP27 and ICP8 promoters compared to IgG controls (Figure 3.1). These results mirror previous findings that H3K27me3 is enriched at the same promoters (129) and indicate that H2AK119ub formation occurs somewhere in the lead up to latency establishment *in vivo*.

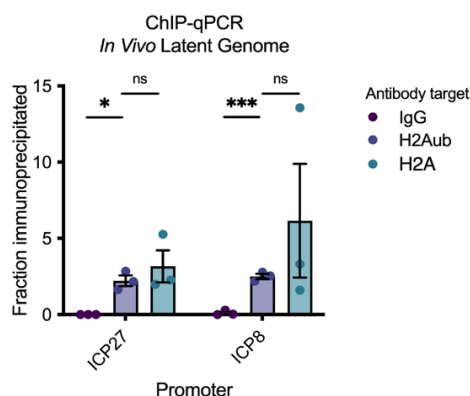


Figure 3.1: HSV-1 genomes from latently infected ganglia show enrichment for H2AK119ub at the lytic ICP27 and ICP8 promoters.

ChIP was performed on latently infected trigeminal ganglia harvested 30 days post-infection, and relative DNA quantity determined by qPCR. IP values were normalized over corresponding sample input material values. IgG is a negative control. Multiple Welch's t-tests, * $p < 0.05$, *** $p < 0.005$. *In vivo* infections performed by Anna Cliffe, ganglia processing, ChIP-qPCR and data analysis by Alison Francois and Anna Cliffe. This data set is also included in Sara Dochnal's dissertation (310).

3.3.2. H2AK119ub is Not Detected on Lytic HSV-1 Chromatin.

Following the finding that H2AK119ub is on latent HSV-1 chromatin *in vivo*, we set out to determine whether the histone modification is deposited during lytic infection. Given our previous findings of repression by PRC2-mediated H3K27me2 on a subset of lytic genomes in fibroblasts, we chose to determine whether a similar phenomenon is seen for H2AK119 formation. Using the colocalization assay previously introduced and EdC-labeled HSV-1 DNA (Chapter 2), we assessed individual viral genomes for colocalization with H2AK119ub at 2 and 4 hours post-infection of human foreskin fibroblasts (HFFs).

Notably, our collaborators in the Rothbart laboratory (Van Andel Institute) screened H2AK119ub antibodies for non-specificity, but technical constraints with recombinant histone peptide generation necessitated western blot analysis instead of the peptide binding arrays featured in chapter 2. Figure 6.4 shows the western blot conducted for two antibodies, Millipore E6C5 and CST 8240S, and found H2AK119ub specificity only for the latter antibody. We thus proceeded with immunostaining using the CST antibody against H2AK119ub.

Representative images are shown in Figure 3.2A. NucSpotA quantification was used to quantify immunostain intensity at the viral genome relative to the whole nucleus, and some instances of co-localization were observed by eye. However, comparison with rotated images (random placement controls) showed H2AK119ub co-localization with HSV-1 DNA was below that expected by chance at 2 HPI and similar to values expected by chance at 4 HPI (Figure 3.2B). This result suggested we were not observing biologically meaningful co-localization of lytic HSV-1 genomes with H2AK119ub.

We next performed chromatin immunoprecipitation (ChIP)-qPCR on HFFs 1 HPI to quantify H2AK119ub enrichment on specific viral promoters, drawing comparison with

enrichment at host promoters using GAPDH as the negative control and HoxA1 as the positive control. These regions were chosen from the antibody product validation data (CST 8240S). Fold enrichment over the input material quantified by qPCR (Figure 3.2C) shows significant enrichment over IgG for both host regions, despite one serving as a negative control. This result likely speaks to non-specific binding, or results from cell type-specific epigenetics causing higher than expected enrichment at the GAPDH promoter. Regardless, enrichment at viral promoters *ICP27* and *ICP8* is significantly lower than either host region, and not significantly different from the IgG negative control. Ultimately, we could not find evidence for H2AK119ub on individual viral genomes by imaging assay, or on bulk chromatin by CHIP-qPCR at 1 HPI.

3.3.3. PRC1 Inhibition Restricts Lytic Gene Transcription.

In case the failure to observe H2AK119ub on lytic HSV-1 chromatin resulted from technical and residue-specific limitations, we also performed gene expression experiments to determine the functional effect of PRC1 inhibition during infection. We first used inhibitor PRT4165, which targets BMI1 and RING1A to inhibit H2AK119 ubiquitination. Cells pre-treated and infected in the presence of the inhibitor were expected to show enhanced lytic gene expression, presuming loss of H2AK119ub would relieve transcriptional repression. However, the opposite phenotype was seen, with PRT4165 treatment significantly impairing lytic gene transcription in HFFs by 5 HPI (Figure 3.4A-B).

To ensure this observation was not a cell type-specific phenomenon, we also infected epithelial cells (ARPE-19s) with PRT4165 treatment and saw the same phenotype (Figure 3.4C-D). Lastly, we used a separate BMI1 inhibitor, PTC-209, in consideration for potential off-target effects caused by PRT4165. PTC-209 recapitulated the phenotype of transcriptional repression by 5 HPI in ARPE-19s (Figure 3.4E-F). This result has also been confirmed by other lab members using a more specific Ring1 inhibitor known as RB-3 (Figure 3.3G-H) (311). These results indicated that PRC1 does functionally impact lytic gene expression, so we next set out to identify the PRC1 subunits involved.

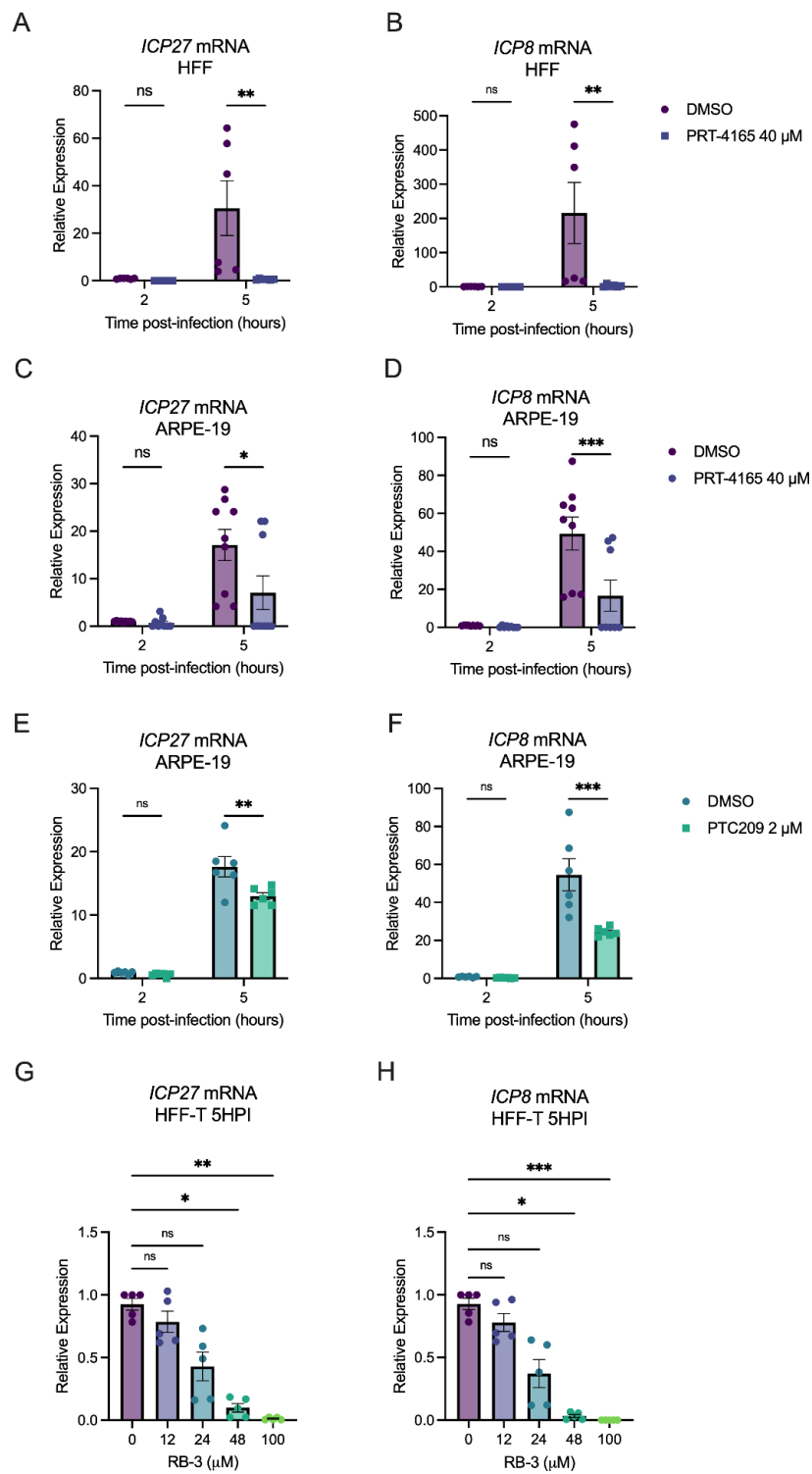


Figure 3.3: Lytic gene expression is restricted by PRC1 inhibition in both fibroblasts (HFFs) and epithelial cells (ARPE-19s).

Cells were pre-treated 1h with inhibitors before infection with inhibitor treatment at MOI 3. Expression is relative to g-actin expression. *ICP27* is used as an immediate early class gene, and *ICP8* as an early gene. RNA lysate was harvested 2 and 5 hours post-addition of inoculum. **A-B.** Lytic gene expression in HFFs treated with PRT4165. **C-D.** Lytic gene expression ARPE-19s treated with PRT4165. **E-F.** Lytic gene expression in ARPE-19s treated with a separate PRC1 inhibitor, PTC209. Multiple Mann-Whitney tests. **G-H.** Dose-response of lytic gene expression in the presence of PRC1 inhibitor RB-3. Immortalized HFFs (HFF-Ts) were not pre-treated, the inhibitor added at the time of infection. Friedman tests. * $p < 0.05$, ** $p < 0.005$, *** $p < 0.0005$ A-B: 2 experimental replicates, $n=3$ data points per replicate. Experiment and data analysis by Alison Francois. C-D: 3 experimental replicates, 2 by Alison Francois and 1 by Sara Dochnal. 3 data points per replicate, collated. E-F: 2 replicates, 3 data points per replicate. Experiments and data analysis by Sara Dochnal. G-H: 3 replicates, 5 collated data points. Experiment and data analysis by James Boehlke.

3.3.4. RING1A/B Co-localize with a Subset of Lytic HSV-1 Genomes.

We next chose to determine whether the enzymatic subunit RING1B (also referred to as RNF1) is associated with HSV-1 DNA during lytic infection of fibroblasts. RING1B is an E3 ubiquitin ligase that facilitates the ubiquitination of H2AK119ub, PRC1 does not necessarily remain bound to chromatin once ubiquitination is complete (312), in contrast with PRC2 stably binding and occupying sites of H3K27me3 (140). Given the functional phenotype we observed with PRC1 inhibitors, we continued pursuing PRC1 activity on HSV-1 gene transcription. We chose to look for co-localization with the enzymatic subunits of PRC1 complexes, RING1A and RING1B, as one of the two will be present in all versions of vPRC1 or cPRC1.

Using our imaging assay, we observed strong co-localization of RING1B with viral EdC-labeled viral DNA in HFFs 2 and 4 HPI. Representative images of infected

nuclei (Figure 3.5A) show three examples of RING1B co-localization with viral DNA 2 HPI (top panels) and 4 HPI (lower panels). An intensity ratio threshold was chosen and calibrated by eye, the dashed lines in Figure 3.5B indicating this threshold and the percentages reflecting the proportion of genomes above the threshold.

Interestingly, by 4 HPI a minority of nuclei showed a punctate staining pattern with only a handful of bright foci (second and third rows of lower panel), demonstrating heterogeneous RING1B patterning during this stage of lytic infection. Comparison with rotated images (random placement controls, Figure 3.5B) showed roughly a third of genomes co-localized with RING1B 2 HPI, but a similar proportion of randomly placed genomes did as well (35% and 30% of genomes fall above the co-localization threshold). By 4 HPI co-localization with RING1B differed significantly from random placement (47% compared to 40%) of genomes above the threshold), indicating a biologically meaningful association with RING1B by at least a subset of lytic genomes.

To validate this RING1B phenotype, we performed siRNA knockdown of RING1B and saw loss of RING1B stain intensity in the knockdown cells. Figure 3.5C shows the mean intensity of RING1B at individual viral genomes, all images standardized to the same visualization parameters. Mean intensity of RING1B at lytic genomes is significantly reduced in knockdown cells, indicating this immunostain phenotype is indeed reflective of RING1B and not resulting from non-specific binding. Figure 3.5D shows NucSpotA quantification of stain intensity across the nucleus, above the threshold chosen to exclude areas without signal. Nuclei treated with siRNA against RING1B showed significantly dimmer RING1B staining, also validating the phenotype seen with this RING1B antibody.

RING1A is the other enzymatic subunit a PRC1 complex can contain. There is a fair amount of redundancy between RING1A and RING1B (313), and any mechanism

regulating lytic gene transcription could also feature a complex with RING1A or RING1B. We also observed co-localization of viral genomes with RING1A, as shown in Figure 3.6A. Rotational analysis showed RING1A co-localization with viral genomes is not greater than that expected by chance 2 HPI (29% and 31% of genomes above the threshold), whereas significantly more were co-localized than by random placement at 4 HPI (42% compared to 28% above the threshold), with very similar results to RING1B. These findings support a role for PRC1 activity in promoting HSV-1 lytic gene transcription.

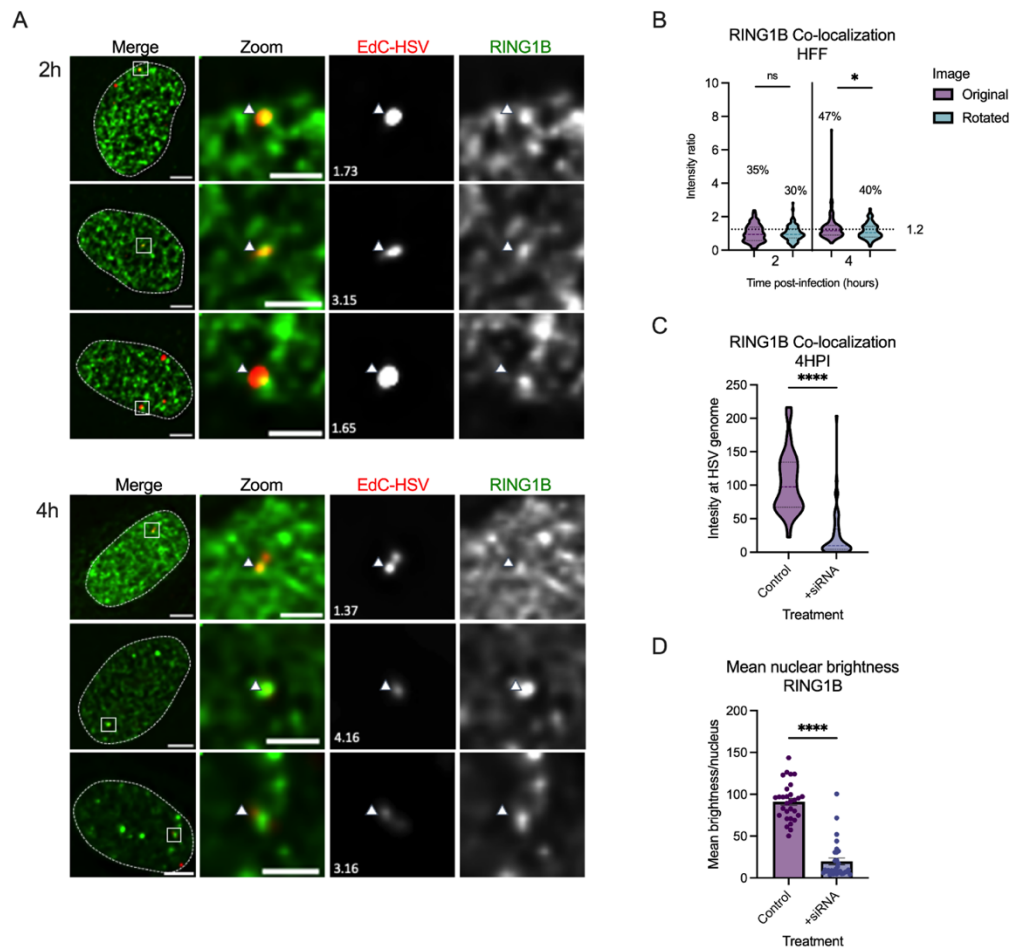


Figure 3.4: RING1B co-localizes with a subset of lytic genomes.

A. Representative images of HFF nuclei 2 and 4 HPI, zoomed in on each viral genome. Arrows indicate the same location in each channel. Intensity ratios are superimposed over each viral genome's image. Merge image scale bars= 10 μm , zoom image scale bars=5 μm . **B.** Violin plots of signal intensity ratios at viral genomes, calculated using NucSpotA. Rotation analysis for RING1B co-localization with lytic genomes. Rotated images were generated by rotating the viral genome channel relative to the others and were used as random placement controls. Percentages indicate the proportion of genomes with intensity ratios above the co-localization threshold (dashed line). Paired Wilcoxon tests, $*p < 0.005$. Data collated from 3 experimental replicates, at least two independent infections imaged each. **C.** RING1B siRNA knockdown in HFFs compared with unmodified cells. RING1B immunostain signal at viral genomes is shown, all images standardized to the same RING1B channel settings. Mann-Whitney test, $****p < 0.0001$. Single experimental replicate, 30 cells analyzed. **D.** Using the same images as C, brightness above the NucSpotA threshold of 65% stain intensity (to select for visually confirmed positive signal) is shown. Mann-Whitney test, $****p < 0.0001$. Single experimental replicate, 30 cells analyzed. *Data collection and analysis by Alison Francois.*

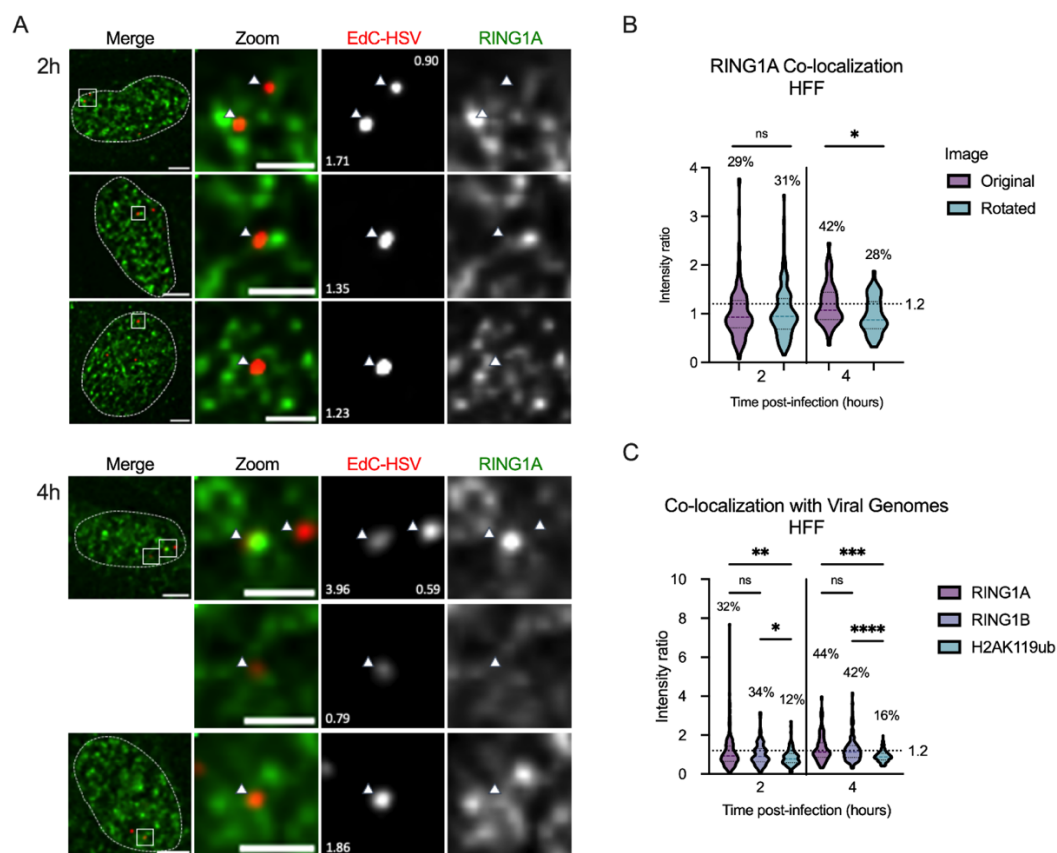


Figure 3.5: RING1A also co-localizes with a subset of lytic HSV-1 genomes 4 HPI.

A. Representative images of HFF nuclei 2 and 4 HPI, zoomed in on each viral genome. Arrows indicate the same location in each channel. Intensity ratios are superimposed over each viral genome's image. Merge image scale bars= 10 μm , zoom image scale bars=5 μm . **B.** Violin plots of signal intensity ratios at viral genomes, calculated using NucSpotA. Rotational analysis for RING1A co-localization with lytic genomes. Rotated images were generated by rotating the viral genome channel relative to the others and were used as random placement controls. Percentages indicate the proportion of genomes with intensity ratios above the co-localization threshold (dashed line). Paired Wilcoxon tests, * $p < 0.005$. Data collated from 2 (2 HPI) and 1 (4 HPI) experimental replicates, at least two independent infections each. **C.** Comparison between the co-localization values for RING1A, RING1B and H2AK119ub at 2 and 4 HPI. Data analysis of the same images analyzed in panel B, and Figures 2A-B and 3A-B. Kruskal Wallis tests, * $p < 0.05$, ** $p < 0.005$, *** $p < 0.0005$, **** $p < 0.0001$. *Data collection and analysis by Alison Francois.*

3.3.5. PRC1 Inhibition Reveals RING1A at Input Genomes in Transcriptionally Active Infected Cells.

We next used a third PRC1 inhibitor, RB-3, to explore the roles of RING1A and RING1B during lytic infection. We first validated that the BMI1/RING1B inhibitor restricts lytic gene expression like the effects of PRT4165 and PTC209 (Figure 3.3). Immortalized HFFs (HFF-Ts) were infected with RB-3 at different concentrations, and a dose response-dependent restriction was observed for immediate early ICP27 and ICP8 transcripts (Figure 3.6A-B). These findings support the phenotypes seen in Figure 3.3, suggesting the restriction is not due to an off-target effect, and further indicating PRC1 activity promotes lytic gene expression.

We next used RB-3 to assay infected cells for H2AK119ub co-localization, with the expectation of seeing lower intensity ratios for RB-3 treated genomes. Cells were categorized by the presence or absence of ICP4 immunostaining anywhere in the nucleus, in an attempt to observe changes only on a subset of lytic genomes (those that are positive for ICP4 have initiated the lytic infection cycle). Intensity ratios for individual genomes, split by ICP4 phenotype, are shown for cells 2 HPI and 5 HPI (Figure 3.6C-D). H2AK119ub co-localization was not impacted by RB-3 treatment in either ICP4+ or ICP4- cells, which was somewhat surprising given the functional effect of PRC1 inhibition observed earlier. However, this does align with the results in Figure 3.2A-B, in which we also could not observe significant H2AK119ub co-localization.

Performing the same assay for RING1A and RING1B immunostaining 5 HPI, we found that RING1A co-localization with lytic genomes in ICP4+ cells was significantly impaired by RB-3 treatment (Figure 3.6E), and co-localization with RING1A was significantly greater for ICP4+ than ICP4- untreated cells. RING1B co-localization was

not impacted by RB-3 treatment (Figure 3.6F) and was not significantly more co-localized in ICP4+ cells. These findings indicate a possible role specifically for RING1A at this time post-infection.

Lastly, categorizing the infected cells within imaged fields of view by the presence of ICP4 protein (Figure 3.6G), determined to be infected by the presence of any EdC-labeled input HSV-1 genomes, revealed that a greater proportion of nuclei were ICP4+ both 2 and 5 HPI than the RB-3-treated nuclei. The percentage of ICP4+ genomes was still relatively high in either case, 77% and 59% (untreated and treated respectively) of nuclei 2 HPI and 80 and 45% (untreated and treated respectively) of nuclei 5 HPI were ICP4+. This finding suggests RB-3 treatment causes some impairment of lytic gene transcription, in agreement with the functional effects of RB-3 treatment on lytic gene expression (Figure 3.6A-B). Collectively, the results from comparing untreated and RB-3-treated cells support a pro-transcriptional role for PRC1 activity in fibroblasts.

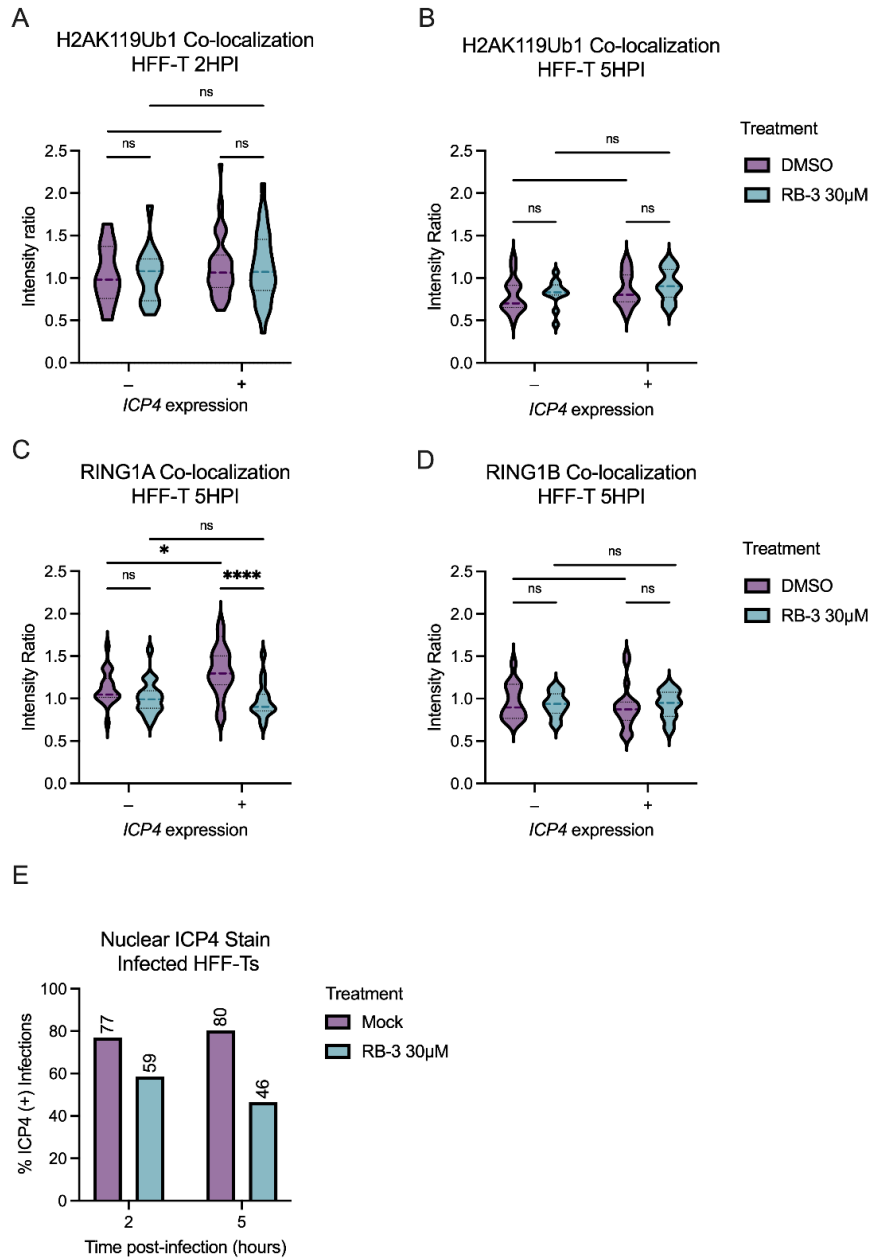


Figure 3.6: PRC1 inhibitor RB-3 causes loss of RING1A at input genomes in cells expressing ICP4.

A-B. Violin plots of signal intensity ratios at viral genomes, calculated using NucSpotA. Co-localization analysis for H2AK119ub with input viral genomes in untreated and RB-3 treated HFF-Ts 2 HPI (A) and 5 HPI (B). Cells were categorized as ICP4+ or ICP4- by visual confirmation of ICP4 immunostaining anywhere in the infected nucleus. 2-way ANOVA. **C.** Violin plots showing co-localization intensity ratios for RING1A with input viral genomes in untreated and RB-3-treated HFF-Ts 5 HPI. 2-way ANOVA. **D.** Violin plots of co-localization intensity ratios for RING1B with input viral genomes in untreated and RB-3-treated HFF-Ts 5 HPI. 2-way ANOVA. **E.** Sampled HFF-T nuclei containing input genome(s) were categorized visually by the presence of any ICP4 immunostain. ICP4 is a lytic transcript, indicative of viral transcription. The percentage of nuclei in each category is listed above the corresponding bar. * $p < 0.05$, **** $p < 0.0001$. *Experiments, data collection and analysis by James Boehlke, with the exception of data analysis for panels A and E by Alison Francois.*

3.3.6. Pro-Transcriptional H2AK119ub Reader ZRF1 Co-Localizes with Lytic HSV-1 Genomes and Replication Compartments.

Following our findings that H2AK119ub deposition promotes lytic transcription, we set out to identify the reader protein that would mediate this activity. Several publications in the last decade have described a pro-transcriptional role for Zuotin-related factor 1 (ZRF1, also DNAJC2 or MPP11) as a reader of H2AK119ub (207, 217, 314). ZRF1 has both cytoplasmic (protein chaperone) and nuclear (H2AK119ub reader) functions and is thus localized throughout the cell (315). We hypothesized that the pro-transcriptional effect of PRC1 activity in HSV-1 lytic infection is mediated by ZRF1.

Initial immunostaining against ZRF1 (Novus rabbit antibody) showed strong co-localization with EdC-labeled input HSV-1 genomes in HFFs 4 HPI (Figure 3.7A). Quantification of ZRF1 colocalization with lytic genomes using this antibody (Figure 3.7B) showed 41% of genomes at 2 HPI and 97% at 4 HPI fall above the chosen

colocalization threshold. An additional antibody (Santa Cruz, mouse) was also used to account for potential non-specific binding by the first antibody, and co-localization was high at both time points with 88% and 95% of genomes above the threshold 2 and 4 HPI (Figure 3.7C). Representative images using the mouse antibody against ZRF1 are shown in Figure 6.5. The staining pattern at 4 HPI (both antibodies) was similar to the shape of replication compartments (RCs), so we also co-stained infected cells for ZRF1 and ICP4 (as an indicator of RCs) and found ZRF1 enrichment overlaps with the ICP4/RC staining (Figure 3.7D).

Lastly, we transfected vero cells with a FLAG-tagged ZRF1 construct and infected them at a high MOI (20 PFU/ml) for 4 hours. An EdC pulse 30 minutes before fixation was performed to allow EdC incorporation into replication compartments. Using click chemistry to visualize replication compartments and immunostaining against the FLAG epitope, we saw exogenously expressed ZRF1 concentrated in replication compartments relative to the surrounding nuclear stain (Figure 3.7F). These findings, and the re-localization to RCs observed for ZRF1 between 1 and 4 HPI (Figure 3.7E) suggest to us that ZRF1 is recruited to replication compartments. The presence of ZRF1 raises the possibility that ZRF1 is functioning as a H2AK119ub reader of the lytic HSV-1 genome and promoting lytic gene transcription.

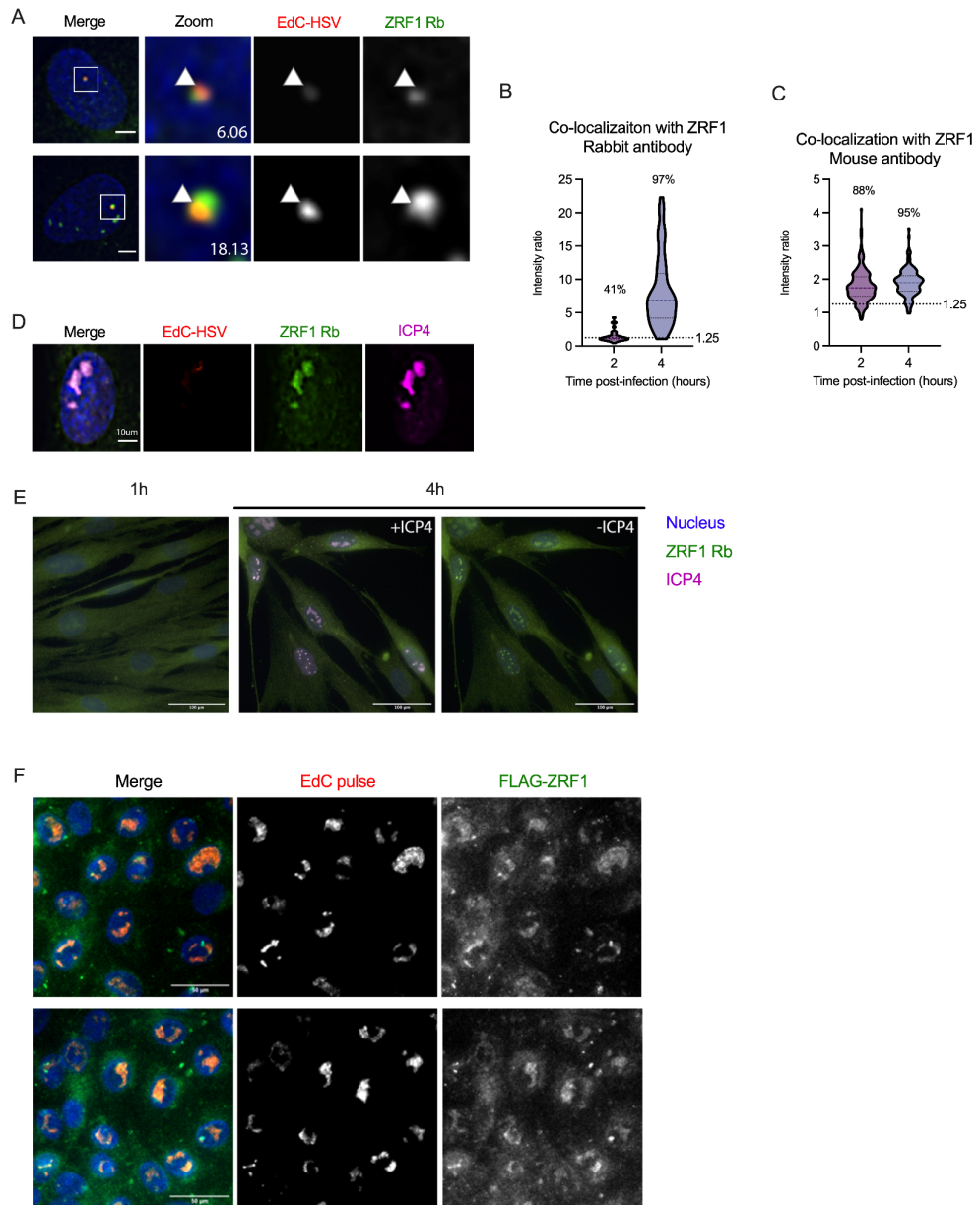


Figure 3.7: H2AK119ub reader ZRF1 co-localizes with lytic genomes and is recruited to replication compartments in fibroblasts.

A. Representative images of HFF nuclei 4 HPI immunostained for ZRF1 with the rabbit antibody (Novus) zoomed in on each viral genome. Arrows indicate the same location in each channel. Intensity ratios are superimposed over each viral genome's image. Merge image scale bars= 10 μm , zoom image scale bars=5 μm . **B.** NucSpotA quantification of co-localization of viral genomes with ZRF1 2 and 4 HPI, including the data represented in A, using the rabbit antibody. Percentages indicate the proportion of genomes with intensity ratios above the co-localization threshold (dashed line). Two experimental replicates, each of two infections in parallel **C.** Quantification of independent infections using a mouse ZRF1 antibody (Santa Cruz), images from 2 experimental replicates of 2 infections each. Percentages indicate the proportion of genomes with intensity ratios above the co-localization threshold (dashed line) **D.** An infected HFF nucleus 4 HPI co-stained for ZRF1 (rabbit antibody) and lytic gene product ICP4, used here to identify replication compartments, and input HSV-1 genomes. **E.** Representative fields of view showing ZRF1 staining (rabbit antibody) 1 and 4 HPI. 4 HPI images are the same field of view, labeled as +ICP4 (including ICP4 staining in the merged image) or -ICP4 (showing only ZRF1 staining). Scale bar=100 μm . **F.** Vero cells transfected with a FLAG-tagged ZRF1 construct, infected at a high MOI (20 PFU/cell) with HSV-1 for 4 hours. An EdC pulse (10 μM) was added 30 minutes prior to fixation, and click chemistry used to visualize replication compartments. Representative fields of view are shown, selected from three transfections performed in parallel. Scale bar=50 μm . *Experiments, data collection and analysis and figure compilation by Alison Francois.*

3.3.7. ZRF1 is Expressed in Neurons and Re-Localizes to Replication Compartments During Neuronal Lytic Infection.

An important aspect of HSV-1 biology is the contrasting infection outcomes of lytic and latent infection. It occurred to us that a pro-transcriptional host factor could be differentially expressed by cell type and could thus be a factor in the cell type-specific outcomes of HSV-1 infection. We first wanted to determine whether ZRF1 expression was detected in neuronal cell lysates. Although ZRF1 has defined roles in neurodevelopment and differentiation, it was not evident whether terminally differentiated

sensory neurons express ZRF1, whether different isoforms are expressed, or where it would be localized in the cell. PRC2 accessory protein and H2AK119ub reader JARID2 was found by our group to exist exclusively in a truncated form without a ubiquitin-binding domain in murine sensory neurons (310).

To address this uncertainty, cell lysates were run on an SDS-PAGE gel, transferred and blotted for ZRF1 protein (Figure 3.8A). Murine dermal fibroblasts and SCG neurons, human mesencephalic (LUHMES) cells and human retinal pigmented epithelial (ARPE-19) cell lysates all showed ZRF1 expression. Each lane showed many bands outside the predicted size (indicated on Figure 3.8A), with some variation in the combination of bands between the cell lysates. This blot confirmed that ZRF1 is expressed in human and murine non-neuronal and neuronal cell types, and the banding pattern indicated the potential for the presence of multiple isoforms. We also blotted with another antibody against ZRF1 (Figure 6.6A-D) and saw a distinct but similarly complex variety of band sizes, and siRNA-mediated knockdown was performed to identify the “correct” band in case the other bands represent off-target protein binding (5.6E).

We next set out to determine whether ZRF1 is involved in lytic infection of a neuron for comparison with our findings in non-neuronal cells. Figure 3.8B shows representative images of lytically infected SCG neurons (infection in the absence of antiviral acyclovir) immunostained for ZRF1 (rabbit antibody). There is a striking pattern of ZRF1 intensity within the nucleus 8 HPI, reminiscent of RCs during non-neuronal infection. This staining pattern also shows re-localization from broadly nuclear and cytoplasmic before infection to intensely bright foci during lytic replication. These findings indicate that ZRF1 is also recruited to RCs in lytic neuronal infection, and thus could mediate transcriptional activation in the neuronal cell environment.

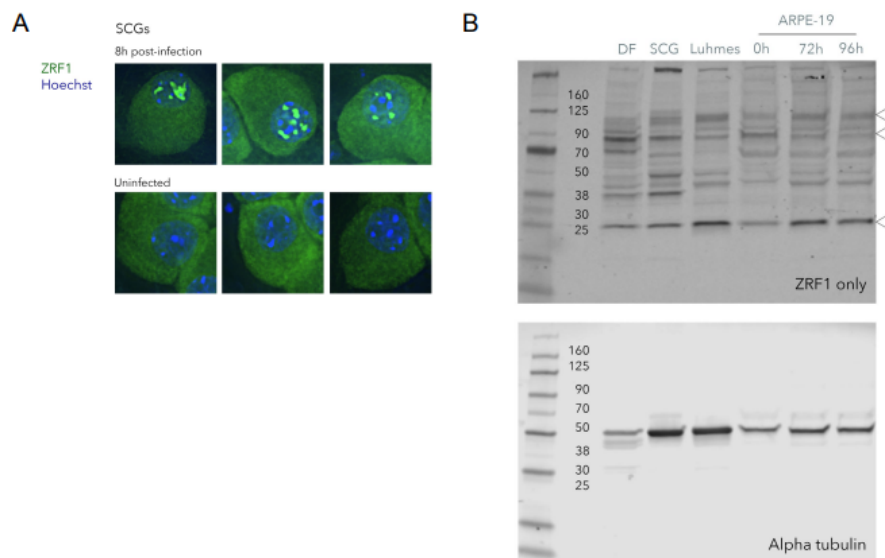


Figure 3.8: ZRF1 is expressed in neuronal cells and recruited to replication compartments during lytic neuronal infection.

A. Superior cervical ganglia (SCG) neurons cultured *in vitro*, uninfected and infected lytically with HSV-1 8 HPI. Staining for ZRF1 (rabbit antibody) is shown for three representative cells in each condition. **B.** Western blots for one membrane sequentially blotted for ZRF1 (top panel, antibody) and loading control alpha tubulin (lower panel). Cells in each lane are, in order: primary dermal fibroblasts (DFs, murine); primary SCG neurons (murine); Lund human mesencephalic neuronal cells (LUHMES), human embryonic neuronal precursor cells induced to differentiate *in vitro*; retinal pigmented epithelial cells (ARPE-19s). Ladder band sizes are labeled with their protein size in kDa. PVDF membrane was visualized using ECL. *Experiments and data analysis by Alison Francois. DF and SCG cell lysates used for panel B were provided by Sara Dochnal.*

3.3.8. Total ZRF1 Expression and S47 Phosphorylation Change as a Consequence of Lytic Infection In Fibroblasts.

HSV-1 is known to modulate the host proteome throughout infection, by means including host protein shutoff (316, 317), targeting proteins for degradation (77, 78, 318) and broadly increasing protein phosphorylation (319). Expanding on the hypothesis that ZRF1 is pro-transcriptional for the viral genome, we wished to determine whether ZRF1 protein levels and phosphorylation are modulated during lytic infection. We blotted uninfected and infected (2, 4 and 6 HPI) HFF cell lysates for total ZRF1 and phospho-S47 ZRF1 (Figure 3.9B-C), stripping and re-probing the same membrane. The lower portion of the membrane was separately probed for H3 (loading control) and ID1. ID1 blocks ZRF1 recruitment (209), and a change in ID1 expression could impact ZRF1 activity without total ZRF1 levels changing.

Total ZRF1 levels at the indicated band size increased from 2-6 HPI, while pZRF1 S47 dropped over the same time frame. ID1 signal was faint but indicated its loss during infection., which is consistent with previous mass spectrometry data published by our collaborator Dr Colin Crump, represented in Figure 3.9A (320) The indicated band intensity was normalized to H3 intensity and plotted in Figure 3.9C. These results suggest that total ZRF1 is upregulated during infection, and ID1 may be targeted for degradation, both changes promoting lytic gene expression.

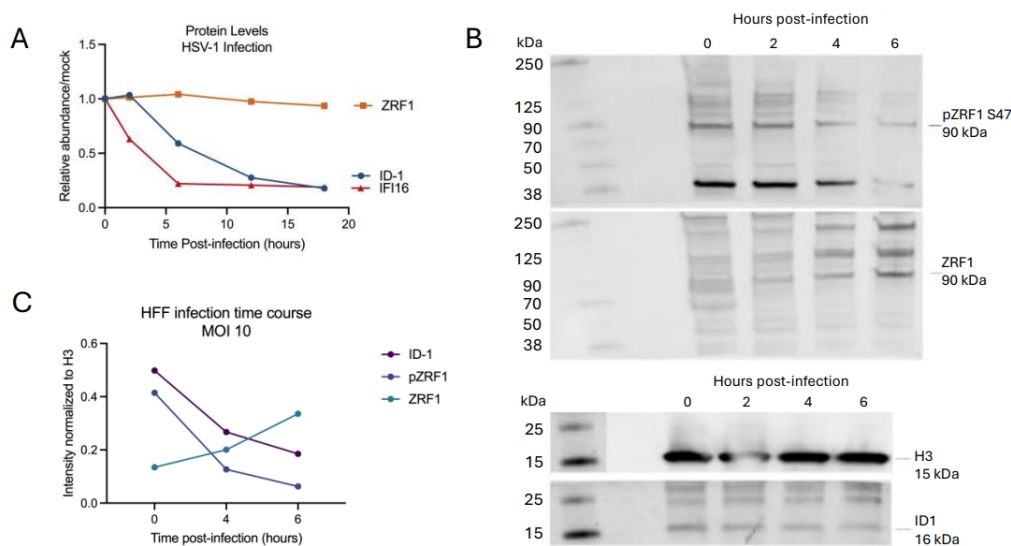


Figure 3.9: ZR1, pZRF1 and ID1 protein levels shift over 6 hours of lytic infection.

A. Mass spectrometry results for relative protein levels during lytic infection of HaCaT cells infected with HSV-1 at an MOI of 10 PFU/cell. IFI16 is included as an example of another host protein. Compiled by Anna Cliffe using published data (Soh et al., 2020) (320). **B.** Cell lysate from mock and HSV-1 infected HFFs (MOI 10 PFU/cell) 2, 4 and 6 HPI was run on an SDS-PAGE gel and sequentially blotted. Upper panel: phosphorylated ZRF1 (pS47) and total ZRF1. PVDF membrane was visualized using ECL. Lower panel: Total H3 and ID1 from the same SDS-PAGE gel, PVDF membrane sliced off the sections in A before blotting. **C.** Quantification of band intensity normalized to total H3 at 0, 4 and 6 HPI. *Experiments and data analysis by Alison Francois*

3.4. Discussion

3.4.1. A Pro-Transcriptional Role for PRC1 in HSV-1 Lytic Infection

The Polycomb complexes have classically been considered repressive to transcription, informing the term Polycomb Silencing (136, 154, 187). Mirroring others' findings that H2AK119ub can be pro-transcriptional on host chromatin (207, 214, 216, 217), our findings support an unanticipated pro-viral role for PRC1 during lytic infection. In comparison with the PRC2 H3K27me2-mediated silencing characterized in our previous work, this PRC1-mediated mechanism seems to be exploited to the virus' advantage. In our proposed mechanism, H2AK119ub deposition on incoming lytic genomes is recognized by the reader protein ZRF1, which can promote transcription. Inhibiting PRC1 impairs transcription, and this PRC1-ZRF1 axis could explain the gene expression phenotypes observed with PRC1 inhibition (Figures 3.3, 3.6A-B). The evident recruitment of ZRF1 to replication compartments is also compelling support for the protein's pro-viral role, and if this observation is further validated, ZRF1 is a previously unidentified pro-viral host factor.

The finding that ZRF1 is recruited to replication compartments in both fibroblasts and neurons leads us to ask what differs between the two cell types such that latency establishment leads to H3K27 methylation. We detected H2AK119ub on the latent genome *in vivo* (Figure 3.1), which raises the possibility that H2AK119ub precedes PRC2 recruitment and eventual H3K27 methylation. This sequence of events would mirror those in *de novo* host heterochromatin formation, which the virus could have exploited in the process of co-evolving with the human host and co-opting host mechanisms. One possible answer to this question is the presence of ID1, which

prevents ZRF1 from binding to H2AK119ub during neural differentiation (209). Although Aloia et al. find ID1 expression falls as differentiation progresses, this result is in the context of mouse embryonic neural development. Whether ID1 levels shift during neuronal infection, and determining baseline ID1 expression levels in sensory neurons will allow the exploration of ID1 as a regulator of ZRF1-mediated lytic gene activation. Our collaborator Dr Colin Crump conducted a tandem mass-spectrometry-based proteomic analysis of lytic infection in keratinocytes (320), and from this data set relative ID1 and ZRF1 (DNAJC2) protein levels are shown in Figure 3.9A. Interestingly, these data show steady ZRF1 throughout infection, with declining ID1. Our western blot of lytically infected HFFs (Figure 3.9B-C) saw ID1 levels dropping, although the band was faint to begin with and requires further optimization. We saw ZRF1 levels increasing, whereas the Crump data set does not, and it will be interesting to determine whether either result is cell type dependent.

Our results point to PRC1 involvement in lytic HSV-1 gene expression but may not indicate any particular PRC1 composition. All three inhibitors used inhibit H2AK119 ubiquitination, but through slightly different mechanisms. PRT4165 inhibits the BMI1/RING1A interaction, but the compound does also inhibit RING1B activity (321). RING1A and RING1B substantially overlap in their functions (321, 322), so it is also difficult to delineate RING1A and RING1B involvement in HSV-1 lytic gene expression. In all likelihood, supported by our co-localization findings for both RING1A and RING1B, both proteins can carry out this function and compensate for each other. BMI1 can be incorporated into either vPRC1 or cPRC1, so do not point to specific complex variants. PTC-209 specifically inhibits BMI1 transcription in addition to BMI1 activity, so this phenotype could be caused by the loss of BMI1-containing PRC1 altogether as opposed to the specific enzymatic activity of RING1A or RING1B. RB-3 targets the RING1B-BMI1

interaction, preventing their interaction with nucleosomes (323). Although off-target effects are certainly possible, multiple inhibitors of global H2AK119 ubiquitination recapitulated the restrictive lytic gene expression phenotype. Knockdown and knock-out experiments will be necessary to rule out off-target effects, but the redundancy between many Polycomb proteins may make that tricky.

3.4.2. Inability to Detect H2AK119ub on Lytic Chromatin

Quantification of H2AK119ub at lytic viral genomes showed no co-localization significantly above that for randomly placed genomes (Figure 3.2A-B), but the functional effect of the modification's deposition being inhibited was striking. Given our observations that three different PRC1 inhibitors restrict lytic gene expression (Figure 3.3), the inability to detect H2AK119ub with our imaging assay does not necessarily indicate complete absence. Technical limitations of the imaging assay could be responsible for this result. We first determined by eye that H2AK119ub was co-localizing with lytic genomes, and our method of generating random placement control images could be inappropriate for this histone modification's staining pattern. A challenge we identified early in this research was quantification of co-localization with a relatively diffuse nuclear stain. In the process of developing NucSpotA, we chose to threshold the immunostaining signal to exclude areas of no signal in the nuclear mean calculation. Although this approach was useful for assessing H3K27 methylation in Chapter 2, H2AK119ub could be too diffuse or abundant for statistically significant co-localization with lytic genomes compared to the rest of the nucleus. In addition to its role in heterochromatin formation and maintenance, H2AK119ub is utilized by the cell to mark sites of DNA damage (206–208, 304). H2AK119ub functions aside from *de novo*

heterochromatin formation, such as nucleotide excision repair, could contribute to the diffuse and abundant nuclear staining pattern. Our result could also be due to insufficient microscopic resolution to identify co-localization with H2AK119ub. This imaging assay should be tested with higher resolution microscopy (such as an Airyscan confocal) to conclusively determine whether H2AK119ub co-localization is above random placement.

Compared to the H3-H4 dimer, an H2A-H2B dimer is more flexible and could thus be sensitive to wash steps during the immunostaining process (324). As discussed in chapters 1 and 2, histone antibodies are tricky to generate with specificity, and post-translational modifications of nearby residues modify the ability of reader proteins to bind the epitope (223–225, 244). This grants an astonishing amount of complexity and tunability to the use of histone post-translational modifications, making it difficult to generate antibodies with high specificity for a single residue. Phosphorylation or other PTMs of adjacent amino acids in the histone tail could occlude antibody binding to H2AK119ub, obscuring the signal for a PTM that is present. H2AT120 is one such residue that can be phosphorylated, and should be considered in this context (325). We did perform the ChIP for H2AK119ub in non-neuronal cells (Figure 3.2C) with a lambda protein phosphatase reaction step to eliminate occlusion by adjacent phosphorylated residues, but other histone modifications could also be occluding antibody binding.

In the specific case of histone H2A, it is also worth noting that H2AK119ub is indistinguishable from H2AXK118Ub as an epitope recognized by histone antibodies (305). High similarity between histone variants further complicates attempts to target the H2AK119ub residue with antibody binding. To ensure the simultaneous fixation/permeabilization step in preparation for click chemistry did not wash out soluble H2AK119ub, we also tested fixation without prior wash steps and permeabilization after fixation. We did not see an increase in lytic genome co-localization with H2AK119ub

compared to the simultaneous fixation/permeabilization method, suggesting we were not washing out the antibody target in processing.

We also faced challenges performing epigenetic assays for H2AK119ub, by CHIP-qPCR and CUT&RUN. As shown in Figure 3.2C, very little H2AK119ub was found on lytic *ICP27* and *ICP8* promoters, whereas more was found on the host negative control promoter than we expected. While this result does indicate some successful immunoprecipitation of the residue, this approach requires further optimization to find appropriate host control regions. To ensure we were not missing regions of H2AK119ub enrichment on the lytic genome we also performed CUT&RUN experiments. This approach had the added benefit of antibody binding within the intact (permeabilized) nucleus and no formaldehyde fixation, which we considered could retain the unmodified epitope with conditions during lytic infection. Our collaborator could not perform the histone peptide binding arrays (discussed in chapter 2) for H2AK119ub due to technical constraints synthesizing the peptide, and instead performed western blots to test antibody specificity (Figure 6.4). The one that showed specificity to the Ub modification (CST 8240S) was used for CUT&RUN experiments, the first of which showed poor binding efficiency when compared to IgG negative control and H3K4me3 positive control reactions (data not shown). We next decided to confirm whether a lack of fixation was beneficial for assay sensitivity, and this time (using the same antibody) we achieved high efficiency in the unfixed sample (Figure 6.7). Sequencing depth and alignment rate were poorer for the fixed sample, leading us to the conclusion that fixation impairs CUT&RUN for H2AK119ub. However, the coverage on the human genome in the unfixed sample was unexpectedly broad, leading us to conclude non-specific binding led to noisy data. A sample coverage plot is shown in Figure 6.8. CUT&RUN for lytic HSV-1 chromatin will require further optimization, and validation of antibody specificity is key in this process.

In summary, we cannot rule out H2AK119ub at the lytic genome evading antibody binding.

3.4.3. Non-specific ZRF1 Antibody Binding

ZRF1 is a relatively understudied protein, at least in its chromatin-modifying capacity. As such, few antibodies are available. Through western blotting (Figure 6.6) we found both antibodies we tested (Novus NBP2-12808 and NBP1-82627) showed strong bands outside the expected band size (indicated with arrows). These antibodies are both polyclonal, which could explain the variety of band sizes, but could also be beneficial for blotting as many isoforms as possible. By comparing these two antibodies' blots, and in combination with knockdown and knockout of ZRF1 expression, we were able to identify a band that is most likely ZRF1. Whether the other bands are also ZRF1 of different isoforms, or a viral gene product recognized by the antibody, remains to be determined. The difference in co-localization intensity ratios at 2 HPI between rabbit and mouse anti-ZRF1 antibodies (Figure 3.6, Figure 6.5) may speak to the antibody recognizing different isoforms of ZRF1, but this remains to be determined.

3.4.4. Future Directions

Our findings point to an exciting pro-transcriptional mechanism during lytic HSV-1 infection mediated by host PRC1 machinery. Technical challenges prevented us from conclusively determining that ZRF1 is at replication compartments, or that H2AK119ub is present on lytic HSV-1 chromatin. We also faced unexpected challenges achieving knockdowns of RING1A, RING1B and ZRF1, which would provide a functional link

between the proteins observed at lytic genomes and the PRC1 inhibitor gene expression phenotypes. More experiments are required to solidify this hypothesis, and many avenues beyond establishing the mechanism can be explored in the future. These include the possible involvement of ID1 in regulating ZRF1 activity, the cell type-specific differences that could promote lytic or latent infection, whether specific ZRF1 isoforms are involved, and whether this mechanism could become a therapeutic target for limiting lytic replication. In addition to its role as a subunit of PRC1, RING1B can write H2AK119ub at sites of DNA damage on host chromatin as part of a separate complex, the UV-RING1B complex (206). In the context of nucleotide excision repair, ZRF1 works with DICER to decondense chromatin (205–208). RING1B could promote lytic HSV-1 gene transcription from outside the PRC1 complex, opening up more possible mechanisms of action that should be considered.

Chapter 4: Implications and Future Directions

4.1 Future Directions

4.1.1. Potential Mechanisms for Repression by PHF20L1 in HSV-1 Infection

PHF20L1 is a Recently Identified H3K27me2 Reader

Our findings in Chapter 2 informed the hypothesis that PHF20L1 contributes to transcriptional repression of incoming HSV-1 genomes by reading H3K27me2. PHF20L1 contributes to the maintenance of pluripotency, the protein shown to antagonize DNMT1-mediated proteasomal degradation in mammalian cells. In this context, PHF20L1 recognizes mono-methylated DNMT1K142 (326). In ovarian cancer cells, PHF20L1 regulates transcription factor Sox2 by binding mono-methylated K42 and K117, preventing degradation (327). Both functions involve recognition of a methylated lysine, but do not involve direct recognition of histone tail PTMs. PHF20L1 has only recently been found to have an epigenetic reader function, binding H3K27me2, but its involvement in lytic infection could point to more host mechanisms' roles regulating lytic gene transcription (258).

PHF20L1 binds H3K27me2 through its TUDOR domain, determined by Hou et al. using a histone peptide array of individual PHF20L1 domains to assess binding strength (258). As with many epigenetic-related proteins, PHF20L1's H3K27me2 reader function has been investigated in the context of cancers. The regulatory mechanisms PHF20L1 contributes to could represent mechanisms regulating lytic HSV-1 chromatin. These mechanisms inform avenues for future exploration, with the aim of identifying the mechanism behind PHF20L1 transcriptional repression of HSV-1 genomes.

Interaction With the NuRD Complex

The Mi-2/nucleosome remodeling and deacetylase (NuRD) complex pairs ATP-dependent remodeling with deacetylation of chromatin (328, 329). NuRD counters the activity of SWI/SNF complexes (328). SWI/SNF complexes open chromatin structure in an ATP-dependent manner to enable gene transcription during embryogenesis and development. NuRD and Polycomb complexes are important negative regulators of gene expression in this process (330).

Unsurprisingly, the NuRD complex shows a similar level of complexity to the Polycomb complexes through combinations of different subunits (331–333). The human complex consists of CHD3, 4 or 5, an ATP-dependent remodeler that can physically slide nucleosomes along the length of DNA to modulate chromatin structure (330, 332). The complex also includes histone deacetylase HDAC 1 or 2, creating a unique combination of HDAC and ATP-dependent chromatin modeling functions (332). RBBP4 or 7 function as histone chaperones in the complex, and other subunits facilitate DNA binding (MTA1/2/3), methylated CpG binding (MBD2 or 3) and regulators of HDAC affinity (GATAD2A or B) (332). The NuRD complex may also remodel chromatin at actively transcribed regions of chromatin. A 2018 study using mESCs determined that NuRD resets transcription by evicting RNA polymerase II and transcriptional factors from transcriptional start sites, which they describe as “fine-tuning” gene expression (334).

The NuRD complex is of particular interest as a candidate mechanism behind PHF20L1 repression of lytic HSV-1 gene transcription. As outlined in Figure 4.1, NuRD can free up H3K27me2 by removing nearby H3K27 acetyl residues. PHF20L1 can then recruit PRC2 to the region of chromatin, allowing PRC2 to carry out H3K27 methylation and repress transcription (258, 329). This model was proposed to repress tumor suppressor genes in breast cancer cells, and a similar role in other cancers is certainly

possible (258, 335). Future studies should aim to determine whether NuRD is the facilitator of H3K27me2 repression of lytic genes. Importantly, Dembowki and DeLuca (2015) performed HSV-1 DNA pulldown (iPOND) and proteomic analysis, from which the data show multiple components of the NuRD complex recruited to replication compartments (alongside several other chromatin remodeling complex subunits) (90). Additionally, CHD3 has been shown to repress incoming HSV-1 genomes during lytic infection, indicating a repressive role for this component of the NuRD complex. Although the many paralogs and subunits complexity to future studies, this evidence and our findings support further investigation into a NuRD-PHF20L1-PRC2 axis repressing HSV-1 transcription.

The NSL and MSL Complexes

PHF20L1 can also be found in the non-specific lethal (NSL) complex, which catalyzes deacetylation of H4K16 residues near pro-transcriptional H3K4me2/3 residues (284–286, 336). It is not known whether PHF20L1-NSL is recruited by H3K27me2, but this should be considered as an alternative to the NuRD complex in the transcriptional repression of HSV-1 genes. It is also notable that the homolog PHF20 is very similar in terms of functional domains, but PHF20 often acts pro-transcriptionally and PHF20L1 repressively (258, 285). We did not look at PHF20 expression in this study, and future experiments could aim to determine whether the homologs have distinct roles in HSV-1 transcriptional regulation. The male-specific lethal (MSL) complex includes PHF20 and acts pro-transcriptionally on host chromatin. The enzymatic subunit lysine acetyltransferase 8 (KAT8) can be incorporated into NSL or MSL complexes, catalyzing H4K5 and H4K8 acetylation or H4K16ac respectively (337). This is an example of the

functional specificity determined by individual NSL or MSL subunits, and PHF20L1 could also be incorporated into the MSL complex.

Remaining questions regarding PHF20L1 in HSV-1 infection

Future investigations based on our findings should address the following questions:

1. Is PHF20L1 repressing transcription on HSV-1 genomes? This proposed function requires experimental validation.
2. Is PHF20L1 acting with the NuRD complex to carry out this repression?
3. Does homolog PHF20 also co-localize with HSV-1 genomes?
4. Does PHF20 have a different functional effect on lytic gene transcription from homolog PHF20L1?
5. What are the expression levels of PHF20L1 and NuRD complex components in our neuronal latency system? Cell type-specific differences shaping infection outcomes could include these components.
6. What is the timing of H3K27me2 formation on incoming genomes prior to latency establishment in neurons, and does PHF20L1 facilitate transcriptional repression during latency establishment?

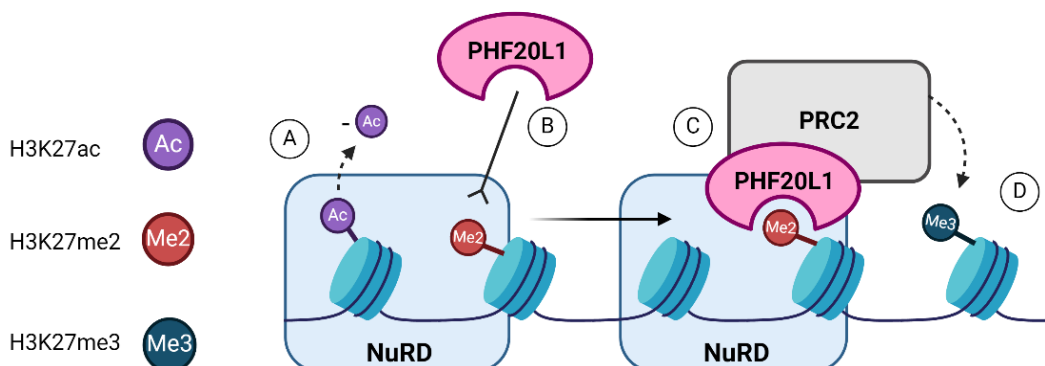


Figure 4.1: The repressive PHF20L1-NuRD-PRC2 mechanism that could be occurring on viral chromatin

A schematic summarizing the model proposed by Hou et al. (2020). (A) The NuRD complex deacetylates H3K27 in which the (B) PHF20L1 can bind nearby H3K27me2. (C) PHF20L1 can recruit PRC2, (D) allowing PRC2 to further methylate nearby H3K27 residues.

4.1.2. An Integrated Model for Polycomb Regulation of HSV-1

Chromatin

Bringing H2AK119 Ubiquitination into our Understanding of HSV-1

Transcriptional Regulation

The findings outlined in chapters 2 and 3 reflect the two branches of Polycomb silencing. Interaction between these two branches is well-established on mammalian chromatin, and it is reasonable to expect interplay between the PRC1 and PRC2-mediated roles in HSV-1 infection. We proposed a mechanism in chapter 1 in which PRC1-mediated H2AK119 ubiquitination precedes PRC2-mediated H3K27 methylation, the former recruiting the latter and reflecting the *de novo* formation of heterochromatin on host chromatin (156, 270). This interaction is outlined in Figure 4.2. Our finding that

H2AK119ub is present on latent chromatin *in vivo* is consistent with a model in which H2AK119ub is first formed on the viral genome in a neuronal nucleus, and PRC2 recruited to sites of H2AK119ub. PRC2 eventually writes H3K27me3, later on in the establishment of latency (10-14 days post-infection *in vivo* (129).) *In vivo* experiments profiling the viral chromatin as latency is established would help establish whether H2AK119ub precedes H3K27me3, as one would expect from the order of events observed on host chromatin.

Our findings of PRC1 activity in lytic infection inform candidates for future study. A preliminary model is shown in Figure 4.2, in which RING1A/B-mediated H2AK119 ubiquitination recruits ZRF1 to activate gene expression. If ID1 is present it can prevent ZRF1 recruitment, which would then leave the ubiquitin open for JARID2 to read and recruit PRC2. PRC2 could then methylate H3K27 and reinforce and maintain transcriptional repression. Aspects of this model could be promoted in specific cell types, promoting lytic infection or latency establishment in the right contexts.

Remaining questions regarding RING1A/B, H2AK119ub and ZRF1

Our findings form the foundation of a mechanism, but aspects of this model require validation or further investigation. As indicated in figure 4.2, these include:

- A) What complex are RING1A and/or RING1B part of when acting on the HSV-1 genome?
- B) Is ZRF1 recruited to H2AK119ub on HSV-1 chromatin?
- C) Is H2AK119ub present on the lytic genome in combination with other modifications that occlude antibody recognition?
- D) What complexes or mechanisms does ZRF1 employ to activate lytic gene transcription?

- E) Do ID1 levels shape infection outcomes by controlling ZRF1 pro-transcriptional activity?
- F) Does ZRF1 recruitment impact JARID2 binding to H2AK119ub and PRC2 recruitment?

Regardless of the outcome of these investigations, our identification of a pro-transcriptional role for PRC1 in lytic HSV-1 infection is an exciting addition to the complexities of Polycomb silencing and the virus' exploitation of host mechanisms.

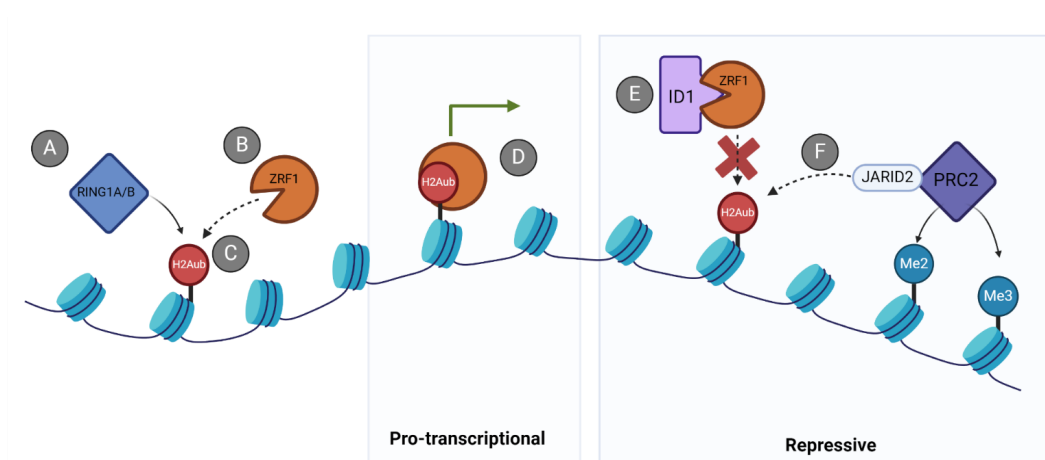


Figure 4.2: An integrated model for PRC1 and PRC2 activity regulating HSV-1 transcription. A proposed model for PRC1 and PRC2-mediated Polycomb activity on the HSV-1 genome. RING1A/B deposits H2AK119ub, recruiting ZRF1 to activate gene transcription. If ID1 is present, it can prevent ZRF1 recruitment, freeing up H2AK119ub for binding by JARID2 and PRC2 recruitment. This combination of PRC1 and PRC2 activity is repressive. Letter labels refer to questions this model raises, described in the main text. Made with Biorender.

4.1.3. HSV-1 as a Tool to Study Host Epigenetics

Virology has long been a means through which to explore cell biology, with many molecular biology tools originating from viruses. Through the process of natural selection, herpesviruses have evolved elegant mechanisms using host transcriptional machinery, cytoskeletal transport mechanisms and more (107, 119, 260, 338, 339). The human species also developed anti-viral measures, many of which HSV-1 specifically defends against to ensure viral replication (340). The interaction between virus and host is a unique opportunity to gain insight into subcellular processes, including those modifying chromatin structure.

De novo chromatin formation is difficult to observe, due to residual epigenetic templates on the host genome. The arrival of naked HSV-1 DNA in a cell nucleus is an opportunity to observe the *de novo* formation of heterochromatin and witness the dynamics of Polycomb silencing. In this study, observing the activities of Polycomb complexes on incoming lytic HSV-1 genomes informed our understanding of the process on host chromatin. H3K27me2 is not well understood as a transcriptional regulator, and we were able to link PHF20L1 with rapid repression and show the balance of H3K27me2 and H3K9me3 shifted by the presence of PML nuclear bodies. Linking H2AK119ub to transcriptional activation through ZRF1 expands our knowledge of the transcriptionally activating side to Polycomb “silencing”, and HSV-1 is perhaps a novel tool with which to study proteins like PHF20L1 and ZRF1 and the surprising roles embodied by epigenetic processes.

4.2. Technical Lessons and Advances

4.2.1. Capturing Heterogeneity During Lytic Infection

The imaging assay introduced in Chapter 2 (Figure 2.2) formed a major component of this work. We aimed to develop a method of observing heterogeneity amongst individual HSV-1 genomes, and the assay can be applied to many aspects of HSV-1 biology. Although the EdC-labeled HSV-1 visualization method using click chemistry was originated and developed by others (72, 79, 80, 150, 341), we had not encountered a method of quantifying histone co-localization with viral genomes from batches of images. We explored other methods including blinding images and scoring by eye, but the diffuse nature of many histone modifications in the nucleus can make subjective scoring difficult. NucSpotA allowed us to adjust thresholds for each immunostain's pattern, calibrating what looked like "real" signal by eye and applying the parameters to a large batch of images. Dr Ali Rohani created NucSpotA at our request, and the customizable nature of the program allows a high degree of optimization and fine-tuning. We determined that regardless of the values obtained from NucSpotA measurements, it was important to compare these values with appropriate controls. These controls consisted of other nuclear proteins associating with HSV-1 DNA (Figure 2.3B, 2.6B), and random placement in the nucleus by image rotation (Figure 2.3C-D, F, 2.6C).

Ultimately, we were able to obtain large enough data sets to identify sub-populations of genomes associating with H3K27me2 in fibroblasts (Chapter 2). In Chapter 3, we visualized the co-localization of both RING1A and RING1B with lytic genomes (Figures 3.4 and 3.5), reflecting possible heterogeneity in the PRC1 complexes that act on lytic genomes. Although RING1A and RING1B carry out largely

redundant activities, we know diversity in complex composition allows for fine-tuning and context-specific regulation of Polycomb silencing (172, 322). Whether HSV-1 associates with RING1A or RING1B could lead to heterogeneous transcriptional outcomes. Our finding that RING1A co-localization is impeded by PRC1 inhibitor RB-3 in cells expressing ICP4 (Figure 3.6) also serves as an example of the value of imaging individual cells and genomes, as we were able to correlate the presence of lytic gene products (ICP4) and RING1A association.

We gained the most insight when combining this approach with variables such as inhibitor treatment. Comparison points proved essential for interpreting NucSpotA data, such as inhibitor treatments that led to increased H3K27me2 association (Figure 2.6) or loss of RING1A association with lytic genomes (Figure 3.6). We were also able to compare cells expressing PML with PML knockout cells and observe shifts in the balance of H3K27me2 and H3K9me3 that may be difficult to detect at a bulk chromatin level (Figure 2.8). A strategic combination of experimental variables, image quantification with thresholds calibrated by eye, and a large batch of images from experimental replicates allowed us to make novel observations about HSV-1 chromatin structure and the host machinery shaping it.

4.2.2. Antibody Specificity is Key

As discussed in Chapters 2 and 3, histone antibodies with high residue specificity proved challenging to find. Our collaborator Dr Rothbart's help in screening a selection of antibodies against histone peptides was invaluable but highlighted the incredible complexity of using histone antibodies. Our results show the importance of screening for

non-specific binding, and the value of testing several antibodies against the same epitope.

Similarly, both PHF20L1 and ZRF1 proved frustrating to work with. Both are relatively understudied in the epigenetic roles we were investigating, with a small handful of papers pushing us in their directions experimentally (206, 207, 216, 217, 258, 335). The nature of these proteins as research subjects meant we had few antibodies to choose from, saw unexpected western blot band sizes, and struggled to validate knockdown or knockout with the reagents available. Figure 6.9 shows the confusing band patterns we saw blotting for PHF20L1, and the variability between different antibodies' expected band size according to product data sheets. Some of the protein band patterning could be attributed to the expression of multiple isoforms, but more research is needed to delineate the roles of individual isoforms. Additionally, attempts to over-express a FLAG-tagged PHF20L1 construct were toxic to the cells, forcing us to limit our exploration to endogenous PHF20L1. While this was frustrating, these proteins both proved exciting roads to go down, and further optimization of knockdown or knockout and better antibody specificity should facilitate insights into their roles in HSV-1 infection.

4.3.3. Next Gen Sequencing Approaches to Viral Chromatin

Although we set out to capture heterogeneous chromatin structures amongst HSV-1 genomes, we also chose to learn and optimize a bulk chromatin assay that uses Next Gen Sequencing, CUT&RUN. The requirement for fewer input cells than ChIP-qPCR was appealing, given the potential applications for neuronal infection as a non-dividing cell. For this project, we also wanted to map coverage across the entire HSV-1 genome,

as it is dense with genomic features that could be missed by choosing the wrong genome region to amplify by qPCR. We were able to successfully perform CUT&RUN for HSV-1 lytic chromatin but had to improvise along the way to account for the unique requirements of viral epigenetics.

My analysis pipeline was developed by closely following and adjusting a tutorial on protocols.io (342), which was not only incredibly informative, but the active discussion in comments between the authors and other scientists troubleshooting also proved helpful. This pipeline is summarized in Figure 4.2. This pipeline has been adapted to analyze ChIP-seq data, standardizing reads to the input sample instead of spike-in DNA (310). Advice from other herpes virologists proved invaluable, particularly Dr Sarah Dremel and Dr Seth Frieze. Dr Dremel's previous work informed our approach to quantifying histone modification enrichment along the viral genome (107), and she explained why certain quality control and other analyses were not appropriate for viral reads. A recent publication by Dr Daphne Avgousti's group also provided insight into why peak calling analysis are not appropriate for heterochromatin, as it constitutes much broader areas of the genome than some other histone modifications at actively transcribed regions of chromatin (260). NGS approaches to viral chromatin feel like the wild west in some ways, but the method adaptation and creative problem solving were instructive.

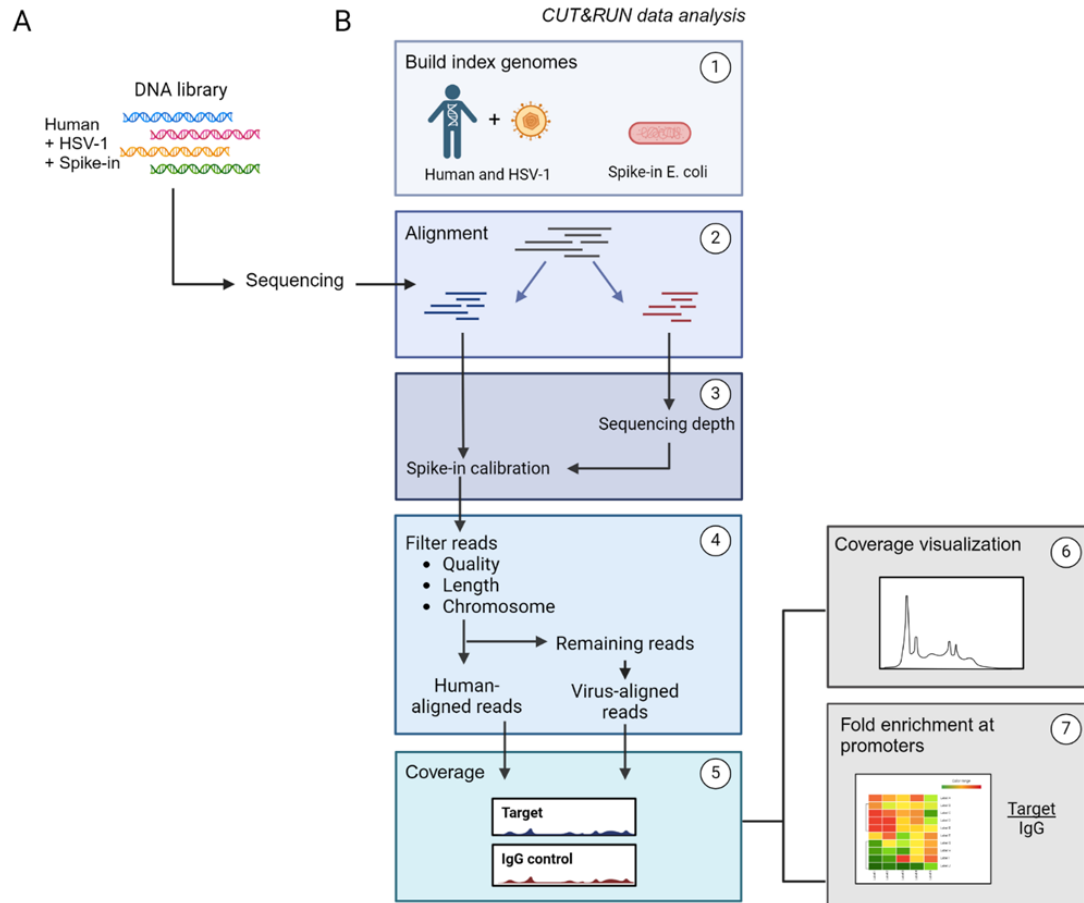


Figure 4.3: An overview of the CUT&RUN data analysis pipeline established for HSV-1 infected cells

A. The nucleus of a cell being processed for CUT&RUN contains both host and viral DNA. During DNA library preparation, a known amount of *E. coli* DNA is spiked in to the sample. This is later used to normalize for sequencing depth. **B.** 1. Two index genomes are built using Bowtie2, one a combined human and viral genome (the viral genome is treated as an extra chromosome) and an *E. coli* genome. 2. After DNA library sequencing, alignment of the reads is performed against both reference genomes. 3. The *E. coli* alignment rate is used to calculate a normalization factor, which is applied to the human and viral alignment results. 4. Reads are then filtered for quality, length and by chromosome, then filtered against the human genome to retain only human-aligned reads. The non-aligned reads are further processed, filtered against the viral genome, leading to a separate file of virus-aligned reads. 5. Coverage files are generated for the normalized, filtered reads as bedgraph files. 6. Coverage can be directly visualized in Integrative Genome Viewer using bedgraph files, or can be normalized to the IgG control. 7. Coverage plots can be used to calculate the sum of scores for each sample's reads at a defined region, such as a promoter. Choosing a sum calculation, rather than mean, accounts for any large spikes in the designated region that could be obscured with a mean value. The score sums for the target and IgG control samples can be compared to calculate the ratio of target to IgG coverage at that region. Heat maps are one way to plot these ratios for each promoter/region.

4.3 Conclusions

It is evident that Polycomb regulatory mechanisms, both of host chromatin and incoming HSV-1 genomes, are multi-faceted. The extent to which Polycomb complexes act redundantly (such as homologs RING1A and RING1B), the existence of variants cPRC1, vPRC1, PRC2.1 and PRC2.2, and the functions of individual subunits and accessory proteins underlie the sophisticated mechanisms behind mammalian Polycomb silencing. HSV-1 infection provides a unique lens through which we can observe *de novo* Polycomb silencing in a differentiated cell. Experimental determination of the involved complexes and components is benefitted by the functional readout of lytic gene expression. The distinct infection outcomes of lytic and latent infection also allow for the study of cell type specific Polycomb silencing mechanisms and teasing out which aspects of non-neuronal and neuronal cell biology shape these. Our studies informed a model integrating the two branches of Polycomb silencing, suggesting that novel systems and approaches can help experimentally identify interplay between PRC2 and PRC1-mediated regulatory mechanisms. The decades of Polycomb research in the contexts of embryogenesis, neurodevelopment and cancer informed our studies, helping us identify the histone modifications, chromatin remodeling complexes and reader proteins we investigated. Our research hopefully demonstrates the value of HSV-1 as another informative context for Polycomb research.

The heterogeneity we observed in the Polycomb silencing of incoming HSV-1 genomes (Chapter 2) likely speaks to the many host and viral factors competing for transcriptional control, as evidenced by our shifting the balance from H3K27me2 to H3K9me3 by modulating PML expression (Figure 2.8). The experimental and analytical methods developed in these studies, including individual viral genome imaging and

quantitative analysis, underline the value of considering heterogeneity during HSV-1 infection. The factors shaping heterogeneous outcomes could be therapeutic targets, aiming to push the balance towards more repressive viral chromatin formation (132). The use of Next Gen Sequencing to characterize bulk viral chromatin also proved informative, and is certainly a direction the HSV-1 field has been moving towards with ChIP-seq and RNA-seq (including single-cell RNA-seq) (80, 145, 222, 343–348). By combining methods capturing heterogeneous outcomes with improved bulk chromatin characterization, we have demonstrated the value of pushing complementary techniques for the study of HSV-1 epigenetics and mammalian Polycomb silencing.

Chapter 5: Materials and Methods

This is an adaptation of the Materials and Methods section of the following publication, with information pertaining to Chapter 3 added:

Francois Alison K., Rohani Ali, Loftus Matt, Dochnal Sara, Hrit Joel, McFarlane Steven, Whitford Abigail, Lewis Anna, Krakowiak Patryk, Boutell Chris, Rothbart Scott B., Kashatus David, Cliffe Anna R. 2024. Single-genome analysis reveals a heterogeneous association of the herpes simplex virus genome with H3K27me2 and the reader PHF20L1 following infection of human fibroblasts. MBio 0:e03278–23.

Blank page

5.1. Reagents

5.1.1. Non-Neuronal Cells

Primary HFF, U2OS, and Vero cells were all obtained from the American Type Culture Collection. Telomerase immortalized retinal pigmented epithelial cells (RPE-T) have been described previously (80). HFF-Ts were generated by telomerase immortalization by lentiviral transduction of HFFs using pLV-hTERT-IRES-hygro [a gift from Tobias Meyer (Addgene plasmid # 85140; <http://n2t.net/addgene:85140>; RRID:Addgene_85140)] (349).

HFF, U2OS, HFF-T, and RPE-T cells were cultured in Dulbecco modified Eagle Medium High Glucose (DMEM, Gibco 11965–092) supplemented with 10% fetal bovine serum (FBS). RPE-Ts were cultured in the presence of 5 µg/mL of Hygromycin. Vero cells were cultured in DMEM supplemented with 10% Fetalplex (GeminiBio 50–753-2987). 293-LTV cells (Cell Biolabs LTV-100) were cultured in DMEM High Glucose with 10% FBS and 1% MEM NEAA (Gibco 11140–050).

5.1.2. Primary Neuronal Cells

Sympathetic neurons from the superior cervical ganglia (SCG) of post-natal days 0–2 (P0-P2) CD1 Mice (Charles River Laboratories) were dissected as previously described (263). Rodent handling and husbandry were carried out under animal protocols approved by the Animal Care and Use Committee of the University of Virginia (UVA). Ganglia were briefly kept in Leibovitz's L-15 media with 2.05 mM L-glutamine before dissociation in Collagenase Type IV (1 mg/mL) followed by Trypsin (2.5 mg/mL) for 20

minutes each at 37°C. Dissociated ganglia were triturated, and approximately 5,000 neurons per well were plated onto rat tail collagen-coated glass coverslips. Sympathetic neurons were maintained in CM1 [Neurobasal Medium supplemented with PRIME-XV IS21 Neuronal Supplement (Irvine Scientific), 50 ng/mL Mouse NGF 2.5S, 2 mM L-Glutamine, and Primocin]. Aphidicolin (3.3 mg/mL) was added to the CM1 for the first 5 days post-dissection.

5.1.3. Viruses

Herpes simplex virus (HSV-1) strain 17Syn+ was grown on Vero cells infected at an MOI of 0.1 PFU/cell and cultured at 34°C for 2 days or until cytopathic effect was observed. Heparin sodium (BP2425, Fisher Scientific) in phosphate-buffered saline (PBS) was added to flasks to a final concentration of 50 µg/mL and incubated at 37°C for 4–6 hours, before supernatant collection and centrifugation at 4°C 150 RCF for 10 minutes. The supernatant was centrifuged at 20,000 RCF for 1 hour at 4°C, and the virus pellet was resuspended in 10% glycerol in PBS, then sonicated at an amplitude of 20% for 20 seconds before aliquoting and storage at –80°C. Stocks of 17Syn+ were titrated on Vero cells. VP16 activation domain mutant (RP5) and rescue (RP5R) HSV-1 stocks were generated by infecting U2OS cells at an MOI of 0.05 PFU/cell. RP5R and RP5 were titrated on U2OS cells as described previously (66). RP5 was propagated and titrated in the presence of hexamethylene bis-acetamide (HMBA) in PBS (Sigma Aldrich 224235–50G) to a final concentration of 3 mM.

5.1.4 Inhibitors

Inhibitors were resuspended in dimethyl sulfoxide (DMSO), and vehicle controls were performed with inhibitor-equivalent volumes of DMSO. Concentrations were chosen by initial kill curve experiments, selecting a range of concentrations surrounding the compound's reported IC50 value and determining the highest concentration that does not cause visible morphological damage or cell death. UNC1999 (Cayman Chemical Company 14621) was used at 1.8 μ M, GSK-J4 (Sigma Aldrich SML0701) at 10 μ M, PRT-4165 (Sigma Aldrich SML1013) at 30 μ M, PTC209 (Tocris 5191) at 2 μ M, and RB-3 (synthesized upon request) at 30 μ M unless otherwise indicated.

5.1.5. PML Nanoblade and Knock-Out Cell Production

Nanoblades were generated as previously described (350) in 293-LTV cells transfected using jetPRIME (Polypus 101000027) with plasmids pCMV-VSV-G (a gift from Bob Weinberg Addgene plasmid # 8454; <https://n2t.net/addgene:8454>; RRID:Addgene_8454), BaEVRLess (gifted by Els Verhoeven; constructed with pCMV-VSV-G) (351), p5349 [pBS-CMV-gagpol, a gift from Patrick Salmon (Addgene plasmid # 35614; <http://n2t.net/addgene:35614>; RRID:Addgene_35614)], BIC-Gag-Cas9 [a gift from Philippe Mangeot & Théophile Ohlmann & Emiliano Ricci (Addgene plasmid # 119942; <https://n2t.net/addgene:119942>; RRID:Addgene_119942)] (350) and pBLADE PML (target sequence GCG GGT GTG TCT GCA CCT AGG GG) or pBLADE non-targeted control (target sequence ATC GTT TCC GCT TAA CGG CG) [BLADE was a gift from Philippe Mangeot & Théophile Ohlmann & Emiliano Ricci (Addgene plasmid # 134912; <https://n2t.net/addgene:134912>; RRID:Addgene_134912)] (350). Cas9 production was quantified by serial dilution as described using Cas9 nuclease (New

England BioLabs M0386S). HFF-hTERT cells were transduced with Nanoblades with 8 $\mu\text{g}/\text{mL}$ polybrene (Boston BioProducts BM-862M-1) and cultured with 5 ng/mL human fibroblast growth factor (FGF, Gemini Bio-Products 300-113P) throughout clonal selection. Knock-out was verified by immunostaining for PML.

5.1.6. Production of EdC-labeled Virus Stocks

The EdC-labeling protocol was adapted from previously published procedures (79, 80). RPE-Ts were infected with 17Syn+ in 0.2% FBS DMEM at an MOI of 0.001 PFU/cell for WT 17Syn+ and RP5R, or 0.5 PFU/cell for RP5 and kept at 33°C. HMBA was included in media at a final concentration of 3 mM during EdC labeling of RP5. EdC (Sigma-Aldrich T511307) pulses diluted in 0.2% FBS DMEM were added at 6–24, 48, and 72 HPI to 1 μM final concentrations. At 72 HPI, heparin sodium was added, incubated, and the supernatant was passed through a 0.45- μm PES syringe filter, and the supernatant virus harvested as above with the inclusion of an additional two wash steps using DMEM containing 0.2% FBS.

Table 5.1: Antibodies used and their applications

Note: CST= Cell Signalling Technology, SC= Santa Cruz, AM= Active Motif

Target	Catalog Number	Application	Figure Used
Alpha tubulin	CST 3873	Western blot	6.6C
FLAG	CST 8146S	Immunofluorescence	3.7F
H2A	CST 12349S	ChIP	3.1
H2AK119ub	CST 8240S	Immunofluorescence, CUT&RUN, ChIP	3.1, 3.2, 3.6, 6.4
H3	Abcam ab176842	Immunofluorescence, western blots	2.3A-C, 2.6B, 3.9B-C 6.2A-B
H3K27me2	AM 39245	Binding array, immunofluorescence	2.6, 2.8C, 2.8E, 6.1B, 6.3A
H3K27me2	Diagenode C15410046-10	Binding array, CUT&RUN optimization	6.1D, 6.3
H3K27me2	CST D18C8, 9728	Binding array, CUT&RUN	2.7, 6.1C
H3K27me2	AM 61435	Binding array, Immunofluorescence	2.6G, 6.1E
H3K27me3	CST 9733S	Binding array, immunofluorescence, CUT&RUN, western blots	2.1, 2.3A-B, 2.3D-F, 6.1A, 6.2A-B, 6.8
H3K4me3	Epicypther 13-0041	CUT&RUN	2.1, 2.7 6.7, 6.8
H3K9me3	Diagenode C15410193	Immunofluorescence, western blot	2.8E, 6.2A
PHF20L1	Novus NBP1-85655	Immunofluorescence	2.9
PHF20L1	Invitrogen PA5- 115749	Western blot	6.9
PML	SC sc-377390	Immunofluorescence	2.8
Rabbit IgG	Epicypther 13-0042	CUT&RUN	6.8

RING1A	CST 13069S	Immunofluorescence	3.5, 3.6
RING1B	CST 5694S	Immunofluorescence, western blot	3.4, 3.6
RNA polymerase II	Millipore 05-623	Immunofluorescence	2.3A, 2.3B
ZRF1 pS47	CST 12397	Western blot	3.9
ZRF1/DNAJC 2	Novus NBP2-12802	Immunofluorescence, western blot	3.8, 3.9B-C 6.6A, 6.6D
ZRF1/DNAJC 2	Novus NBP1-82627	Western blot	6.6B, 6.6D
ZRF1/DNAJC 2	SC sc-393426	Immunofluorescence, western blot	3.7, 6.5

Table 5.2: Oligonucleotide primer sequences used for qPCR

Name	Forward 5' to 3'	Reverse 5' to 3'
ICP27 mRNA	GCA TCT TCT CTC CGA CCC CG	GCA TCC TTC GTG TTT GTC ATT CTG
ICP4 mRNA	TGC TGC TGC TGT CCA CGC	CGG TGT TGA CCA CGA TGA GCC
UL30 mRNA	CGC GCT TGG CGG GTA TTA ACA T	TGG GTG TCC GGC AGA ATA AAG
VP16 mRNA	GGA CCG GAC GGA CCT TAT	GGT TGC TTA AAT GCG TGG TG
human g-Actin	CAC CGC CGC ATC CTC CTC TTC	TGT GTG CCG CCC GAC AGC
Human GAPDH promoter	CAG CCT TTG AAA GAA AGA AAG GG	ACT TTG GGA ACG ACT GAG ATG
Human HoxA1 promoter	GGT GGT TAT TGT GAC GGT AGT G	GGG TGA GTG ATG AGG TGT AAA G

Table 5.3: Promoter locations on reference genome used for CUT&RUN data analysis

Genome	Chromosome	Start	End	Name	Strand
hg38	chr12	6532516	6536516	GAPDH	+
hg38	chr20	64162450	64166450	Myt1pr	+
hg38	chr14	94388635	94392635	SERPINA1	-
HSV-1 S17	NC_001806.2	2031	2281	RL2	+
HSV-1 S17	NC_001806.2	113525	113775	UL54	+
HSV-1 S17	NC_001806.2	131253	131502	RS1	-
HSV-1 S17	NC_001806.2	132046	132296	US12	-
HSV-1 S17	NC_001806.2	132049	132299	US1	+
HSV-1 S17	NC_001806.2	9659	9909	UL2	+
HSV-1 S17	NC_001806.2	15406	15656	UL5	-
HSV-1 S17	NC_001806.2	20345	20595	UL8	-
HSV-1 S17	NC_001806.2	23211	23461	UL9	-
HSV-1 S17	NC_001806.2	26871	27121	UL12	-
HSV-1 S17	NC_001806.2	47727	47977	UL23	-
HSV-1 S17	NC_001806.2	62135	62383	UL29	-
HSV-1 S17	NC_001806.2	62540	62788	UL30	+
HSV-1 S17	NC_001806.2	86150	86400	UL39	+
HSV-1 S17	NC_001806.2	89695	89945	UL40	+
HSV-1 S17	NC_001806.2	92857	93105	UL42	+
HSV-1 S17	NC_001806.2	106759	107009	UL50	+
HSV-1 S17	NC_001806.2	108909	109159	UL52	+
HSV-1 S17	NC_001806.2	10878	11128	UL3	+
HSV-1 S17	NC_001806.2	46403	46653	UL22	-
HSV-1 S17	NC_001806.2	105077	105326	UL48	-

5.2. Infections

5.2.1. Lytic Infections

Cells were plated into 24-well plates 24 hours prior to infection. Where specified, cells were pre-treated for 1–2 hours prior to infection with inhibitors. The virus was diluted in PBS containing 0.1% glucose and 1% FBS. In all experiments, this represents the 0-hour time-point post-infection. After 1 hour of adsorption at 37°C, cells were washed twice with PBS containing 0.1% glucose and 1% FBS. Cells were overlaid with DMEM containing 1% FBS and incubated at 37°C.

5.2.2. Establishment of Latent HSV-1 Infection in Primary Neurons

Neonatal SCGs were infected at postnatal days 6–8 with EdC-labeled HSV at an MOI of 7.5 PFU/cell assuming 5,000 cells/well in PBS supplemented with 1% FBS, 4.5 g/L glucose, and 10 mM Acyclovir (ACV) for 3 hours at 37°C. Post-infection, the inoculum was replaced with CM1 containing 50 mM ACV.

5.2.3. *In Vivo* Latent Infection

CD-1 mice (Charles River Laboratories) were anesthetized, inoculated with HSV-1 by ocular scarification as described previously (129, 352). Trigeminal ganglia were removed 30 days post-infection, fixed with formaldehyde and tissue dissociated before processing for chromatin immunoprecipitation, all as described previously (129).

5.3. Immunofluorescence

5.3.1. Click Chemistry and Immunofluorescence

Cells were plated onto glass coverslips in 24-well plates and infected at the indicated MOIs. Cells were washed twice with cytoskeletal (CSK) buffer (10 mM HEPES, 100 mM NaCl, 300 mM Sucrose, 3 mM MgCl₂, 5 mM EGTA), then simultaneously fixed and permeabilized in 1.8% formaldehyde (methanol-free, Thermo Fisher Scientific 28906) and 0.5% Triton-X100 in CSK for 10 minutes. Cells were washed three times in PBS and twice in CSK post-fixation. Coverslips were blocked with 3% bovine serum albumin (BSA, Fisher Bioreagents BP1600-100) prior to Click-chemistry followed by immunostaining. EdC-labeled HSV was detected using the Click-iT Plus EdU Alexa Fluor 555 Imaging Kit (Thermo Fisher Scientific C10638) according to the manufacturer's instructions, using a working stock of picoyl azide-Alexa Fluor 555 (PCA-AF 555). For immunostaining, samples were incubated overnight with primary antibodies in 3% BSA and washed in PBS three times. Following primary antibody treatment, coverslips were incubated for 1 hour in Alexa Fluor-conjugated secondary antibodies (Invitrogen A-11008). Nuclei were stained with Hoechst 33258 (Life Technologies H3570).

5.3.2. Image Analysis

Epifluorescence microscopy images were acquired at 60× using an sCMOS charge-coupled device camera (pco.edge) mounted on a Nikon Eclipse Ti Inverted Epifluorescent microscope using NIS-Elements software (Nikon). Individual nuclei were

isolated from this field of view and 3D deconvolved using the Landweber method (10 iterations) in NIS-Elements software. Deconvolved z-stacks processed by NucSpotA, which is part of the Mitogenie suite, using thresholds to isolate positive immunostaining signal (visually determined) as follows:

Chapter 2: 70.5% (H3, H3K27me2, H3K27me3) and 65% (PHF20L1) for 17Syn+ infection of HFFs; 75% (H3K27me2), 70% (H3K9me3 and PHF20L1) for RP5 infection of HFF-Ts and PML knock-out HFF-Ts. Rotation control images were generated from original channel combination images using FIJI, prior to analysis with NucSpotA. Images processed for this analysis were rotated by 90°.

Chapter 3: 70% (H2AK119ub and RING1A), 65% (RING1B) Rotation control images were generated from original channel combination images using FIJI, prior to analysis with NucSpotA. Rotation control images were generated from original channel combination images using FIJI, prior to analysis with NucSpotA. Images processed for this analysis were rotated by 180° (a change made to optimize the number of rotated genomes kept within the bounds of the nucleus). The stated co-localization intensity ratio thresholds (dashed lines on violin plots) were blindly calibrated by eye.

5.3.3. Expressing FLAG-tagged ZRF1

Vero cells plated on glass coverslips were transfected with 1 µg per well pcDNA FLAG ZRF1 (a gift from Mario Pende (353)), using Opti-MEM Reduced Serum Medium (Gibco 31985070) and lipofectamine 3000 (Invitrogen L3000015) with 1.5 µl Lipofectamine 3000 reagent per well. Cells were infected with 17Syn+ at an MOI of 20 PFU/cell 30 hours post-transfection. 30 minutes before fixation (as described for click chemistry, 5.3.1) an EdC pulse (Sigma-Aldrich T511307, 10 µM) was added to the media to allow

incorporation into replication compartments. Slides were processed for click chemistry and immunostaining against the FLAG epitope (Cell Signalling Technology 8146S).

5.4. Other Quantitative Methods

5.4.1. Quantification of Viral Gene Expression

Analysis of mRNA expression by RT-qPCR. To analyze HSV mRNA relative expression, total RNA was extracted using the Zymo Research Quick-RNA MiniPrep Kit (R1055) with an on-column DNase digestion. Reverse transcription was carried out on equivalent amounts of RNA using Maxima Maxima First Strand cDNA Synthesis Kit (Thermo Scientific K1642), RiboLock RNase Inhibitor (Thermo Scientific EO0382), Random Hexamer Primer (Thermo Scientific SO142) and dNTP Set (Thermo Scientific R0181), and qPCR was carried out using PowerUp SYBR Green Master Mix (Applied Biosystems A25741). The relative mRNA copy number was determined using the $2^{-\Delta\Delta C_t}$ method and viral mRNAs were normalized to that of the human reference gene mRNA transcript from ACTG1 (actin gamma 1). All samples were run in duplicate on an Applied Biosystems Quantstudio 6 Flex Real-Time PCR System, and the analysis carried out using QuantStudio Real-Time PCR Software v1.7. Primer sequences: ICP8 as published (262); TK as published (10); and others are listed in Table 5.2.

5.4.2. Western Blotting

Confluent HFFs cultured in a six-well plate were treated with indicated concentrations of GSK-J4 or UNC1999 in 10% FBS DMEM for 4 days, with a media change including fresh inhibitor on day 2. Untreated cells were cultured in parallel.

Chapter 2: Histones were isolated from inhibitor-treated or untreated cells using the histone extraction kit (Active Motif, 40028), and western blots were performed. Histone

extracts were combined with Li-cor 4X Protein Loading Buffer (928-40004) and resolved on Bio-Rad Mini-PROTEAN TGX 4-20% gel (4561094) in Boston BioProducts Tris-Glycine-SDS Running Buffer (BP-150), and transferred onto an Immobilon-FL PVDF membrane (IPFL00010) using Boston BioProducts Transfer Buffer (BP-190) made to 20% vol/vol methanol. Membranes were blocked in Odyssey Blocking Buffer (OBB, 10 mM Tris-HCl pH 7.5, 150 mM NaCl, 2% Fish gelatin, 1% ovalbumin) for a minimum of 1 hour at room temperature, washed with TBS-T (Research Products International T60075-4000.0 with 0.1% Tween 20, and incubated with primary antibody (diluted in OBB with 0.2% Tween 20) overnight at 4°C. Li-cor secondary antibodies (925-32211, 925-68070) were diluted in OBB (with 0.2% Tween 20, 0.02% SDS) and blots imaged on a Li-Cor Odyssey CLX-1374. Band intensity quantification was performed using Li-Cor Image Studio v5.2. Li-Cor Chameleon Duo Pre-Stained Protein Ladder (928-60000) was used. **Chapter 3:** Lysates were harvested directly into Licor 4X Protein Loading Buffer, sonicated and boiled for 10 minutes at 95°C. SDS-PAGE gels and transfers to PVDF were run as described above. PVDF membranes were blocked with PVDF Blocking Reagent for Can Get Signal (Toyobo NYPBR01), antibody application was performed using Can Get Signal Enhancer Solution 1 & 2 (Toyobo NKB-101) and bands visualized with Vector Laboratories HRP-conjugated secondary antibodies (PI-1000-1 and PI-2000-1) and Western Lightning Plus-ECL Enhanced Chemiluminescence Substrate (Perkin Elmer). Blots were visualized on a Li-Cor chemidoc .

5.4.3. Histone Peptide Array

Peptide synthesis and validation, array fabrication, and antibody analysis were performed as described (223, 225, 244, 354). Each peptide was spotted in triplicate

twice per array. Triplicate spots were averaged and treated as a single value for subsequent statistical analysis as described (224).

5.5. Epigenetic Assays

5.5.1 ChIP-qPCR

10 mm dishes of HFFs infected with 17Syn+ at MOI 3 PFU/cell were formaldehyde fixed and processed for ChIP as previously described (96). Pellets were treated with lambda protein phosphatase for 30 minutes before sonication (New England Biolabs P0753S). qPCR was carried out on the same apparatus and software as described in 5.4.1. SsoAdvanced Universal SYBR Green Supermix (Bio-Rad 1725270) was used, and relative standard curves made with serially diluted DNA (HFFs infected at MOI 10 PFU/cell with Syn17+) extracted with the Monarch Genomic DNA Purification Kit (New England Biolabs T3010S). Fold enrichment over the input sample was calculated using relative copy numbers. Ganglia from *in vivo* infected mice were processed for ChIP as previously described (129), harvested 30 days post-infection. The antibodies used are included in Table 5.1.

5.5.2. CUT&RUN

CUT&RUN was carried out using the Epiccypher CUTANA Chic/CUT&RUN Kit and workflow (14–1048). Antibodies used for CUT&RUN are included in Table 5.1. Dual-indexed DNA libraries were prepared using Epiccypher CUTANA CUT&RUN Library Prep Kit (14-1001). Pair-ended, partial lane sequencing and de-multiplexing were carried out using NovaSeq (Novogene). Data analysis was performed using command line and R code, and workflow, adapted from the cited tutorial (342). The Rivanna high-

performance computing environment (UVA Research Computing) was used for the command line data processing.

The HSV-1 Syn17+ genome sequence (NCBI NC_001806.2) was used in combination with the hg38 human genome assembly (RefSeq GCF_000001405.40) to make a joint Bowtie2 index genome. Sequence alignment was performed with bowtie2 with the following settings: --end-to-end --very-sensitive --no-mixed --no-discordant --phred33 -I 10X 700. Separate alignments were performed to spike-in E. Coli DNA (MG1655, Genbank U00096.3), from which sequencing depth was calculated and reads normalized accordingly before filtering into separate human and viral bedgraph files. Data quality control and visualization were performed using R. Data are available in the SRA database (PRJNA1047640).

Viral gene promoter coordinates previously identified for KOS strain (259) were BLAST sequenced against the 17Syn+ genome, and the equivalent region on the 17Syn+ genome was used to generate viral promoter coordinates. Bedtools Mapbed was used to calculate the sum of scores at each defined promoter region, using normalized bedgraph files as input (promoter coordinates are listed in Table 5.3). Where a region lacked coverage, resulting in no score in the bedgraph file, a pseudo-value of 0.005 was used to allow fold enrichment calculation. Viral gene body coordinates were defined from the reference sequence NC_001806.2. Human promoters were located using the Eukaryotic Promoter Database (<https://epd.expasy.org>). The ratio between the sums for H3K27me2/3 and IgG was calculated to determine fold enrichment. MACS2 bdgcmp was used to generate linear fold enrichment bedgraph files for visualization, and the Integrative Genome Viewer Web interface (<https://igv.org/app/>) and software v2.16.1 were used to visualize bedgraph coverage files. Bedgraph coverage files from two

experimental replicates were combined using the Bedtools Bedgraph Merge Files function.

Appendix: Supplementary Data

Blank page

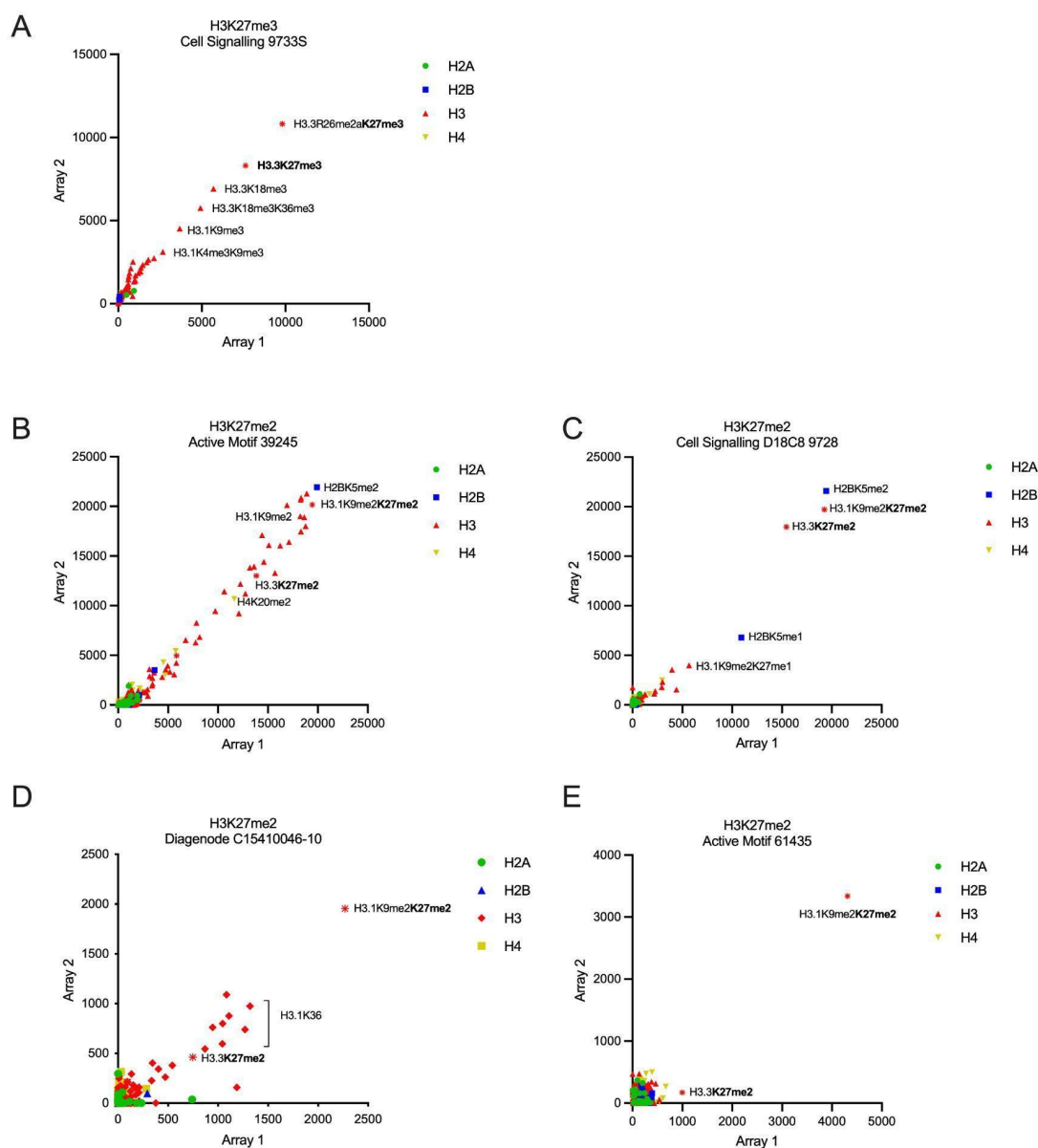


Figure 6.1: Histone peptide binding arrays for H3K27me3 and H3K27me2 antibodies show variable target specificity and non-specific binding affinities.

Scatter plots of two binding array data sets from the same antibody sample, one dataset on each axis to indicate reproducibility. Depicted are the relative binding intensities for the chosen commercial antibodies. Labels are bolded where the antibody's target residue is included in a combination of histone peptide modifications. Other notable non-specific binding partners are also labeled. *Arrays and data analysis performed by Joel Hrit of the Rothbart lab. Figure compiled by Alison Francois.*

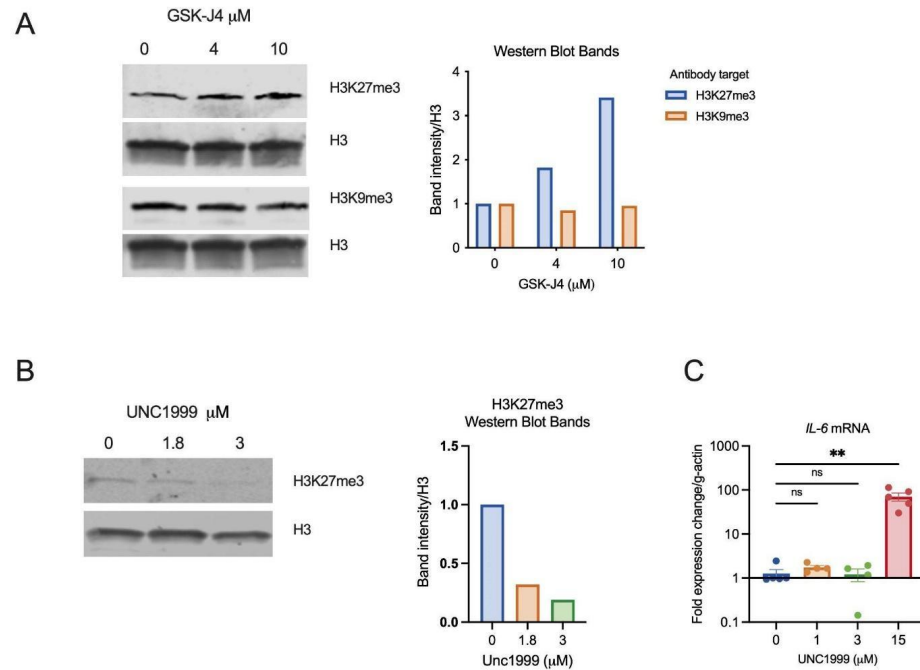


Figure 6.2: Validation of inhibitor activity and lack of interferon-stimulated gene induction.

A. HFFs were treated with UNC1999 at indicated concentrations for 4 days, with fresh inhibitor added once on day 2. The cumulative effect of UNC1999 on cellular chromatin was assessed from histone extracts blotted for H3K27me3. Li-Cor band quantification is normalized to total H3 bands, relative to untreated cells. **B.** Cumulative effects of treatment with GSK-J4 for four days on cellular chromatin, assessed by blotting histone extracts for both H3K27me3 and H3K9me3. Li-Cor band quantification in A and B was normalized to total H3 bands, relative to untreated cells. **C.** IL-6 expression measured by RT-qPCR of cDNA made from HFFs treated with indicated concentrations of UNC1999 for 5 hours. *Experiments and data analysis by Alison Francois.*

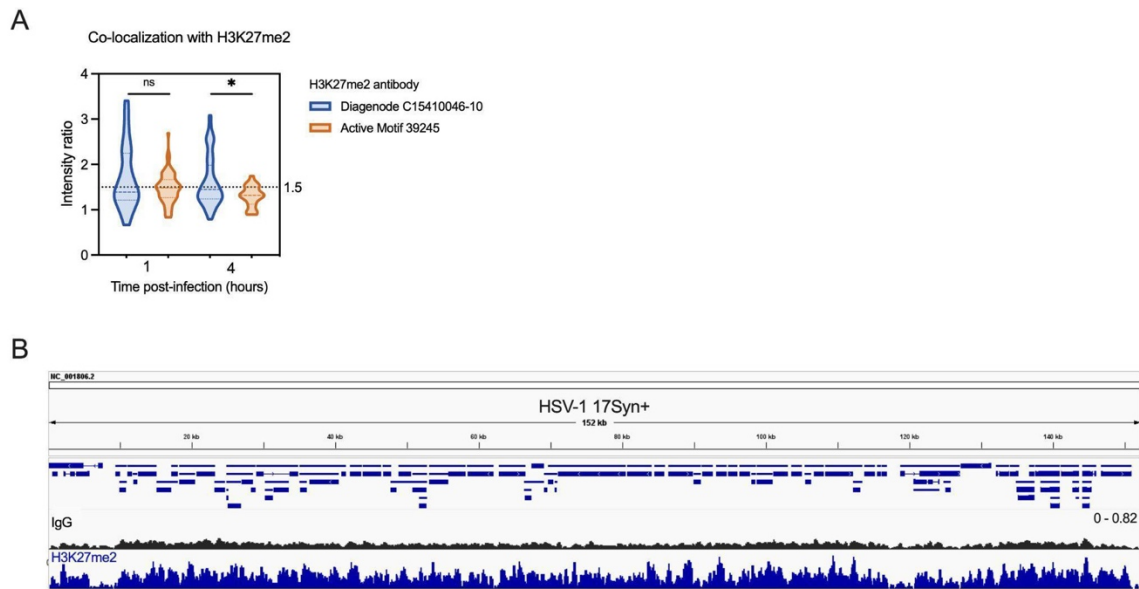


Figure 6.3: Certain H3K27me2 antibodies show evidence of non-specific binding to the viral genome.

A. Comparison of co-localization with H3K27me2 immunostained with two different antibodies at 4 HPI (Kolmogorov-Smirnov test.) Adjusted p-value $^* = < 0.05$. **B.** 17Syn+ genome coverage from HFFs 1 HPI, from a single replicate of CUT&RUN with control IgG and H3K27me2 antibodies (Diagenode C15410046-10). Experiments and data analysis by Alison Francois. Sequencing from panel B performed by Novogene, visualized on Integrative Genome Viewer.

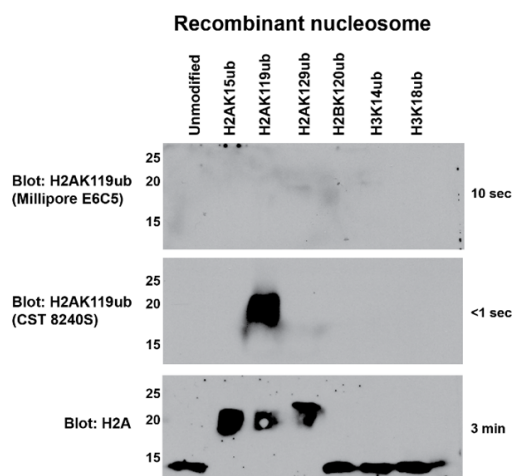


Figure 6.4: H2AK119ub antibody binding specificity assessed by western blot.

Assay performed by Joel Hrit of the Rothbart group (Van Andel institute), testing the listed antibodies for H2AK119ub against recombinant nucleosomes with different ubiquitination histone tail modifications. *Data and figure provided by Joel Hrit.*

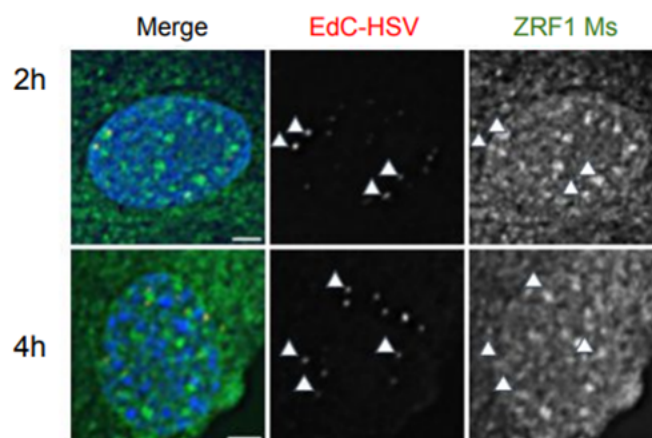


Figure 6.5: ZRF1 staining with a mouse antibody shows concentration at replication compartments.

High MOI (approximately 10 genomes/cell) infected HFFs 2 and 4 HPI stained for ZRF1 with the mouse (Santa Cruz) antibody. Blue= nuclear Hoechst stain. Arrows point to the same points on each image, a randomly chosen sampling of the viral genomes within that nucleus. *Experiments and data analysis by Alison Francois.*

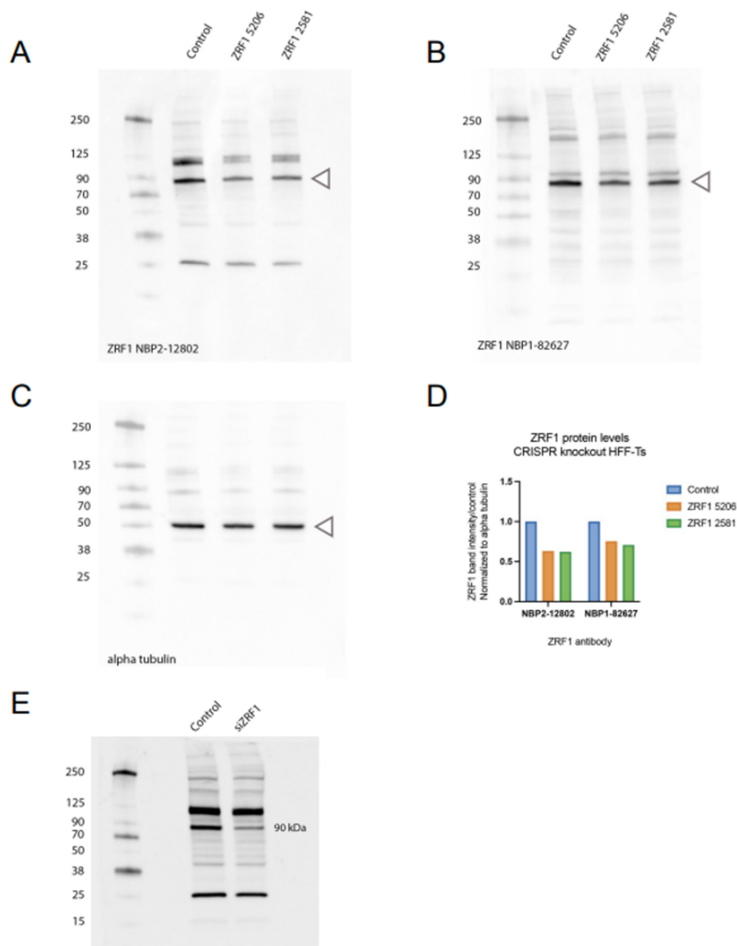


Figure 6.6: Western blots of ZRF1 showed non-specific protein bands.

A-B. Cell lysates from HFF-Ts treated with CRISPR-Cas9 to remove ZRF1 expression. Lysates were harvested following selection and blotted with the indicated antibody against ZRF1. The partial reduction in ZRF1 signal indicates a mixed population of CRISPR-modified and unmodified cells. **C.** Loading control for A and B, blotted for alpha tubulin. **D.** ImageJ quantification of band intensity at the band indicated by arrows in A and B. **E.** siRNA-mediated knockdown of ZRF1 were attempted in HFFs, cell lysates harvested 72h post-transfection and run on an SDS-PAGE gel and transferred to PVDF for western blotting. Expected band size is indicated on the right hand side of the blot, as reported by the antibody manufacturer.

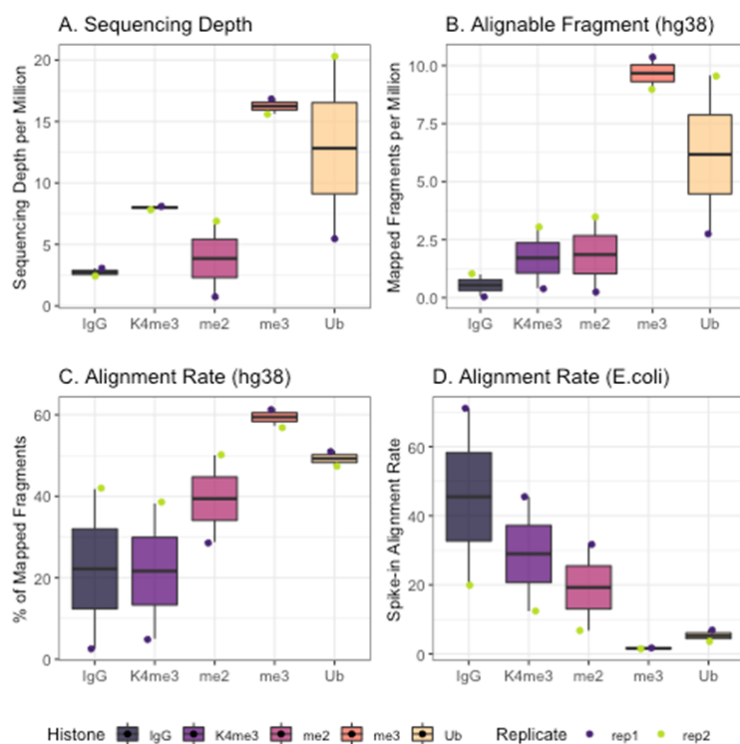


Figure 6.7: Optimizing CUT&RUN for H2AK119ub in HFF cells.

Quality control analysis comparing aligned sequencing data with antibodies for IgG (negative control), K4me3 (positive control included in product), H3K27me2, H3K27me3 and H2AK119ub. Rep 1= formaldehyde fixed, rep 2= unfixed. Hg38 is a human genome assembly, E. coli DNA was spiked in to normalize reads to sequencing depth later. **A.** Sequencing depth for reach sample, calculated using spike-in E. coli DNA. **B.** The fraction of fragments alignable to the reference genome. **C.** Rate of fragment alignment to the human genome. **D.** Rate of alignment to the spike-in E. coli genome. *Data analysis by Alison Francois using RStudio, following a published tutorial (342)*

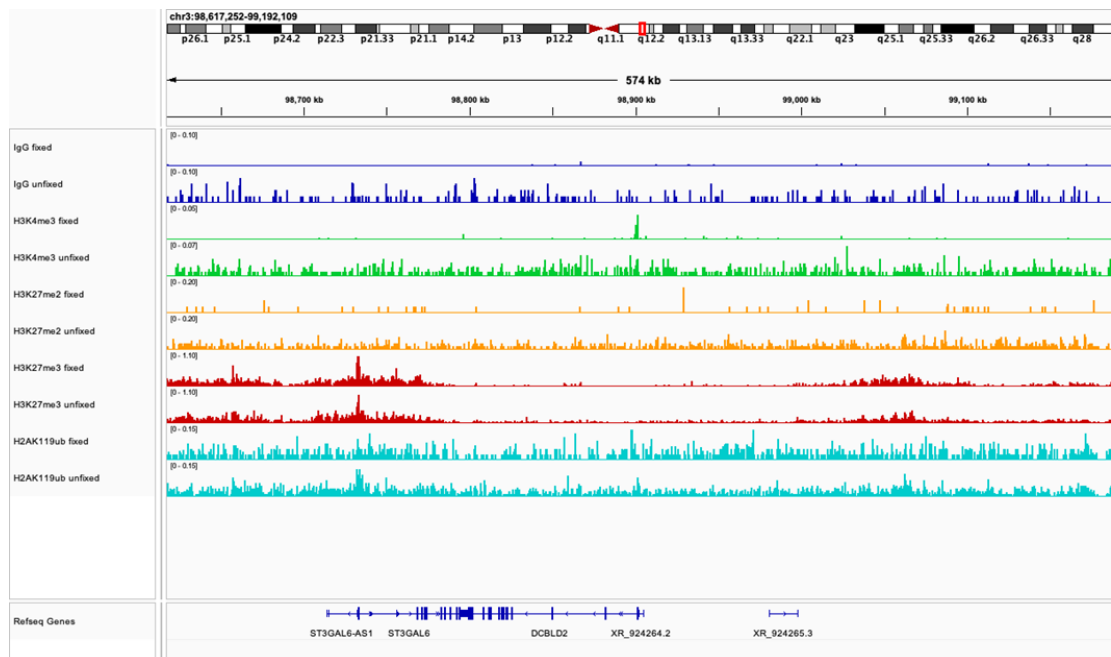


Figure 6.8: Integrative Genome Viewer coverage plots for CUT&RUN samples.

A sample region of the human genome (chromosome 3) comparing coverage (normalized to sequencing depth) for the fixed and unfixed samples (each within a pair set to the same scale). The scale is displayed in the top left corner of each coverage plot. Coverage for the negative control IgG (blue), H3K4me3 (green), H3K27me2 (yellow), H3K27me3 (red), and H2AK119ub (teal) are shown. Host genes are annotated in the lower panel. *Experiment and data analysis by Alison Francois.*

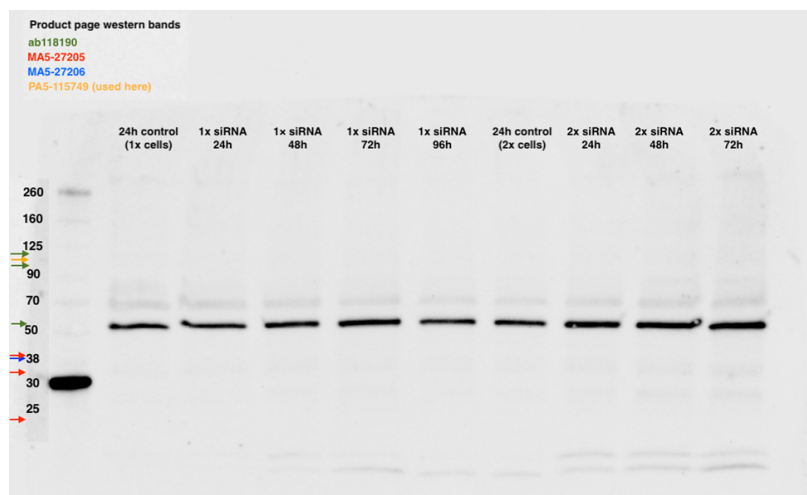


Figure 6.9: Assessing PHF20L1 protein levels by western blot is made complicated by bands of unexpected sizes.

A western blot from an SDS-PAGE gel run with HFF cell lysate following single or double siRNA-mediated knockdown against PHF20L1. The arrows to the left indicate expected band size according to the manufacturer of several antibodies against PHF20L1. The expected band size for the antibody used on this blot (PA5-115749) is indicated by the yellow arrow. *Experiments and data analysis by Alison Francois.*

References

1. Dochnal SA, Francois AK, Cliffe AR. 2021. De Novo Polycomb Recruitment: Lessons from Latent Herpesviruses. *Viruses* 13:1470.
2. Cohen JI. 2020. Herpesvirus latency. *J Clin Invest* 130:3361–3369.
3. Dolan A, Jamieson FE, Cunningham C, Barnett BC, McGeoch DJ. 1998. The genome sequence of herpes simplex virus type 2. *J Virol* 72:2010–2021.
4. Kimberlin D. 2004. Herpes simplex virus, meningitis and encephalitis in neonates. *Herpes* 11 Suppl 2:65A-76A.
5. Berkhout A, Kapoor V, Heney C, Jones CA, Clark JE, Britton PN, Vaska VL, Lai MM, Nourse C. 2022. Epidemiology and long-term neurological sequelae of childhood herpes simplex CNS infection. *J Paediatr Child Health* 58:1372–1378.
6. Naesens L, Muppala S, Acharya D, Nemegeer J, Bogaert D, Lee J-H, Staes K, Debacker V, De Bleser P, De Bruyne M, De Baere E, van Gent M, Liu G, Lambrecht BN, Staal J, Kerre T, Beyaert R, Maelfait J, Tavernier SJ, Gack MU, Haerynck F. 2022. GTF3A mutations predispose to herpes simplex encephalitis by disrupting biogenesis of the host-derived RIG-I ligand RNA5SP141. *Sci Immunol* 7:eabq4531.
7. Tyler KL. 2004. Herpes simplex virus infections of the central nervous system: encephalitis and meningitis, including Mollaret's. *Herpes* 11 Suppl 2:57A-64A.
8. Ibáñez FJ, Farías MA, Gonzalez-Troncoso MP, Corrales N, Duarte LF, Retamal-Díaz A, González PA. 2018. Experimental Dissection of the Lytic Replication Cycles of Herpes Simplex Viruses in vitro. *Front Microbiol* 9:2406.
9. Herpes simplex virus. <https://www.who.int/news-room/fact-sheets/detail/herpes-simplex-virus>. Retrieved 20 March 2024.
10. Xu F, Sternberg MR, Kottiri BJ, McQuillan GM, Lee FK, Nahmias AJ, Berman SM, Markowitz LE. 2006. Trends in herpes simplex virus type 1 and type 2 seroprevalence in the United States. *JAMA* 296:964–973.
11. Reeves WC, Corey L, Adams HG, Vontver LA, Holmes KK. 1981. Risk of recurrence after first episodes of genital herpes. Relation to HSV type and antibody response. *N Engl J Med* 305:315–319.
12. Lafferty WE, Coombs RW, Benedetti J, Critchlow C, Corey L. 1987. Recurrences after oral and genital herpes simplex virus infection. Influence of site of infection and viral type. *N Engl J Med* 316:1444–1449.
13. Lee S, Ives AM, Bertke AS. 2015. Herpes Simplex Virus 1 Reactivates from Autonomic Ciliary Ganglia Independently from Sensory Trigeminal Ganglia To Cause Recurrent Ocular Disease. *J Virol* 89:8383–8391.

14. James C, Harfouche M, Welton NJ, Turner KM, Abu-Raddad LJ, Gottlieb SL, Looker KJ. 2020. Herpes simplex virus: global infection prevalence and incidence estimates, 2016. *Bull World Health Organ* 98:315–329.
15. Marcocci ME, Napoletani G, Protto V, Kolesova O, Piacentini R, Li Puma DD, Lomonte P, Grassi C, Palamara AT, De Chiara G. 2020. Herpes Simplex Virus-1 in the Brain: The Dark Side of a Sneaky Infection. *Trends Microbiol* 28:808–820.
16. Jamieson GA, Maitland NJ, Wilcock GK, Craske J, Itzhaki RF. 1991. Latent herpes simplex virus type 1 in normal and Alzheimer's disease brains. *J Med Virol* 33:224–227.
17. Beffert U, Bertrand P, Champagne D, Gauthier S, Poirier J. 1998. HSV-1 in brain and risk of Alzheimer's disease. *Lancet*.
18. Itzhaki RF. 2021. Overwhelming Evidence for a Major Role for Herpes Simplex Virus Type 1 (HSV1) in Alzheimer's Disease (AD); Underwhelming Evidence against. *Vaccines (Basel)* 9.
19. Wainberg M, Luquez T, Koelle DM, Readhead B, Johnston C, Darvas M, Funk CC. 2021. The viral hypothesis: how herpesviruses may contribute to Alzheimer's disease. *Mol Psychiatry* 26:5476–5480.
20. Yong SJ, Yong MH, Teoh SL, Soga T, Parhar I, Chew J, Lim WL. 2021. The Hippocampal Vulnerability to Herpes Simplex Virus Type I Infection: Relevance to Alzheimer's Disease and Memory Impairment. *Front Cell Neurosci* 15:695738.
21. Varicella. <https://www.who.int/teams/health-product-policy-and-standards/standards-and-specifications/vaccine-standardization/varicella>. Retrieved 20 March 2024.
22. Harpaz R, Leung JW. 2019. The Epidemiology of Herpes Zoster in the United States During the Era of Varicella and Herpes Zoster Vaccines: Changing Patterns Among Children. *Clin Infect Dis* 69:345–347.
23. Sorel O, Messaoudi I. 2018. Varicella Virus-Host Interactions During Latency and Reactivation: Lessons From Simian Varicella Virus. *Front Microbiol* 9:3170.
24. Kennedy PGE, Gershon AA. 2018. Clinical Features of Varicella-Zoster Virus Infection. *Viruses* 10.
25. Kennedy PGE, Mogensen TH, Cohrs RJ. 2021. Recent Issues in Varicella-Zoster Virus Latency. *Viruses* 13.
26. Sampathkumar P, Drage LA, Martin DP. 2009. Herpes zoster (shingles) and postherpetic neuralgia. *Mayo Clin Proc* 84:274–280.

27. Collins-McMillen D, Buehler J, Peppenelli M, Goodrum F. 2018. Molecular Determinants and the Regulation of Human Cytomegalovirus Latency and Reactivation. *Viruses* 10.
28. Zuhair M, Smit GSA, Wallis G, Jabbar F, Smith C, Devleeschauwer B, Griffiths P. 2019. Estimation of the worldwide seroprevalence of cytomegalovirus: A systematic review and meta-analysis. *Rev Med Virol* 29:e2034.
29. 2023. Cytomegalovirus (CMV) and Congenital CMV Infection. <https://www.cdc.gov/cmvi/index.html>. Retrieved 20 March 2024.
30. Forte E, Zhang Z, Thorp EB, Hummel M. 2020. Cytomegalovirus Latency and Reactivation: An Intricate Interplay With the Host Immune Response. *Front Cell Infect Microbiol* 10:130.
31. Goodrum F. 2016. Human Cytomegalovirus Latency: Approaching the Gordian Knot. *Annu Rev Virol* 3:333–357.
32. Leng SX, Kamil J, Purdy JG, Lemmermann NA, Reddehase MJ, Goodrum FD. 2017. Recent advances in CMV tropism, latency, and diagnosis during aging. *Geroscience* 39:251–259.
33. Crawford LB, Diggins NL, Caposio P, Hancock MH. 2022. Advances in Model Systems for Human Cytomegalovirus Latency and Reactivation. *MBio* 13:e0172421.
34. Mohanna S, Maco V, Bravo F, Gotuzzo E. 2005. Epidemiology and clinical characteristics of classic Kaposi's sarcoma, seroprevalence, and variants of human herpesvirus 8 in South America: a critical review of an old disease. *Int J Infect Dis* 9:239–250.
35. Stănescu L, Foarfă C, Georgescu AC, Georgescu I. 2007. Kaposi's sarcoma associated with AIDS. *Rom J Morphol Embryol* 48:181–187.
36. Dunmire SK, Verghese PS, Balfour HH Jr. 2018. Primary Epstein-Barr virus infection. *J Clin Virol* 102:84–92.
37. Bjornevik K, Cortese M, Healy BC, Kuhle J, Mina MJ, Leng Y, Elledge SJ, Niebuhr DW, Scher AI, Munger KL, Ascherio A. 2022. Longitudinal analysis reveals high prevalence of Epstein-Barr virus associated with multiple sclerosis. *Science* 375:296–301.
38. Sundaresan B, Shirafkan F, Ripperger K, Rattay K. 2023. The Role of Viral Infections in the Onset of Autoimmune Diseases. *Viruses* 15.
39. Wang W, Ji M. 2019. Efficacy of acyclovir for herpes simplex encephalitis: A protocol for a systematic review of randomized controlled trial. *Medicine* 98:e15254.

40. Pisitpayat P, Jongkhajornpong P, Lekhanont K, Nonpassopon M. 2021. Role of Intravenous Acyclovir in Treatment of Herpes Simplex Virus Stromal Keratitis with Ulceration: A Review of 2 Cases. *Am J Case Rep* 22:e930467.
41. Brandariz-Nuñez D, Correas-Sanahuja M, Maya-Gallego S, Martín Herranz I. 2021. Neurotoxicity associated with acyclovir and valacyclovir: A systematic review of cases. *J Clin Pharm Ther* 46:918–926.
42. Boyd MR, Safrin S, Kern ER. 1993. Penciclovir: a review of its spectrum of activity, selectivity, and cross-resistance pattern. *Antivir Chem Chemother* 4:3–11.
43. Pottage JC Jr, Kessler HA. 1995. Herpes simplex virus resistance to acyclovir: clinical relevance. *Infect Agents Dis* 4:115–124.
44. Reusser P. 1996. Herpesvirus resistance to antiviral drugs: a review of the mechanisms, clinical importance and therapeutic options. *J Hosp Infect* 33:235–248.
45. Moomaw MD, Cornea P, Rathbun RC, Wendel KA. 2003. Review of antiviral therapy for herpes labialis, genital herpes and herpes zoster. *Expert Rev Anti Infect Ther* 1:283–295.
46. Schalkwijk HH, Snoeck R, Andrei G. 2022. Acyclovir resistance in herpes simplex viruses: Prevalence and therapeutic alternatives. *Biochem Pharmacol* 206:115322.
47. Sharma D, Sharma S, Akojwar N, Dondulkar A, Yenorkar N, Pandita D, Prasad SK, Dhobi M. 2023. An Insight into Current Treatment Strategies, Their Limitations, and Ongoing Developments in Vaccine Technologies against Herpes Simplex Infections. *Vaccines (Basel)* 11.
48. Dong H, Wang Z, Zhao D, Leng X, Zhao Y. 2021. Antiviral strategies targeting herpesviruses. *J Virus Erad* 7:100047.
49. Kim Y, Anderson JL, Lewin SR. 2018. Getting the “Kill” into “Shock and Kill”: Strategies to Eliminate Latent HIV. *Cell Host Microbe* 23:14–26.
50. Abner E, Jordan A. 2019. HIV “shock and kill” therapy: In need of revision. *Antiviral Res* 166:19–34.
51. Nehme Z, Pasquereau S, Herbein G. 2019. Control of viral infections by epigenetic-targeted therapy. *Clin Epigenetics* 11:55.
52. Liang Y, Vogel JL, Arbuckle JH, Rai G, Jadhav A, Simeonov A, Maloney DJ, Kristie TM. 2013. Targeting the JMJD2 histone demethylases to epigenetically control herpesvirus infection and reactivation from latency. *Sci Transl Med* 5:167ra5.

53. Shimeld C, Tullo AB, Hill TJ, Blyth WA, Easty DL. 1985. Spread of herpes simplex virus and distribution of latent infection after intraocular infection of the mouse. *Arch Virol* 85:175–187.
54. Dyson H, Shimeld C, Hill TJ, Blyth WA, Easty DL. 1987. Spread of herpes simplex virus within ocular nerves of the mouse: demonstration of viral antigen in whole mounts of eye tissue. *J Gen Virol* 68 (Pt 12):2989–2995.
55. Döhner K, Cornelius A, Serrero MC, Sodeik B. 2021. The journey of herpesvirus capsids and genomes to the host cell nucleus. *Curr Opin Virol* 50:147–158.
56. McElwee M, Vijayakrishnan S, Rixon F, Bhella D. 2018. Structure of the herpes simplex virus portal-vertex. *PLoS Biol* 16:e2006191.
57. Evilevitch A, Lavelle L, Knobler CM, Raspaud E, Gelbart WM. 2003. Osmotic pressure inhibition of DNA ejection from phage. *Proc Natl Acad Sci U S A* 100:9292–9295.
58. Petrov AS, Harvey SC. 2007. Structural and thermodynamic principles of viral packaging. *Structure* 15:21–27.
59. Liashkovich I, Hafezi W, Kühn JM, Oberleithner H, Shahin V. 2011. Nuclear delivery mechanism of herpes simplex virus type 1 genome. *J Mol Recognit* 24:414–421.
60. Brandariz-Nuñez A, Liu T, Du T, Evilevitch A. 2019. Pressure-driven release of viral genome into a host nucleus is a mechanism leading to herpes infection. *Elife* 8.
61. Brandariz-Nuñez A, Robinson SJ, Evilevitch A. 2020. Pressurized DNA state inside herpes capsids-A novel antiviral target. *PLoS Pathog* 16:e1008604.
62. Strang BL, Stow ND. 2005. Circularization of the herpes simplex virus type 1 genome upon lytic infection. *J Virol* 79:12487–12494.
63. Roizman B, Knipe DM, Whitley RJ. 2013. *Fields Virology*, 6th ed. Lippincott Williams & Wilkins. <https://play.google.com/store/books/details?id=QCyMAwAAQBAJ>.
64. Wysocka J, Herr W. 2003. The herpes simplex virus VP16-induced complex: the makings of a regulatory switch. *Trends Biochem Sci* 28:294–304.
65. Hancock MH, Cliffe AR, Knipe DM, Smiley JR. 2010. Herpes simplex virus VP16, but not ICP0, is required to reduce histone occupancy and enhance histone acetylation on viral genomes in U2OS osteosarcoma cells. *J Virol* 84:1366–1375.
66. Suk H, Knipe DM. 2015. Proteomic analysis of the herpes simplex virus 1 virion protein 16 transactivator protein in infected cells. *Proteomics* 15:1957–1967.
67. Ahmad I, Wilson DW. 2020. HSV-1 Cytoplasmic Envelopment and Egress. *Int J Mol*

Sci 21.

68. Antinone SE, Smith GA. 2010. Retrograde axon transport of herpes simplex virus and pseudorabies virus: a live-cell comparative analysis. *J Virol* 84:1504–1512.
69. Hafezi W, Lorentzen EU, Eing BR, Müller M, King NJC, Klupp B, Mettenleiter TC, Kühn JE. 2012. Entry of herpes simplex virus type 1 (HSV-1) into the distal axons of trigeminal neurons favors the onset of nonproductive, silent infection. *PLoS Pathog* 8:e1002679.
70. Cereghini S, Yaniv M. 1984. Assembly of transfected DNA into chromatin: structural changes in the origin-promoter-enhancer region upon replication. *EMBO J* 3:1243–1253.
71. Kobilier O, Brodersen P, Taylor MP, Ludmir EB, Enquist LW. 2011. Herpesvirus replication compartments originate with single incoming viral genomes. *MBio* 2.
72. Sekine E, Schmidt N, Gaboriau D, O'Hare P. 2017. Spatiotemporal dynamics of HSV genome nuclear entry and compaction state transitions using bioorthogonal chemistry and super-resolution microscopy. *PLoS Pathog* 13:e1006721.
73. Everett RD, Sourvinos G, Leiper C, Clements JB, Orr A. 2004. Formation of nuclear foci of the herpes simplex virus type 1 regulatory protein ICP4 at early times of infection: localization, dynamics, recruitment of ICP27, and evidence for the de novo induction of ND10-like complexes. *J Virol* 78:1903–1917.
74. Taylor TJ, Knipe DM. 2004. Proteomics of herpes simplex virus replication compartments: association of cellular DNA replication, repair, recombination, and chromatin remodeling proteins with ICP8. *J Virol* 78:5856–5866.
75. Honess RW, Roizman B. 1974. Regulation of herpesvirus macromolecular synthesis. I. Cascade regulation of the synthesis of three groups of viral proteins. *J Virol* 14:8–19.
76. Honess RW, Roizman B. 1975. Regulation of herpesvirus macromolecular synthesis: sequential transition of polypeptide synthesis requires functional viral polypeptides. *Proc Natl Acad Sci U S A* 72:1276–1280.
77. Boutell C, Cuchet-Lourenço D, Vanni E, Orr A, Glass M, McFarlane S, Everett RD. 2011. A viral ubiquitin ligase has substrate preferential SUMO targeted ubiquitin ligase activity that counteracts intrinsic antiviral defence. *PLoS Pathog* 7:e1002245.
78. Cuchet-Lourenço D, Vanni E, Glass M, Orr A, Everett RD. 2012. Herpes simplex virus 1 ubiquitin ligase ICP0 interacts with PML isoform I and induces its SUMO-independent degradation. *J Virol* 86:11209–11222.

79. Alandijany T, Roberts APE, Conn KL, Loney C, McFarlane S, Orr A, Boutell C. 2018. Distinct temporal roles for the promyelocytic leukaemia (PML) protein in the sequential regulation of intracellular host immunity to HSV-1 infection. *PLoS Pathog* 14:e1006769.
80. McFarlane S, Orr A, Roberts APE, Conn KL, Iliev V, Loney C, da Silva Filipe A, Smollett K, Gu Q, Robertson N, Adams PD, Rai TS, Boutell C. 2019. The histone chaperone HIRA promotes the induction of host innate immune defences in response to HSV-1 infection. *PLoS Pathog* 15:e1007667.
81. Rodríguez MC, Dybas JM, Hughes J, Weitzman MD, Boutell C. 2020. The HSV-1 ubiquitin ligase ICP0: Modifying the cellular proteome to promote infection. *Virus Res* 285:198015.
82. Everett RD, Parada C, Gripon P, Sirma H, Orr A. 2008. Replication of ICP0-null mutant herpes simplex virus type 1 is restricted by both PML and Sp100. *J Virol* 82:2661–2672.
83. Gu H, Zheng Y. 2016. Role of ND10 nuclear bodies in the chromatin repression of HSV-1. *Virol J* 13:62.
84. Xu P, Roizman B. 2017. The SP100 component of ND10 enhances accumulation of PML and suppresses replication and the assembly of HSV replication compartments. *Proc Natl Acad Sci U S A* 114:E3823–E3829.
85. Cohen C, Corpet A, Roubille S, Maroui MA, Poccardi N, Rousseau A, Kleijwegt C, Binda O, Texier P, Sawtell N, Labetoulle M, Lomonte P. 2018. Promyelocytic leukemia (PML) nuclear bodies (NBs) induce latent/quiescent HSV-1 genomes chromatinization through a PML NB/Histone H3.3/H3.3 Chaperone Axis. *PLoS Pathog* 14:e1007313.
86. Merkl PE, Orzalli MH, Knipe DM. 2018. Mechanisms of Host IFI16, PML, and Daxx Protein Restriction of Herpes Simplex Virus 1 Replication. *J Virol* 92.
87. Mertens ME, Knipe DM. 2021. Herpes Simplex Virus 1 Manipulates Host Cell Antiviral and Proviral DNA Damage Responses. *MBio* 12.
88. Suzich JB, Cuddy SR, Baidas H, Dochnal S, Ke E, Schinlever AR, Babnis A, Boutell C, Cliffe AR. 2021. PML-NB-dependent type I interferon memory results in a restricted form of HSV latency. *EMBO Rep* 22:e52547.
89. Ma Y, Li J, Dong H, Yang Z, Zhou L, Xu P. 2022. PML Body Component Sp100A Restricts Wild-Type Herpes Simplex Virus 1 Infection. *J Virol* 96:e0027922.
90. Dembowski JA, DeLuca NA. 2015. Selective recruitment of nuclear factors to productively replicating herpes simplex virus genomes. *PLoS Pathog* 11:e1004939.

91. Dembowski JA, DeLuca NA. 2018. Temporal Viral Genome-Protein Interactions Define Distinct Stages of Productive Herpesviral Infection. *MBio* 9:01182–01118.
92. Leinbach SS, Summers WC. 1980. The structure of herpes simplex virus type 1 DNA as probed by micrococcal nuclease digestion. *J Gen Virol* 51:45–59.
93. Lentine AF, Bachenheimer SL. 1990. Intracellular organization of herpes simplex virus type 1 DNA assayed by staphylococcal nuclease sensitivity. *Virus Res* 16:275–292.
94. Kent JR, Zeng P-Y, Atanasiu D, Gardner J, Fraser NW, Berger SL. 2004. During lytic infection herpes simplex virus type 1 is associated with histones bearing modifications that correlate with active transcription. *J Virol* 78:10178–10186.
95. Herrera FJ, Triezenberg SJ. 2004. VP16-dependent association of chromatin-modifying coactivators and underrepresentation of histones at immediate-early gene promoters during herpes simplex virus infection. *J Virol* 78:9689–9696.
96. Cliffe AR, Knipe DM. 2008. Herpes simplex virus ICP0 promotes both histone removal and acetylation on viral DNA during lytic infection. *J Virol* 82:12030–12038.
97. Huang J, Kent JR, Placek B, Whelan KA, Hollow CM, Zeng P-Y, Fraser NW, Berger SL. 2006. Trimethylation of histone H3 lysine 4 by Set1 in the lytic infection of human herpes simplex virus 1. *J Virol* 80:5740–5746.
98. Narayanan A, Ruyechan WT, Kristie TM. 2007. The coactivator host cell factor-1 mediates Set1 and MLL1 H3K4 trimethylation at herpesvirus immediate early promoters for initiation of infection. *Proc Natl Acad Sci U S A* 104:10835–10840.
99. Kristie TM. 2016. Chromatin Modulation of Herpesvirus Lytic Gene Expression: Managing Nucleosome Density and Heterochromatic Histone Modifications. *MBio* 7:e00098-16.
100. Kutluay SB, DeVos SL, Klomp JE, Triezenberg SJ. 2009. Transcriptional coactivators are not required for herpes simplex virus type 1 immediate-early gene expression in vitro. *J Virol* 83:3436–3449.
101. Liang Y, Vogel JL, Narayanan A, Peng H, Kristie TM. 2009. Inhibition of the histone demethylase LSD1 blocks alpha-herpesvirus lytic replication and reactivation from latency. *Nat Med* 15:1312–1317.
102. Roizman B. 2011. The checkpoints of viral gene expression in productive and latent infection: the role of the HDAC/CoREST/LSD1/REST repressor complex. *J Virol* 85:7474–7482.
103. Raja P, Lee JS, Pan D, Pesola JM, Coen DM, Knipe DM. 2016. A Herpesviral

- Lytic Protein Regulates the Structure of Latent Viral Chromatin. *MBio* 7.
104. Oh HS, Bryant KF, Nieland TJF, Mazumder A, Bagul M, Bathe M, Root DE, Knipe DM. 2014. A targeted RNA interference screen reveals novel epigenetic factors that regulate herpesviral gene expression. *MBio* 5:e01086-13.
 105. Shapira L, Ralph M, Tomer E, Cohen S, Kobilier O. 2016. Histone Deacetylase Inhibitors Reduce the Number of Herpes Simplex Virus-1 Genomes Initiating Expression in Individual Cells. *Front Microbiol* 7:1970.
 106. Hu M, Depledge DP, Flores Cortes E, Breuer J, Schang LM. 2019. Chromatin dynamics and the transcriptional competence of HSV-1 genomes during lytic infections. *PLoS Pathog* 15:e1008076.
 107. Dremel SE, DeLuca NA. 2019. Herpes simplex viral nucleoprotein creates a competitive transcriptional environment facilitating robust viral transcription and host shut off. *Elife* 8.
 108. Knipe DM, Cliffe A. 2008. Chromatin control of herpes simplex virus lytic and latent infection. *Nat Rev Microbiol* 6:211–221.
 109. Delbarre E, Ivanauskiene K, Küntziger T, Collas P. 2013. DAXX-dependent supply of soluble (H3.3-H4) dimers to PML bodies pending deposition into chromatin. *Genome Res* 23:440–451.
 110. Lorković ZJ, Park C, Goiser M, Jiang D, Kurzbauer M-T, Schlögelhofer P, Berger F. 2017. Compartmentalization of DNA Damage Response between Heterochromatin and Euchromatin Is Mediated by Distinct H2A Histone Variants. *Curr Biol* 27:1192–1199.
 111. Zink L-M, Delbarre E, Eberl HC, Keilhauer EC, Bönisch C, Pünzeler S, Bartkuhn M, Collas P, Mann M, Hake SB. 2017. H3.Y discriminates between HIRA and DAXX chaperone complexes and reveals unexpected insights into human DAXX-H3.3-H4 binding and deposition requirements. *Nucleic Acids Res* 45:5691–5706.
 112. Wang Y, Long H, Yu J, Dong L, Wassef M, Zhuo B, Li X, Zhao J, Wang M, Liu C, Wen Z, Chang L, Chen P, Wang Q-F, Xu X, Margueron R, Li G. 2018. Histone variants H2A.Z and H3.3 coordinately regulate PRC2-dependent H3K27me3 deposition and gene expression regulation in mES cells. *BMC Biol* 16:107.
 113. Dunjić M, Jonas F, Yaakov G, More R, Mayshar Y, Rais Y, Orenbuch A-H, Cheng S, Barkai N, Stelzer Y. 2023. Histone exchange sensors reveal variant specific dynamics in mouse embryonic stem cells. *Nat Commun* 14:3791.
 114. Cabral JM, Cushman CH, Sodroski CN, Knipe DM. 2021. ATRX limits the accessibility of histone H3-occupied HSV genomes during lytic infection. *PLoS*

Pathog 17:e1009567.

115. Placek BJ, Huang J, Kent JR, Dorsey J, Rice L, Fraser NW, Berger SL. 2009. The histone variant H3.3 regulates gene expression during lytic infection with herpes simplex virus type 1. *J Virol* 83:1416–1421.
116. Conn KL, Hendzel MJ, Schang LM. 2013. The differential mobilization of histones H3.1 and H3.3 by herpes simplex virus 1 relates histone dynamics to the assembly of viral chromatin. *PLoS Pathog* 9:e1003695.
117. Conn KL, Schang LM. 2013. Chromatin dynamics during lytic infection with herpes simplex virus 1. *Viruses* 5:1758–1786.
118. Yu M, Liu K, Mao Z, Luo J, Gu W, Zhao W. 2016. USP11 Is a Negative Regulator to γ H2AX Ubiquitylation by RNF8/RNF168*. *J Biol Chem* 291:959–967.
119. Lilley CE, Carson CT, Muotri AR, Gage FH, Weitzman MD. 2005. DNA repair proteins affect the lifecycle of herpes simplex virus 1. *Proc Natl Acad Sci U S A* 102:5844–5849.
120. Lilley CE, Chaurushiya MS, Boutell C, Everett RD, Weitzman MD. 2011. The intrinsic antiviral defense to incoming HSV-1 genomes includes specific DNA repair proteins and is counteracted by the viral protein ICP0. *PLoS Pathog* 7:e1002084.
121. Packard JE, Dembowski JA. 2021. HSV-1 DNA Replication-Coordinated Regulation by Viral and Cellular Factors. *Viruses* 13:2015.
122. Perng GC, Slanina SM, Yukht A, Ghiasi H, Nesburn AB, Wechsler SL. 2000. The latency-associated transcript gene enhances establishment of herpes simplex virus type 1 latency in rabbits. *J Virol* 74:1885–1891.
123. Bertke AS, Swanson SM, Chen J, Imai Y, Kinchington PR, Margolis TP. 2011. A5-positive primary sensory neurons are nonpermissive for productive infection with herpes simplex virus 1 in vitro. *J Virol* 85:6669–6677.
124. Nicoll MP, Hann W, Shivkumar M, Harman LER, Connor V, Coleman HM, Proença JT, Efstathiou S. 2016. The HSV-1 Latency-Associated Transcript Functions to Repress Latent Phase Lytic Gene Expression and Suppress Virus Reactivation from Latently Infected Neurons. *PLoS Pathog* 12:e1005539.
125. Kubat NJ, Amelio AL, Giordani NV, Bloom DC. 2004. The herpes simplex virus type 1 latency-associated transcript (LAT) enhancer/rcr is hyperacetylated during latency independently of LAT transcription. *J Virol* 78:12508–12518.
126. Amelio AL, Giordani NV, Kubat NJ, O'neil JE, Bloom DC. 2006. Deacetylation of the herpes simplex virus type 1 latency-associated transcript (LAT) enhancer and a

- decrease in LAT abundance precede an increase in ICP0 transcriptional permissiveness at early times postexplant. *J Virol* 80:2063–2068.
127. Amelio AL, McAnany PK, Bloom DC. 2006. A chromatin insulator-like element in the herpes simplex virus type 1 latency-associated transcript region binds CCCTC-binding factor and displays enhancer-blocking and silencing activities. *J Virol* 80:2358–2368.
128. Cliffe AR, Garber DA, Knipe DM. 2009. Transcription of the herpes simplex virus latency-associated transcript promotes the formation of facultative heterochromatin on lytic promoters. *J Virol* 83:8182–8190.
129. Cliffe AR, Coen DM, Knipe DM. 2013. Kinetics of facultative heterochromatin and polycomb group protein association with the herpes simplex viral genome during establishment of latent infection. *MBio* 4:e00590-12.
130. Wang Q-Y, Zhou C, Johnson KE, Colgrove RC, Coen DM, Knipe DM. 2005. Herpesviral latency-associated transcript gene promotes assembly of heterochromatin on viral lytic-gene promoters in latent infection. *Proc Natl Acad Sci U S A* 102:16055–16059.
131. Catez F, Picard C, Held K, Gross S, Rousseau A, Theil D, Sawtell N, Labetoulle M, Lomonte P. 2012. HSV-1 genome subnuclear positioning and associations with host-cell PML-NBs and centromeres regulate LAT locus transcription during latency in neurons. *PLoS Pathog* 8:e1002852.
132. Whitford AL, Cliffe AR. 2022. Key questions on the epigenetics of herpes simplex virus latency. *PLoS Pathog* 18:e1010587.
133. Deshmane SL, Fraser NW. 1989. During latency, herpes simplex virus type 1 DNA is associated with nucleosomes in a chromatin structure. *J Virol* 63:943–947.
134. Healy E, Mucha M, Glancy E, Fitzpatrick DJ, Conway E, Neikes HK, Monger C, Van Mierlo G, Baltissen MP, Koseki Y, Vermeulen M, Koseki H, Bracken AP. 2019. PRC2.1 and PRC2.2 Synergize to Coordinate H3K27 Trimethylation. *Mol Cell* 76:437-452.e6.
135. Delbarre E, Ivanauskiene K, Spirkoski J, Shah A, Vekterud K, Moskaug JØ, Bøe SO, Wong LH, Küntziger T, Collas P. 2017. PML protein organizes heterochromatin domains where it regulates histone H3.3 deposition by ATRX/DAXX. *Genome Res* 27:913–921.
136. Chammas P, Mocavini I, Di Croce L. 2020. Engaging chromatin: PRC2 structure meets function. *Br J Cancer* 122:315–328.
137. Hill JM, Quenelle DC, Cardin RD, Vogel JL, Clement C, Bravo FJ, Foster TP,

- Bosch-Marce M, Raja P, Lee JS, Bernstein DI, Krause PR, Knipe DM, Kristie TM. 2014. Inhibition of LSD1 reduces herpesvirus infection, shedding, and recurrence by promoting epigenetic suppression of viral genomes. *Sci Transl Med* 6:265ra169.
138. Messer HGP, Jacobs D, Dhummakupt A, Bloom DC. 2015. Inhibition of H3K27me3-specific histone demethylases JMJD3 and UTX blocks reactivation of herpes simplex virus 1 in trigeminal ganglion neurons. *J Virol* 89:3417–3420.
139. Lee JS, Raja P, Knipe DM. 2016. Herpesviral ICP0 Protein Promotes Two Waves of Heterochromatin Removal on an Early Viral Promoter during Lytic Infection. *MBio* 7:e02007-15.
140. Oksuz O, Narendra V, Lee C-H, Descostes N, LeRoy G, Raviram R, Blumenberg L, Karch K, Rocha PP, Garcia BA, Skok JA, Reinberg D. 2018. Capturing the Onset of PRC2-Mediated Repressive Domain Formation. *Mol Cell* 70:1149-1162.e5.
141. Sawtell NM, Thompson RL. 2004. Comparison of herpes simplex virus reactivation in ganglia in vivo and in explants demonstrates quantitative and qualitative differences. *J Virol* 78:7784–7794.
142. Proença JT, Coleman HM, Connor V, Winton DJ, Efstathiou S. 2008. A historical analysis of herpes simplex virus promoter activation in vivo reveals distinct populations of latently infected neurones. *J Gen Virol* 89:2965–2974.
143. Cohen EM, Kobiler O. 2016. Gene Expression Correlates with the Number of Herpes Viral Genomes Initiating Infection in Single Cells. *PLoS Pathog* 12:e1006082.
144. Drayman N, Patel P, Vistain L, Tay S. 2019. HSV-1 single-cell analysis reveals the activation of anti-viral and developmental programs in distinct sub-populations. *Elife* 8:566489.
145. Wyler E, Franke V, Menegatti J, Kocks C, Boltengagen A, Praktijnjo S, Walch-Rückheim B, Bosse J, Rajewsky N, Grässer F, Akalin A, Landthaler M. 2019. Single-cell RNA-sequencing of herpes simplex virus 1-infected cells connects NRF2 activation to an antiviral program. *Nat Commun* 10:4878.
146. Cohen EM, Avital N, Shamay M, Kobiler O. 2020. Abortive herpes simplex virus infection of nonneuronal cells results in quiescent viral genomes that can reactivate. *Proc Natl Acad Sci U S A* 117:635–640.
147. Charman M, Weitzman MD. 2020. Replication Compartments of DNA Viruses in the Nucleus: Location, Location, Location. *Viruses* 12.
148. Tomer E, Cohen EM, Drayman N, Afriat A, Weitzman MD, Zaritsky A, Kobiler O. 2019. Coalescing replication compartments provide the opportunity for

- recombination between coinfecting herpesviruses. *FASEB J* 33:9388–9403.
149. Seyffert M, Georgi F, Tobler K, Bourqui L, Anfossi M, Michaelsen K, Vogt B, Greber UF, Fraefel C. 2021. The HSV-1 Transcription Factor ICP4 Confers Liquid-Like Properties to Viral Replication Compartments. *Int J Mol Sci* 22.
 150. Dembowski JA, DeLuca NA. 2017. Purification of Viral DNA for the Identification of Associated Viral and Cellular Proteins. *J Vis Exp* <https://doi.org/10.3791/56374>.
 151. Dembowski JA, Dremel SE, DeLuca NA. 2017. Replication-Coupled Recruitment of Viral and Cellular Factors to Herpes Simplex Virus Type 1 Replication Forks for the Maintenance and Expression of Viral Genomes. *PLoS Pathog* 13:e1006166.
 152. Cao R, Wang L, Wang H, Xia L, Erdjument-Bromage H, Tempst P, Jones RS, Zhang Y. 2002. Role of histone H3 lysine 27 methylation in Polycomb-group silencing. *Science* 298:1039–1043.
 153. Laugesen A, Højfeldt JW, Helin K. 2019. Molecular Mechanisms Directing PRC2 Recruitment and H3K27 Methylation. *Mol Cell* 74:8–18.
 154. Yu J-R, Lee C-H, Oksuz O, Stafford JM, Reinberg D. 2019. PRC2 is high maintenance. *Genes Dev* 33:903–935.
 155. Wang L, Brown JL, Cao R, Zhang Y, Kassis JA, Jones RS. 2004. Hierarchical recruitment of polycomb group silencing complexes. *Mol Cell* 14:637–646.
 156. Blackledge NP, Farcas AM, Kondo T, King HW, McGouran JF, Hanssen LLP, Ito S, Cooper S, Kondo K, Koseki Y, Ishikura T, Long HK, Sheahan TW, Brockdorff N, Kessler BM, Koseki H, Klose RJ. 2014. Variant PRC1 complex-dependent H2A ubiquitylation drives PRC2 recruitment and polycomb domain formation. *Cell* 157:1445–1459.
 157. Cao R, Zhang Y. 2004. SUZ12 is required for both the histone methyltransferase activity and the silencing function of the EED-EZH2 complex. *Mol Cell* 15:57–67.
 158. Ferrari KJ, Scelfo A, Jammula S, Cuomo A, Barozzi I, Stützer A, Fischle W, Bonaldi T, Pasini D. 2014. Polycomb-dependent H3K27me1 and H3K27me2 regulate active transcription and enhancer fidelity. *Mol Cell* 53:49–62.
 159. Højfeldt JW, Laugesen A, Willumsen BM, Damhofer H, Hedehus L, Tvardovskiy A, Mohammad F, Jensen ON, Helin K. 2018. Accurate H3K27 methylation can be established de novo by SUZ12-directed PRC2. *Nat Struct Mol Biol* 25:225–232.
 160. van Mierlo G, Veenstra GJC, Vermeulen M, Marks H. 2019. The Complexity of PRC2 Subcomplexes. *Trends Cell Biol* 29:660–671.

161. Fursova NA, Blackledge NP, Nakayama M, Ito S, Koseki Y, Farcas AM, King HW, Koseki H, Klose RJ. 2019. Synergy between Variant PRC1 Complexes Defines Polycomb-Mediated Gene Repression. *Mol Cell* 74:1020-1036.e8.
162. Al-Raawi D, Jones R, Wijesinghe S, Halsall J, Petric M, Roberts S, Hotchin NA, Kanhere A. 2019. A novel form of JARID2 is required for differentiation in lineage-committed cells. *EMBO J* 38.
163. Conway E, Jerman E, Healy E, Ito S, Holoch D, Oliviero G, Deevy O, Glancy E, Fitzpatrick DJ, Mucha M, Watson A, Rice AM, Chammas P, Huang C, Pratt-Kelly I, Koseki Y, Nakayama M, Ishikura T, Streubel G, Wynne K, Hokamp K, McLysaght A, Ciferri C, Di Croce L, Cagney G, Margueron R, Koseki H, Bracken AP. 2018. A Family of Vertebrate-Specific Polycombs Encoded by the LCOR/LCORL Genes Balance PRC2 Subtype Activities. *Mol Cell* 70:408-421.e8.
164. Beringer M, Pisano P, Di Carlo V, Blanco E, Chammas P, Vizán P, Gutiérrez A, Aranda S, Payer B, Wierer M, Di Croce L. 2016. EPOP Functionally Links Elongin and Polycomb in Pluripotent Stem Cells. *Mol Cell* 64:645–658.
165. Liefke R, Karwacki-Neisius V, Shi Y. 2016. EPOP Interacts with Elongin BC and USP7 to Modulate the Chromatin Landscape. *Mol Cell* 64:659–672.
166. Youmans DT, Gooding AR, Dowell RD, Cech TR. 2021. Competition between PRC2.1 and 2.2 subcomplexes regulates PRC2 chromatin occupancy in human stem cells. *Mol Cell* 81:488-501.e9.
167. Petracovici A, Bonasio R. 2021. Distinct PRC2 subunits regulate maintenance and establishment of Polycomb repression during differentiation. *Mol Cell* 81:2625-2639.e5.
168. Højfeldt JW, Hedehus L, Laugesen A, Tatar T, Wiehle L, Helin K. 2019. Non-core Subunits of the PRC2 Complex Are Collectively Required for Its Target-Site Specificity. *Mol Cell* 76:423-436.e3.
169. Margueron R, Li G, Sarma K, Blais A, Zavadil J, Woodcock CL, Dynlacht BD, Reinberg D. 2008. Ezh1 and Ezh2 maintain repressive chromatin through different mechanisms. *Mol Cell* 32:503–518.
170. Stojic L, Jasencakova Z, Prezioso C, Stützer A, Bodega B, Pasini D, Klingberg R, Mozzetta C, Margueron R, Puri PL, Schwarzer D, Helin K, Fischle W, Orlando V. 2011. Chromatin regulated interchange between polycomb repressive complex 2 (PRC2)-Ezh2 and PRC2-Ezh1 complexes controls myogenin activation in skeletal muscle cells. *Epigenetics Chromatin* 4:16.
171. Son J, Shen SS, Margueron R, Reinberg D. 2013. Nucleosome-binding activities within JARID2 and EZH1 regulate the function of PRC2 on chromatin. *Genes Dev*

- 27:2663–2677.
172. Connelly KE, Dykhuizen EC. 2017. Compositional and functional diversity of canonical PRC1 complexes in mammals. *Biochim Biophys Acta Gene Regul Mech* 1860:233–245.
 173. Piunti A, Shilatifard A. 2021. The roles of Polycomb repressive complexes in mammalian development and cancer. *Nat Rev Mol Cell Biol* 22:326–345.
 174. Gao Z, Zhang J, Bonasio R, Strino F, Sawai A, Parisi F, Kluger Y, Reinberg D. 2012. PCGF homologs, CBX proteins, and RYBP define functionally distinct PRC1 family complexes. *Mol Cell* 45:344–356.
 175. Fischle W, Wang Y, Jacobs SA, Kim Y, Allis CD, Khorasanizadeh S. 2003. Molecular basis for the discrimination of repressive methyl-lysine marks in histone H3 by Polycomb and HP1 chromodomains. *Genes Dev* 17:1870–1881.
 176. Min J, Zhang Y, Xu R-M. 2003. Structural basis for specific binding of Polycomb chromodomain to histone H3 methylated at Lys 27. *Genes Dev* 17:1823–1828.
 177. Moussa HF, Bsteh D, Yelagandula R, Pribitzer C, Stecher K, Bartalska K, Michetti L, Wang J, Zepeda-Martinez JA, Elling U, Stuckey JI, James LI, Frye SV, Bell O. 2019. Canonical PRC1 controls sequence-independent propagation of Polycomb-mediated gene silencing. *Nat Commun* 10:1931.
 178. García E, Marcos-Gutiérrez C, del Mar Lorente M, Moreno JC, Vidal M. 1999. RYBP, a new repressor protein that interacts with components of the mammalian Polycomb complex, and with the transcription factor YY1. *EMBO J* 18:3404–3418.
 179. Tavares L, Dimitrova E, Oxley D, Webster J, Poot R, Demmers J, Bezstarosti K, Taylor S, Ura H, Koide H, Wutz A, Vidal M, Elderkin S, Brockdorff N. 2012. RYBP-PRC1 complexes mediate H2A ubiquitylation at polycomb target sites independently of PRC2 and H3K27me3. *Cell* 148:664–678.
 180. Farcas AM, Blackledge NP, Sudbery I, Long HK, McGouran JF, Rose NR, Lee S, Sims D, Cerase A, Sheahan TW, Koseki H, Brockdorff N, Ponting CP, Kessler BM, Klose RJ. 2012. KDM2B links the Polycomb Repressive Complex 1 (PRC1) to recognition of CpG islands. *Elife* 1:e00205.
 181. Ren X, Kerppola TK. 2011. REST interacts with Cbx proteins and regulates polycomb repressive complex 1 occupancy at RE1 elements. *Mol Cell Biol* 31:2100–2110.
 182. Lagarou A, Mohd-Sarip A, Moshkin YM, Chalkley GE, Bezstarosti K, Demmers JAA, Verrijzer CP. 2008. dKDM2 couples histone H2A ubiquitylation to histone H3 demethylation during Polycomb group silencing. *Genes Dev* 22:2799–2810.

183. Blackledge NP, Fursova NA, Kelley JR, Huseyin MK, Feldmann A, Klose RJ. 2020. PRC1 Catalytic Activity Is Central to Polycomb System Function. *Mol Cell* 77:857-874.e9.
184. Tamburri S, Lavarone E, Fernández-Pérez D, Conway E, Zanotti M, Manganaro D, Pasini D. 2020. Histone H2AK119 Mono-Ubiquitination Is Essential for Polycomb-Mediated Transcriptional Repression. *Mol Cell* 77:840-856.e5.
185. Stock JK, Giadrossi S, Casanova M, Brookes E, Vidal M, Koseki H, Brockdorff N, Fisher AG, Pombo A. 2007. Ring1-mediated ubiquitination of H2A restrains poised RNA polymerase II at bivalent genes in mouse ES cells. *Nat Cell Biol* 9:1428–1435.
186. Zhou W, Zhu P, Wang J, Pascual G, Ohgi KA, Lozach J, Glass CK, Rosenfeld MG. 2008. Histone H2A monoubiquitination represses transcription by inhibiting RNA polymerase II transcriptional elongation. *Mol Cell* 29:69–80.
187. Di Croce L, Helin K. 2013. Transcriptional regulation by Polycomb group proteins. *Nat Struct Mol Biol* 20:1147–1155.
188. Illingworth RS. 2019. Chromatin folding and nuclear architecture: PRC1 function in 3D. *Curr Opin Genet Dev* 55:82–90.
189. Morey L, Aloia L, Cozzuto L, Benitah SA, Di Croce L. 2013. RYBP and Cbx7 define specific biological functions of polycomb complexes in mouse embryonic stem cells. *Cell Rep* 3:60–69.
190. Klauke K, Radulović V, Broekhuis M, Weersing E, Zwart E, Olthof S, Ritsema M, Bruggeman S, Wu X, Helin K, Bystrykh L, de Haan G. 2013. Polycomb Cbx family members mediate the balance between haematopoietic stem cell self-renewal and differentiation. *Nat Cell Biol* 15:353–362.
191. Plys AJ, Davis CP, Kim J, Rizki G, Keenen MM, Marr SK, Kingston RE. 2019. Phase separation of Polycomb-repressive complex 1 is governed by a charged disordered region of CBX2. *Genes Dev* 33:799–813.
192. Tsuboi M, Kishi Y, Yokozeki W, Koseki H, Hirabayashi Y, Gotoh Y. 2018. Ubiquitination-Independent Repression of PRC1 Targets during Neuronal Fate Restriction in the Developing Mouse Neocortex. *Dev Cell* 47:758-772.e5.
193. Chen JJ, Stermer D, Tanny JC. 2022. Decoding histone ubiquitylation. *Front Cell Dev Biol* 10:968398.
194. Cooper S, Grijzenhout A, Underwood E, Ancelin K, Zhang T, Nesterova TB, Anil-Kirmizitas B, Bassett A, Kooistra SM, Agger K, Helin K, Heard E, Brockdorff N. 2016. Jarid2 binds mono-ubiquitylated H2A lysine 119 to mediate crosstalk between Polycomb complexes PRC1 and PRC2. *Nat Commun* 7:13661.

195. Perino M, van Mierlo G, Loh C, Wardle SMT, Zijlmans DW, Marks H, Veenstra GJC. 2020. Two Functional Axes of Feedback-Enforced PRC2 Recruitment in Mouse Embryonic Stem Cells. *Stem Cell Reports* 15:1287–1300.
196. Kasinath V, Beck C, Sauer P, Poepsel S, Kosmatka J, Faini M, Toso D, Aebersold R, Nogales E. 2021. JARID2 and AEBP2 regulate PRC2 in the presence of H2AK119ub1 and other histone modifications. *Science* 371.
197. Kaneko S, Bonasio R, Saldaña-Meyer R, Yoshida T, Son J, Nishino K, Umezawa A, Reinberg D. 2014. Interactions between JARID2 and noncoding RNAs regulate PRC2 recruitment to chromatin. *Mol Cell* 53:290–300.
198. Kaneko S, Son J, Bonasio R, Shen SS, Reinberg D. 2014. Nascent RNA interaction keeps PRC2 activity poised and in check. *Genes Dev* 28:1983–1988.
199. Arrigoni R, Alam SL, Wamstad JA, Bardwell VJ, Sundquist WI, Schreiber-Agus N. 2006. The Polycomb-associated protein Rybp is a ubiquitin binding protein. *FEBS Lett* 580:6233–6241.
200. Rose NR, King HW, Blackledge NP, Fursova NA, Ember KJ, Fischer R, Kessler BM, Klose RJ. 2016. RYBP stimulates PRC1 to shape chromatin-based communication between Polycomb repressive complexes. *Elife* 5.
201. Loyola A, Huang J-Y, LeRoy G, Hu S, Wang Y-H, Donnelly RJ, Lane WS, Lee S-C, Reinberg D. 2003. Functional analysis of the subunits of the chromatin assembly factor RSF. *Mol Cell Biol* 23:6759–6768.
202. Zhang Z, Jones AE, Wu W, Kim J, Kang Y, Bi X, Gu Y, Popov IK, Renfrow MB, Vassilyeva MN, Vassilyev DG, Giles KE, Chen D, Kumar A, Fan Y, Tong Y, Liu C-F, An W, Chang C, Luo J, Chow LT, Wang H. 2017. Role of remodeling and spacing factor 1 in histone H2A ubiquitination-mediated gene silencing. *Proc Natl Acad Sci U S A* 114:E7949–E7958.
203. Li Y, Gong H, Wang P, Zhu Y, Peng H, Cui Y, Li H, Liu J, Wang Z. 2021. The emerging role of ISWI chromatin remodeling complexes in cancer. *J Exp Clin Cancer Res* 40:346.
204. Cai G, Yang Q, Sun W. 2021. RSF1 in cancer: interactions and functions. *Cancer Cell Int* 21:315.
205. De Magis A, Limmer M, Mudiya V, Monchaud D, Juranek S, Paeschke K. 2023. UV-induced G4 DNA structures recruit ZRF1 which prevents UV-induced senescence. *Nat Commun* 14:6705.
206. Chitale S, Richly H. 2017. Nuclear organization of nucleotide excision repair is mediated by RING1B dependent H2A-ubiquitylation. *Oncotarget* 8:30870–30887.

207. Chitale S, Richly H. 2017. DICER and ZRF1 contribute to chromatin decondensation during nucleotide excision repair. *Nucleic Acids Res* 45:5901–5912.
208. Gracheva E, Chitale S, Wilhelm T, Rapp A, Byrne J, Stadler J, Medina R, Cardoso MC, Richly H. 2016. ZRF1 mediates remodeling of E3 ligases at DNA lesion sites during nucleotide excision repair. *J Cell Biol* 213:185–200.
209. Aloia L, Gutierrez A, Caballero JM, Di Croce L. 2015. Direct interaction between Id1 and Zrf1 controls neural differentiation of embryonic stem cells. *EMBO Rep* 16:63–70.
210. Aloia L, Di Stefano B, Sessa A, Morey L, Santanach A, Gutierrez A, Cozzuto L, Benitah SA, Graf T, Broccoli V, Di Croce L. 2014. Zrf1 is required to establish and maintain neural progenitor identity. *Genes Dev* 28:182–197.
211. Kaymak A, Richly H. 2016. Zrf1 controls mesoderm lineage genes and cardiomyocyte differentiation. *Cell Cycle* 15:3306–3317.
212. Demajo S, Uribealago I, Gutiérrez A, Ballaré C, Capdevila S, Roth M, Zuber J, Martín-Caballero J, Di Croce L. 2014. ZRF1 controls the retinoic acid pathway and regulates leukemogenic potential in acute myeloid leukemia. *Oncogene* 33:5501–5510.
213. Aloia L, Demajo S, Di Croce L. 2015. ZRF1: a novel epigenetic regulator of stem cell identity and cancer. *Cell Cycle* 14:510–515.
214. Zhao J, Lan J, Wang M, Liu C, Fang Z, Song A, Zhang T, Wang L, Zhu B, Chen P, Yu J, Li G. 2024. H2AK119ub1 differentially fine-tunes gene expression by modulating canonical PRC1- and H1-dependent chromatin compaction. *Mol Cell* <https://doi.org/10.1016/j.molcel.2024.02.017>.
215. Sanulli S, Justin N, Teissandier A, Ancelin K, Portoso M, Caron M, Michaud A, Lombard B, da Rocha ST, Offer J, Loew D, Servant N, Wassef M, Burlina F, Gambin SJ, Heard E, Margueron R. 2015. Jarid2 Methylation via the PRC2 Complex Regulates H3K27me3 Deposition during Cell Differentiation. *Mol Cell* 57:769–783.
216. Richly H, Rocha-Viegas L, Ribeiro JD, Demajo S, Gundem G, Lopez-Bigas N, Nakagawa T, Rospert S, Ito T, Di Croce L. 2010. Transcriptional activation of polycomb-repressed genes by ZRF1. *Nature* 468:1124–1128.
217. Richly H, Di Croce L. 2011. The flip side of the coin: role of ZRF1 and histone H2A ubiquitination in transcriptional activation. *Cell Cycle* 10:745–750.
218. Arora M, Packard CZ, Banerjee T, Parvin JD. 2016. RING1A and BMI1 bookmark active genes via ubiquitination of chromatin-associated proteins. *Nucleic*

Acids Res 44:2136–2144.

219. Cohen I, Bar C, Ezhkova E. 2020. Activity of PRC1 and Histone H2AK119 Monoubiquitination: Revising Popular Misconceptions. *Bioessays* 42:e1900192.
220. Toth Z, Maglinte DT, Lee SH, Lee H-R, Wong L-Y, Brulois KF, Lee S, Buckley JD, Laird PW, Marquez VE, Jung JU. 2010. Epigenetic analysis of KSHV latent and lytic genomes. *PLoS Pathog* 6:e1001013.
221. Toth Z, Brulois K, Lee H-R, Izumiya Y, Tepper C, Kung H-J, Jung JU. 2013. Biphasic euchromatin-to-heterochromatin transition on the KSHV genome following de novo infection. *PLoS Pathog* 9:e1003813.
222. Günther T, Fröhlich J, Herrde C, Ohno S, Burkhardt L, Adler H, Grundhoff A. 2019. A comparative epigenome analysis of gammaherpesviruses suggests cis-acting sequence features as critical mediators of rapid polycomb recruitment. *PLoS Pathog* 15:e1007838.
223. Rothbart SB, Krajewski K, Strahl BD, Fuchs SM. 2012. Peptide microarrays to interrogate the “histone code.” *Methods Enzymol* 512:107–135.
224. Dickson BM, Cornett EM, Ramjan Z, Rothbart SB. 2016. ArrayNinja: An Open Source Platform for Unified Planning and Analysis of Microarray Experiments. *Methods Enzymol* 574:53–77.
225. Cornett EM, Dickson BM, Rothbart SB. 2017. Analysis of Histone Antibody Specificity with Peptide Microarrays. *J Vis Exp* <https://doi.org/10.3791/55912>.
226. Sun R, Tan X, Wang X, Wang X, Yang L, Robertson ES, Lan K. 2017. Epigenetic Landscape of Kaposi’s Sarcoma-Associated Herpesvirus Genome in Classic Kaposi’s Sarcoma Tissues. *PLoS Pathog* 13:e1006167.
227. Skene PJ, Henikoff S. 2017. An efficient targeted nuclease strategy for high-resolution mapping of DNA binding sites. *Elife* 6.
228. Meers MP, Bryson TD, Henikoff JG, Henikoff S. 2019. Improved CUT&RUN chromatin profiling tools. *Elife* 8:e46314.
229. Reeves MB, MacAry PA, Lehner PJ, Sissons JGP, Sinclair JH. 2005. Latency, chromatin remodeling, and reactivation of human cytomegalovirus in the dendritic cells of healthy carriers. *Proc Natl Acad Sci U S A* 102:4140–4145.
230. Günther T, Grundhoff A. 2010. The epigenetic landscape of latent Kaposi sarcoma-associated herpesvirus genomes. *PLoS Pathog* 6:e1000935.
231. Ramasubramanyan S, Osborn K, Flower K, Sinclair AJ. 2012. Dynamic

- chromatin environment of key lytic cycle regulatory regions of the Epstein-Barr virus genome. *J Virol* 86:1809–1819.
232. Jha HC, Lu J, Verma SC, Banerjee S, Mehta D, Robertson ES. 2014. Kaposi's sarcoma-associated herpesvirus genome programming during the early stages of primary infection of peripheral blood mononuclear cells. *MBio* 5:e02261-14.
233. Buschle A, Hammerschmidt W. 2020. Epigenetic lifestyle of Epstein-Barr virus. *Semin Immunopathol* 42:131–142.
234. Kobiler O, Afriat A. 2021. The Fate of Incoming HSV-1 Genomes Entering the Nucleus. *Curr Issues Mol Biol* 41:221–266.
235. Woellmer A, Arteaga-Salas JM, Hammerschmidt W. 2012. BZLF1 governs CpG-methylated chromatin of Epstein-Barr Virus reversing epigenetic repression. *PLoS Pathog* 8:e1002902.
236. Abraham CG, Kulesza CA. 2013. Polycomb repressive complex 2 silences human cytomegalovirus transcription in quiescent infection models. *J Virol* 87:13193–13205.
237. Saviola AJ, Zimmermann C, Mariani MP, Signorelli SA, Gerrard DL, Boyd JR, Wight DJ, Morissette G, Gravel A, Dubuc I, Flamand L, Kaufer BB, Fietze S. 2019. Chromatin Profiles of Chromosomally Integrated Human Herpesvirus-6A. *Front Microbiol* 10:1408.
238. Trojer P, Reinberg D. 2007. Facultative heterochromatin: is there a distinctive molecular signature? *Mol Cell* 28:1–13.
239. Kim JJ, Kingston RE. 2022. Context-specific Polycomb mechanisms in development. *Nat Rev Genet* 23:680–695.
240. Linard M, Baillet M, Letenneur L, Garrigue I, Catheline G, Dartigues J-F, Peres K, Helmer C. 2021. Herpes simplex virus, early neuroimaging markers and incidence of Alzheimer's disease. *Transl Psychiatry* 11:414.
241. Kutluay SB, Triezenberg SJ. 2009. Role of chromatin during herpesvirus infections. *Biochim Biophys Acta* 1790:456–466.
242. Kwiatkowski DL, Thompson HW, Bloom DC. 2009. The polycomb group protein Bmi1 binds to the herpes simplex virus 1 latent genome and maintains repressive histone marks during latency. *J Virol* 83:8173–8181.
243. Sodroski CN, Knipe DM. 2023. Nuclear interferon-stimulated gene product maintains heterochromatin on the herpes simplex viral genome to limit lytic infection. *Proc Natl Acad Sci U S A* 120:e2310996120.

244. Rothbart SB, Dickson BM, Raab JR, Grzybowski AT, Krajewski K, Guo AH, Shanle EK, Josefowicz SZ, Fuchs SM, Allis CD, Magnuson TR, Ruthenburg AJ, Strahl BD. 2015. An Interactive Database for the Assessment of Histone Antibody Specificity. *Mol Cell* 59:502–511.
245. Drayman N, Karin O, Mayo A, Danon T, Shapira L, Rafael D, Zimmer A, Bren A, Kobilier O, Alon U. 2017. Dynamic Proteomics of Herpes Simplex Virus Infection. *MBio* 8.
246. Scherer KM, Manton JD, Soh TK, Mascheroni L, Connor V, Crump CM, Kaminski CF. 2021. A fluorescent reporter system enables spatiotemporal analysis of host cell modification during herpes simplex virus-1 replication. *J Biol Chem* 296:100236.
247. Orzalli MH, Conwell SE, Berrios C, DeCaprio JA, Knipe DM. 2013. Nuclear interferon-inducible protein 16 promotes silencing of herpesviral and transfected DNA. *Proc Natl Acad Sci U S A* 110:E4492-501.
248. Carraro M, Hendriks IA, Hammond CM, Solis-Mezarino V, Völker-Albert M, Elsborg JD, Weisser MB, Spanos C, Montoya G, Rappsilber J, Imhof A, Nielsen ML, Groth A. 2023. DAXX adds a de novo H3.3K9me3 deposition pathway to the histone chaperone network. *Mol Cell* 83:1075-1092.e9.
249. Cho S, Park JS, Kang Y-K. 2011. Dual functions of histone-lysine N-methyltransferase Setdb1 protein at promyelocytic leukemia-nuclear body (PML-NB): maintaining PML-NB structure and regulating the expression of its associated genes. *J Biol Chem* 286:41115–41124.
250. Corpet A, Olbrich T, Gwerder M, Fink D, Stucki M. 2014. Dynamics of histone H3.3 deposition in proliferating and senescent cells reveals a DAXX-dependent targeting to PML-NBs important for pericentromeric heterochromatin organization. *Cell Cycle* 13:249–267.
251. Rapkin LM, Ahmed K, Dulev S, Li R, Kimura H, Ishov AM, Bazett-Jones DP. 2015. The histone chaperone DAXX maintains the structural organization of heterochromatin domains. *Epigenetics Chromatin* 8:44.
252. Park J, Lee H, Han N, Kwak S, Lee H-T, Kim J-H, Kang K, Youn BH, Yang J-H, Jeong H-J, Kang J-S, Kim S-Y, Han J-W, Youn H-D, Cho E-J. 2018. Long non-coding RNA ChRO1 facilitates ATRX/DAXX-dependent H3.3 deposition for transcription-associated heterochromatin reorganization. *Nucleic Acids Res* 46:11759–11775.
253. Everett RD, Murray J, Orr A, Preston CM. 2007. Herpes simplex virus type 1 genomes are associated with ND10 nuclear substructures in quiescently infected human fibroblasts. *J Virol* 81:10991–11004.

254. Lukashchuk V, Everett RD. 2010. Regulation of ICP0-null mutant herpes simplex virus type 1 infection by ND10 components ATRX and hDaxx. *J Virol* 84:4026–4040.
255. Everett RD. 2013. The spatial organization of DNA virus genomes in the nucleus. *PLoS Pathog* 9:e1003386.
256. Cuddy SR, Cliffe AR. 2023. The Intersection of Innate Immune Pathways with the Latent Herpes Simplex Virus Genome. *J Virol* 97:e0135222.
257. Alvarez F, Muñoz F, Schilcher P, Imhof A, Almouzni G, Loyola A. 2011. Sequential establishment of marks on soluble histones H3 and H4. *J Biol Chem* 286:17714–17721.
258. Hou Y, Liu W, Yi X, Yang Y, Su D, Huang W, Yu H, Teng X, Yang Y, Feng W, Zhang T, Gao J, Zhang K, Qiu R, Wang Y. 2020. PHF20L1 as a H3K27me2 reader coordinates with transcriptional repressors to promote breast tumorigenesis. *Sci Adv* 6:eaaz0356.
259. Dremel SE, DeLuca NA. 2019. Genome replication affects transcription factor binding mediating the cascade of herpes simplex virus transcription. *Proc Natl Acad Sci U S A* 116:3734–3739.
260. Lewis HC, Kelnhofer-Millevolte LE, Brinkley MR, Arbach HE, Arnold EA, Sanders S, Bosse JB, Ramachandran S, Avgousti DC. 2023. HSV-1 exploits host heterochromatin for nuclear egress. *J Cell Biol* 222:e202304106.
261. Oh J, Fraser NW. 2008. Temporal association of the herpes simplex virus genome with histone proteins during a lytic infection. *J Virol* 82:3530–3537.
262. Cliffe AR, Arbuckle JH, Vogel JL, Geden MJ, Rothbart SB, Cusack CL, Strahl BD, Kristie TM, Deshmukh M. 2015. Neuronal Stress Pathway Mediating a Histone Methyl/Phospho Switch Is Required for Herpes Simplex Virus Reactivation. *Cell Host Microbe* 18:649–658.
263. Cuddy SR, Schinlever AR, Dochnal S, Seegren PV, Suzich J, Kundu P, Downs TK, Farah M, Desai BN, Boutell C, Cliffe AR. 2020. Neuronal hyperexcitability is a DLK-dependent trigger of herpes simplex virus reactivation that can be induced by IL-1. *Elife* 9:e58037.
264. Dochnal S, Merchant HY, Schinlever AR, Babnis A, Depledge DP, Wilson AC, Cliffe AR. 2022. DLK-Dependent Biphasic Reactivation of Herpes Simplex Virus Latency Established in the Absence of Antivirals. *J Virol* 96:e0050822.
265. Maroui MA, Callé A, Cohen C, Streichenberger N, Texier P, Takissian J, Rousseau A, Poccardi N, Welsch J, Corpet A, Schaeffer L, Labetoulle M, Lomonte

- P. 2016. Latency Entry of Herpes Simplex Virus 1 Is Determined by the Interaction of Its Genome with the Nuclear Environment. *PLoS Pathog* 12:e1005834.
266. Dunn KW, Kamocka MM, McDonald JH. 2011. A practical guide to evaluating colocalization in biological microscopy. *Am J Physiol Cell Physiol* 300:C723-42.
267. Konze KD, Ma A, Li F, Barsyte-Lovejoy D, Parton T, Macnevin CJ, Liu F, Gao C, Huang X-P, Kuznetsova E, Rougie M, Jiang A, Pattenden SG, Norris JL, James LI, Roth BL, Brown PJ, Frye SV, Arrowsmith CH, Hahn KM, Wang GG, Vedadi M, Jin J. 2013. An orally bioavailable chemical probe of the Lysine Methyltransferases EZH2 and EZH1. *ACS Chem Biol* 8:1324–1334.
268. Kruidenier L, Chung C-W, Cheng Z, Liddle J, Che K, Joberty G, Bantscheff M, Bountra C, Bridges A, Diallo H, Eberhard D, Hutchinson S, Jones E, Katso R, Leveridge M, Mander PK, Mosley J, Ramirez-Molina C, Rowland P, Schofield CJ, Sheppard RJ, Smith JE, Swales C, Tanner R, Thomas P, Tumber A, Drewes G, Oppermann U, Patel DJ, Lee K, Wilson DM. 2012. A selective jumonji H3K27 demethylase inhibitor modulates the proinflammatory macrophage response. *Nature* 488:404–408.
269. Arbuckle JH, Gardina PJ, Gordon DN, Hickman HD, Yewdell JW, Pierson TC, Myers TG, Kristie TM. 2017. Inhibitors of the Histone Methyltransferases EZH2/1 Induce a Potent Antiviral State and Suppress Infection by Diverse Viral Pathogens. *MBio* 8:e01141-17.
270. Hernández-Romero IA, Valdes VJ. 2022. De Novo Polycomb Recruitment and Repressive Domain Formation. *Epigenomes* 6:25.
271. Lee H-G, Kahn TG, Simcox A, Schwartz YB, Pirrotta V. 2015. Genome-wide activities of Polycomb complexes control pervasive transcription. *Genome Res* 25:1170–1181.
272. Blackledge NP, Klose RJ. 2021. The molecular principles of gene regulation by Polycomb repressive complexes. *Nat Rev Mol Cell Biol* 22:815–833.
273. Tal-Singer R, Pichyangkura R, Chung E, Lasner TM, Randazzo BP, Trojanowski JQ, Fraser NW, Triezenberg SJ. 1999. The transcriptional activation domain of VP16 is required for efficient infection and establishment of latency by HSV-1 in the murine peripheral and central nervous systems. *Virology* 259:20–33.
274. Schmidt N, Hennig T, Serwa RA, Marchetti M, O'Hare P. 2015. Remote Activation of Host Cell DNA Synthesis in Uninfected Cells Signaled by Infected Cells in Advance of Virus Transmission. *J Virol* 89:11107–11115.
275. Renner DW, Szpara ML. 2018. Impacts of Genome-Wide Analyses on Our Understanding of Human Herpesvirus Diversity and Evolution. *J Virol* 92.

276. Song B, Sheng X, Justice JL, Lum KK, Metzger PJ, Cook KC, Kostas JC, Cristea IM. 2023. Intercellular communication within the virus microenvironment affects the susceptibility of cells to secondary viral infections. *Sci Adv* 9:eadg3433.
277. Schmitges FW, Prusty AB, Faty M, Stützer A, Lingaraju GM, Aiwasian J, Sack R, Hess D, Li L, Zhou S, Bunker RD, Wirth U, Bouwmeester T, Bauer A, Ly-Hartig N, Zhao K, Chan H, Gu J, Gut H, Fischle W, Müller J, Thomä NH. 2011. Histone methylation by PRC2 is inhibited by active chromatin marks. *Mol Cell* 42:330–341.
278. Wang X, Goodrich KJ, Gooding AR, Naeem H, Archer S, Paucek RD, Youmans DT, Cech TR, Davidovich C. 2017. Targeting of Polycomb Repressive Complex 2 to RNA by Short Repeats of Consecutive Guanines. *Mol Cell* 65:1056-1067.e5.
279. Zhang Q, McKenzie NJ, Warneford-Thomson R, Gail EH, Flanigan SF, Owen BM, Lauman R, Levina V, Garcia BA, Schittenhelm RB, Bonasio R, Davidovich C. 2019. RNA exploits an exposed regulatory site to inhibit the enzymatic activity of PRC2. *Nat Struct Mol Biol* 26:237–247.
280. Cooper S, Dienstbier M, Hassan R, Schermelleh L, Sharif J, Blackledge NP, De Marco V, Elderkin S, Koseki H, Klose R, Heger A, Brockdorff N. 2014. Targeting polycomb to pericentric heterochromatin in embryonic stem cells reveals a role for H2AK119u1 in PRC2 recruitment. *Cell Rep* 7:1456–1470.
281. Song R, Koyuncu OO, Greco TM, Diner BA, Cristea IM, Enquist LW. 2016. Two Modes of the Axonal Interferon Response Limit Alphaherpesvirus Neuroinvasion. *MBio* 7:e02145-15.
282. Salazar S, Luong KTY, Nua T, Koyuncu OO. 2023. Interferon- λ Activates a Differential Response in Peripheral Neurons That Is Effective against Alpha Herpesvirus Infections. *Pathogens* 12.
283. Schulte I, Batty EM, Pole JCM, Blood KA, Mo S, Cooke SL, Ng C, Howe KL, Chin S-F, Brenton JD, Caldas C, Howarth KD, Edwards PAW. 2012. Structural analysis of the genome of breast cancer cell line ZR-75-30 identifies twelve expressed fusion genes. *BMC Genomics* 13:719.
284. Cai Y, Jin J, Swanson SK, Cole MD, Choi SH, Florens L, Washburn MP, Conaway JW, Conaway RC. 2010. Subunit composition and substrate specificity of a MOF-containing histone acetyltransferase distinct from the male-specific lethal (MSL) complex. *J Biol Chem* 285:4268–4272.
285. Van HT, Harkins PR, Patel A, Jain AK, Lu Y, Bedford MT, Santos MA. 2022. Methyl-lysine readers PHF20 and PHF20L1 define two distinct gene expression-regulating NSL complexes. *J Biol Chem* 298:101588.
286. Sheikh BN, Guhathakurta S, Akhtar A. 2019. The non-specific lethal (NSL)

complex at the crossroads of transcriptional control and cellular homeostasis. *EMBO Rep* 20:e47630.

287. Kang S-J, Chun T. 2020. Structural heterogeneity of the mammalian polycomb repressor complex in immune regulation. *Exp Mol Med* 52:1004–1015.
288. Tamburri S, Conway E, Pasini D. 2022. Polycomb-dependent histone H2A ubiquitination links developmental disorders with cancer. *Trends Genet* 38:333–352.
289. Arecco N, Mocavini I, Blanco E, Ballaré C, Libman E, Bonnal S, Irimia M, Di Croce L. 2024. Alternative splicing decouples local from global PRC2 activity. *Mol Cell* <https://doi.org/10.1016/j.molcel.2024.02.011>.
290. de Potter B, Raas MWD, Seidl MF, Verrijzer CP, Snel B. 2023. Uncoupled evolution of the Polycomb system and deep origin of non-canonical PRC1. *Commun Biol* 6:1144.
291. Kalb R, Latwiel S, Baymaz HI, Jansen PWTC, Müller CW, Vermeulen M, Müller J. 2014. Histone H2A monoubiquitination promotes histone H3 methylation in Polycomb repression. *Nat Struct Mol Biol* 21:569–571.
292. Schwartz YB, Pirrotta V. 2014. Ruled by ubiquitylation: a new order for polycomb recruitment. *Cell Rep* 8:321–325.
293. Pengelly AR, Kalb R, Finkl K, Müller J. 2015. Transcriptional repression by PRC1 in the absence of H2A monoubiquitylation. *Genes Dev* 29:1487–1492.
294. Dorafshan E, Kahn TG, Schwartz YB. 2017. Hierarchical recruitment of Polycomb complexes revisited. *Nucleus* 8:496–505.
295. Francis NJ, Kingston RE, Woodcock CL. 2004. Chromatin compaction by a polycomb group protein complex. *Science* 306:1574–1577.
296. Le HQ, Ghatak S, Yeung C-YC, Tellkamp F, Günschmann C, Dieterich C, Yeroslaviz A, Habermann B, Pombo A, Niessen CM, Wickström SA. 2016. Mechanical regulation of transcription controls Polycomb-mediated gene silencing during lineage commitment. *Nat Cell Biol* 18:864–875.
297. Zepeda-Martinez JA, Pribitzer C, Wang J, Bsteh D, Golumbeanu S, Zhao Q, Burkard TR, Reichholf B, Rhie SK, Jude J, Moussa HF, Zuber J, Bell O. 2020. Parallel PRC2/cPRC1 and vPRC1 pathways silence lineage-specific genes and maintain self-renewal in mouse embryonic stem cells. *Sci Adv* 6:eaax5692.
298. Almeida M, Pintacuda G, Masui O, Koseki Y, Gdula M, Cerase A, Brown D, Mould A, Innocent C, Nakayama M, Schermelleh L, Nesterova TB, Koseki H, Brockdorff N. 2017. PCGF3/5-PRC1 initiates Polycomb recruitment in X

- chromosome inactivation. *Science* 356:1081–1084.
299. Żylicz JJ, Bousard A, Žumer K, Dossin F, Mohammad E, da Rocha ST, Schwalb B, Syx L, Dingli F, Loew D, Cramer P, Heard E. 2019. The Implication of Early Chromatin Changes in X Chromosome Inactivation. *Cell* 176:182-197.e23.
300. Żylicz JJ, Heard E. 2020. Molecular Mechanisms of Facultative Heterochromatin Formation: An X-Chromosome Perspective. *Annu Rev Biochem* 89:255–282.
301. Vogel T, Stoykova A, Gruss P. 2006. Differential expression of polycomb repression complex 1 (PRC1) members in the developing mouse brain reveals multiple complexes. *Dev Dyn* 235:2574–2585.
302. Desai D, Pethe P. 2020. Polycomb repressive complex 1: Regulators of neurogenesis from embryonic to adult stage. *J Cell Physiol* 235:4031–4045.
303. Liu Y, Hu G, Yang S, Yao M, Liu Z, Yan C, Wen Y, Ping W, Wang J, Song Y, Dong X, Pan G, Yao H. 2023. Functional dissection of PRC1 subunits RYBP and YAF2 during neural differentiation of embryonic stem cells. *Nat Commun* 14:7164.
304. Kapetanaki MG, Guerrero-Santoro J, Bisi DC, Hsieh CL, Rapić-Otrin V, Levine AS. 2006. The DDB1-CUL4A^{DDB2} ubiquitin ligase is deficient in xeroderma pigmentosum group E and targets histone H2A at UV-damaged DNA sites. *Proc Natl Acad Sci U S A* 103:2588–2593.
305. Barbour H, Daou S, Hendzel M, Affar EB. 2020. Polycomb group-mediated histone H2A monoubiquitination in epigenome regulation and nuclear processes. *Nat Commun* 11:5947.
306. Ito T, Teo YV, Evans SA, Neretti N, Sedivy JM. 2018. Regulation of Cellular Senescence by Polycomb Chromatin Modifiers through Distinct DNA Damage- and Histone Methylation-Dependent Pathways. *Cell Rep* 22:3480–3492.
307. Naik NG, Nguyen TH, Roberts L, Fischer LT, Glickman K, Golas G, Papp B, Toth Z. 2020. Epigenetic factor siRNA screen during primary KSHV infection identifies novel host restriction factors for the lytic cycle of KSHV. *PLoS Pathog* 16:e1008268.
308. Lee S-C, Toth Z. 2022. PRC1-independent binding and activity of RYBP on the KSHV genome during de novo infection. *PLoS Pathog* 18:e1010801.
309. Hopcraft SE, Pattenden SG, James LI, Frye S, Dittmer DP, Damania B. 2018. Chromatin remodeling controls Kaposi's sarcoma-associated herpesvirus reactivation from latency. *PLoS Pathog* 14:e1007267.
310. Dochnal SA. 2023. Regulation of Herpes Simplex Virus-1 Latent Infection and Reactivation by Facultative Heterochromatin and Neuronal Stress Signaling

determined using a Novel Primary Neuronal Model. PhD Microbiology. University of Virginia School of Medicine .

311. Shukla S, Ying W, Gray F, Yao Y, Simes ML, Zhao Q, Miao H, Cho HJ, González-Alonso P, Winkler A, Lund G, Purohit T, Kim E, Zhang X, Ray JM, He S, Nikolaidis C, Ndoj J, Wang J, Jaremko Ł, Jaremko M, Ryan RJH, Guzman ML, Grembecka J, Cierpicki T. 2021. Small-molecule inhibitors targeting Polycomb repressive complex 1 RING domain. *Nat Chem Biol* 17:784–793.
312. Huseyin MK, Klose RJ. 2021. Live-cell single particle tracking of PRC1 reveals a highly dynamic system with low target site occupancy. *Nat Commun* 12:887.
313. Zhu Y, Dong L, Wang C, Hao K, Wang J, Zhao L, Xu L, Xia Y, Jiang Q, Qin J. 2022. Functional redundancy among Polycomb complexes in maintaining the pluripotent state of embryonic stem cells. *Stem Cell Reports* 17:1198–1214.
314. Papadopoulou T, Richly H. 2016. On-site remodeling at chromatin: How multiprotein complexes are rebuilt during DNA repair and transcriptional activation. *Bioessays* 38:1130–1140.
315. Otto H, Conz C, Maier P, Wölfle T, Suzuki CK, Jenö P, Rücknagel P, Stahl J, Rospert S. 2005. The chaperones MPP11 and Hsp70L1 form the mammalian ribosome-associated complex. *Proc Natl Acad Sci U S A* 102:10064–10069.
316. Jurak I, Silverstein LB, Sharma M, Coen DM. 2012. Herpes simplex virus is equipped with RNA- and protein-based mechanisms to repress expression of ATRX, an effector of intrinsic immunity. *J Virol* 86:10093–10102.
317. Pheasant K, Möller-Levet CS, Jones J, Depledge D, Breuer J, Elliott G. 2018. Nuclear-cytoplasmic compartmentalization of the herpes simplex virus 1 infected cell transcriptome is co-ordinated by the viral endoribonuclease vhs and cofactors to facilitate the translation of late proteins. *PLoS Pathog* 14:e1007331.
318. Vanni E, Gatherer D, Tong L, Everett RD, Boutell C. 2012. Functional characterization of residues required for the herpes simplex virus 1 E3 ubiquitin ligase ICP0 to interact with the cellular E2 ubiquitin-conjugating enzyme UBE2D1 (UbcH5a). *J Virol* 86:6323–6333.
319. Kulej K, Avgousti DC, Sidoli S, Herrmann C, Della Fera AN, Kim ET, Garcia BA, Weitzman MD. 2017. Time-resolved Global and Chromatin Proteomics during Herpes Simplex Virus Type 1 (HSV-1) Infection. *Mol Cell Proteomics* 16:S92–S107.
320. Soh TK, Davies CTR, Muenzner J, Hunter LM, Barrow HG, Connor V, Bouton CR, Smith C, Emmott E, Antrobus R, Graham SC, Weekes MP, Crump CM. 2020. Temporal Proteomic Analysis of Herpes Simplex Virus 1 Infection Reveals Cell-Surface Remodeling via pUL56-Mediated GOPC Degradation. *Cell Rep* 33:108235.

321. Ismail IH, McDonald D, Strickfaden H, Xu Z, Hendzel MJ. 2013. A small molecule inhibitor of polycomb repressive complex 1 inhibits ubiquitin signaling at DNA double-strand breaks. *J Biol Chem* 288:26944–26954.
322. Gil J, O’Loughlen A. 2014. PRC1 complex diversity: where is it taking us? *Trends Cell Biol* 24:632–641.
323. Kreso A, van Galen P, Pedley NM, Lima-Fernandes E, Frelin C, Davis T, Cao L, Baiazitov R, Du W, Sydorenko N, Moon Y-C, Gibson L, Wang Y, Leung C, Iscove NN, Arrowsmith CH, Szentgyorgyi E, Gallinger S, Dick JE, O’Brien CA. 2014. Self-renewal as a therapeutic target in human colorectal cancer. *Nat Med* 20:29–36.
324. Kniazeva AS, Armeev GA, Shaytan AK. 2022. H2A-H2B Histone Dimer Plasticity and Its Functional Implications. *Cells* 11.
325. Aihara H, Nakagawa T, Mizusaki H, Yoneda M, Kato M, Doiguchi M, Imamura Y, Higashi M, Ikura T, Hayashi T, Kodama Y, Oki M, Nakayama T, Cheung E, Aburatani H, Takayama K-I, Koseki H, Inoue S, Takeshima Y, Ito T. 2016. Histone H2A T120 Phosphorylation Promotes Oncogenic Transformation via Upregulation of Cyclin D1. *Mol Cell* 64:176–188.
326. Estève P-O, Terragni J, Deepti K, Chin HG, Dai N, Espejo A, Corrêa IR Jr, Bedford MT, Pradhan S. 2014. Methyllysine reader plant homeodomain (PHD) finger protein 20-like 1 (PHF20L1) antagonizes DNA (cytosine-5) methyltransferase 1 (DNMT1) proteasomal degradation. *J Biol Chem* 289:8277–8287.
327. Zhang C, Hoang N, Leng F, Saxena L, Lee L, Alejo S, Qi D, Khal A, Sun H, Lu F, Zhang H. 2018. LSD1 demethylase and the methyl-binding protein PHF20L1 prevent SET7 methyltransferase-dependent proteolysis of the stem-cell protein SOX2. *J Biol Chem* 293:3663–3674.
328. Bracken AP, Brien GL, Verrijzer CP. 2019. Dangerous liaisons: interplay between SWI/SNF, NuRD, and Polycomb in chromatin regulation and cancer. *Genes Dev* 33:936–959.
329. Reynolds N, Salmon-Divon M, Dvinge H, Hynes-Allen A, Balasooriya G, Leaford D, Behrens A, Bertone P, Hendrich B. 2012. NuRD-mediated deacetylation of H3K27 facilitates recruitment of Polycomb Repressive Complex 2 to direct gene repression. *EMBO J* 31:593–605.
330. Kolla V, Naraparaju K, Zhuang T, Higashi M, Kolla S, Blobel GA, Brodeur GM. 2015. The tumour suppressor CHD5 forms a NuRD-type chromatin remodelling complex. *Biochem J* 468:345–352.
331. Smits AH, Jansen PWTC, Poser I, Hyman AA, Vermeulen M. 2013. Stoichiometry of chromatin-associated protein complexes revealed by label-free

- quantitative mass spectrometry-based proteomics. *Nucleic Acids Res* 41:e28.
332. Boulasiki P, Tan XW, Spinelli M, Riccio A. 2023. The NuRD Complex in Neurodevelopment and Disease: A Case of Sliding Doors. *Cells* 12.
333. Reid XJ, Low JKK, Mackay JP. 2023. A NuRD for all seasons. *Trends Biochem Sci* 48:11–25.
334. Bornelöv S, Reynolds N, Xenophontos M, Gharbi S, Johnstone E, Floyd R, Ralser M, Signolet J, Loos R, Dietmann S, Bertone P, Hendrich B. 2018. The Nucleosome Remodeling and Deacetylation Complex Modulates Chromatin Structure at Sites of Active Transcription to Fine-Tune Gene Expression. *Mol Cell* 71:56-72.e4.
335. Alberto-Aguilar DR, Hernández-Ramírez VI, Osorio-Trujillo JC, Gallardo-Rincón D, Toledo-Leyva A, Talamás-Rohana P. 2022. PHD finger protein 20-like protein 1 (PHF20L1) in ovarian cancer: from its overexpression in tissue to its upregulation by the ascites microenvironment. *Cancer Cell Int* 22:6.
336. Liu H, Wei T, Sun L, Wu T, Li F, Zhao J, Chu J, Wang F, Cai Y, Jin J. 2022. The Non-Specific Lethal (NSL) Histone Acetyltransferase Complex Transcriptionally Regulates Yin Yang 1-Mediated Cell Proliferation in Human Cells. *Int J Mol Sci* 23.
337. Radzishuskaya A, Shliaha PV, Grinev VV, Shlyueva D, Damhofer H, Koche R, Gorshkov V, Kovalchuk S, Zhan Y, Rodriguez KL, Johnstone AL, Keogh M-C, Hendrickson RC, Jensen ON, Helin K. 2021. Complex-dependent histone acetyltransferase activity of KAT8 determines its role in transcription and cellular homeostasis. *Mol Cell* 81:1749-1765.e8.
338. Miranda-Saksena M, Denes CE, Diefenbach RJ, Cunningham AL. 2018. Infection and Transport of Herpes Simplex Virus Type 1 in Neurons: Role of the Cytoskeleton. *Viruses* 10.
339. Dremel SE, Sivrich FL, Tucker JM, Glaunsinger BA, DeLuca NA. 2022. Manipulation of RNA polymerase III by Herpes Simplex Virus-1. *Nat Commun* 13:623.
340. Zhao J, Qin C, Liu Y, Rao Y, Feng P. 2020. Herpes Simplex Virus and Pattern Recognition Receptors: An Arms Race. *Front Immunol* 11:613799.
341. Su Hui Teo C, Serwa RA, O'Hare P. 2016. Spatial and Temporal Resolution of Global Protein Synthesis during HSV Infection Using Bioorthogonal Precursors and Click Chemistry. *PLoS Pathog* 12:e1005927.
342. Zheng Y, Ahmad K, Henikoff S. 2020. CUT&Tag data processing and analysis tutorial v1.

343. Fox HL, Dembowski JA, DeLuca NA. 2017. A Herpesviral Immediate Early Protein Promotes Transcription Elongation of Viral Transcripts. *MBio* 8.
344. Lang F, Li X, Vladimirova O, Hu B, Chen G, Xiao Y, Singh V, Lu D, Li L, Han H, Wickramasinghe JMASP, Smith ST, Zheng C, Li Q, Lieberman PM, Fraser NW, Zhou J. 2017. CTCF interacts with the lytic HSV-1 genome to promote viral transcription. *Sci Rep* 7:39861.
345. Washington SD, Singh P, Johns RN, Edwards TG, Mariani M, Fietze S, Bloom DC, Neumann DM. 2019. The CCCTC Binding Factor, CTRL2, Modulates Heterochromatin Deposition and the Establishment of Herpes Simplex Virus 1 Latency In Vivo. *J Virol* 93.
346. Rivas T, Goodrich JA, Kugel JF. 2021. The Herpes Simplex Virus 1 Protein ICP4 Acts as both an Activator and a Repressor of Host Genome Transcription during Infection. *Mol Cell Biol* 41:e0017121.
347. Harkness JM, Kader M, DeLuca NA. 2014. Transcription of the herpes simplex virus 1 genome during productive and quiescent infection of neuronal and nonneuronal cells. *J Virol* 88:6847–6861.
348. Depledge DP, Srinivas KP, Sadaoka T, Bready D, Mori Y, Placantonakis DG, Mohr I, Wilson AC. 2019. Direct RNA sequencing on nanopore arrays redefines the transcriptional complexity of a viral pathogen. *Nat Commun* 10:754.
349. Hayer A, Shao L, Chung M, Joubert L-M, Yang HW, Tsai F-C, Bisaria A, Betzig E, Meyer T. 2016. Engulfed cadherin fingers are polarized junctional structures between collectively migrating endothelial cells. *Nat Cell Biol* 18:1311–1323.
350. Mangeot PE, Risson V, Fusil F, Marnef A, Laurent E, Blin J, Mournetas V, Massouridès E, Sohier TJM, Corbin A, Aubé F, Teixeira M, Pinset C, Schaeffer L, Legube G, Cosset F-L, Verhoeyen E, Ohlmann T, Ricci EP. 2019. Genome editing in primary cells and in vivo using viral-derived Nanoblades loaded with Cas9-sgRNA ribonucleoproteins. *Nat Commun* 10:45.
351. Girard-Gagnepain A, Amirache F, Costa C, Lévy C, Frecha C, Fusil F, Nègre D, Lavillette D, Cosset F-L, Verhoeyen E. 2014. Baboon envelope pseudotyped LVs outperform VSV-G-LVs for gene transfer into early-cytokine-stimulated and resting HSCs. *Blood* 124:1221–1231.
352. Whitford AL, Clinton CA, Kennedy EBL, Dochnal SA, Suzich JB, Cliffe AR. 2022. Ex Vivo Herpes Simplex Virus Reactivation Involves a Dual Leucine Zipper Kinase-Dependent Wave of Lytic Gene Expression That Is Independent of Histone Demethylase Activity and Viral Genome Synthesis. *J Virol* 96:e0047522.
353. Barilari M, Bonfils G, Treins C, Koka V, De Villeneuve D, Fabrega S, Pende M.

2017. ZRF1 is a novel S6 kinase substrate that drives the senescence programme. *EMBO J* 36:736–750.
354. Fuchs SM, Krajewski K, Baker RW, Miller VL, Strahl BD. 2011. Influence of combinatorial histone modifications on antibody and effector protein recognition. *Curr Biol* 21:53–58.